TRANSACTIONS OF POWDER METALLURGY ASSOCIATION OF INDIA

ISSN 0377-9416

PMAI

Vol. 37, December 2011

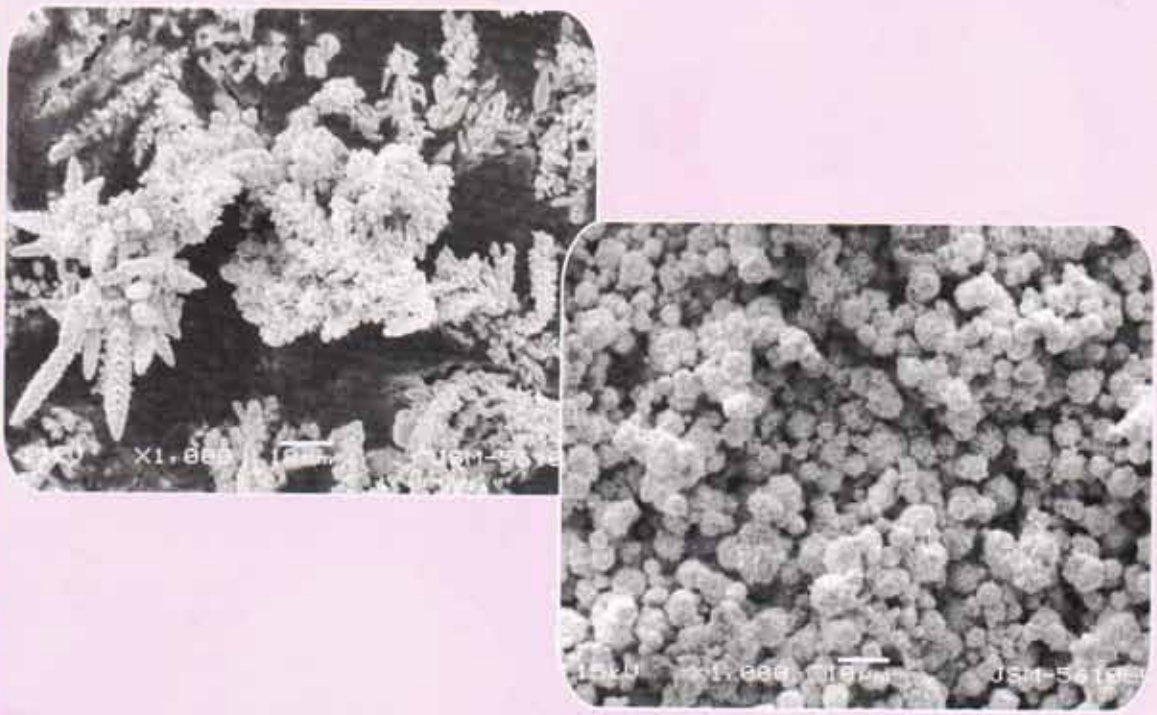

Editor - **P. Ramakrishnan**

Powder Metallurgy Association of India

TRANSACTIONS OF POWDER METALLURGY ASSOCIATION OF INDIA

Vol. 37, December 2011

Editor
P. Ramakrishnan

Powder Metallurgy Association of India

Office Bearers

President :
Shri PNS Sivan

Vice President :
Shri N. Chandrachud
Shri N. Gopinath
Shri P. M. Agarwala
Shri Deepak Grover
Shri P. V. Hegde

Honorary General Secretary :
Dr. Murli Gopal Krishnamoorty

Honorary Treasurer :
Shri K. S. Samant

Honorary Jt. Secretaries :
Dr. Anish Upadhyaya
Shri Jayesh Patel
Dr. Narendra Dhokey

Vol. 37, December 2011

Published by

Powder Metallurgy Association of India (PMAI)
Office : 1002, B-Wing, Kingston, High Street, Hiranandani Complex,
Near D-Mart, Powai, Mumbai. Tel. : 25704588 / E-mail : pmai_pm@yahoo.com

Note : Neither the Powder Metallurgy Association of India nor the editor assumes responsibility of opinions expressed by the authors of the papers published in this transaction.

Price : Rs. 400/- for Indian subscribers and US $ 50 for Overseas subscribers.

Cover : SEM Micrographs of Copper & Nickel Powders, Page 37

Editorial

PMAI organized the International Conference on PM for Automotive and Engineering Industries along with 37th Annual Technical Meeting on Particulate Materials during 3 to 5 Feb., 2011, at The Hotel Westin Pune, Koregaon Park.

Transactions of PMAI, Vol.37, December 2011 contains selected papers from this event. The influence of hydrogen recirculation on the reduction and properties of sponge iron from the blue dust have been established and 20 tons of new grade powder produced is the subject matter of the first paper. The next is the PMAI award winning paper of 2011, explaining the effect of iron powder dilution on the properties of M3/2 sintered steel. The articles following these two are on magnetic materials, investigate the development of Fe-P-Al alloy and nanocrystalline Fe-Co-B-Mo alloy. The next article is on characterization of Yitria stabilised mechanically alloyed (ODS) ferritic stainless steel, followed by boriding of PM, Fe and Fe-2cu-2Ni-0.2C alloy. Two articles are on electrical contact materials and the first one indicate the remarkable improvements in properties attained by the alumina dispersion strengthened cu-Ni matrix nano-composites by high energy milling while the other paper deals with the possibility of replacing infiltration process by liquid phase sintering of Cu-Cr contacts advantageously.

The paper entitled, the investigation on the development and wear studies of PM processed iron based brake pads for heavy duty aircraft applications is discussing the hot powder perform forging approach. The article on the flow through conical converging die of sintered perform is on the investigation of the various aspects of extrusion of powder performs. The two papers on nuclear fuel fabrication deal with the annular mixed oxide fuel pellets for FBTR & PFBR and Th-U , mixed oxide fuel pellets for experimental irradiation. The final paper provides a continuous environmental friendly hydrothermal process for the production of ZnO particles.

We are pleased to announce PM-12, International Conference & Exhibition on New vistas in Particulate Materials Technology and 38th.Annual Technical Meeting during Feb.2 to 4, at the Residence Hotel & Convention Centre, Mumbai.

PMAI wishes its readers a Very Happy & Prosperous New Year 2012.

P. Ramakrishnan

TRANSACTIONS OF
POWDER METALLURGY ASSOCIATION OF INDIA
Vol. 37, December 2011

CONTENTS

HYDROGEN RECIRCULATION AFFECTS ON REDUCTION PROCESS AND PROPERTIES OF THE SPONGE IRON POWDER OF BDP-18 GRADE.

Dr. Dmytro Fedorov

Scientific Expert, Fluidtherm Technology/PC Ladotherm, Ukraine.

Abstract

Production of sponged iron powder from blue dust has been implemented by the author and Fluidtherm Technology, Chennai, at Research and Development Center of NMDC, Hyderabad. The background of the technological route is gas-tight furnace with hydrogen recirculation. During Preliminary Acceptance trials there were a lot of different situations and regimes of the process, which provided with valuable statistical data of the industrial scale. Statistically accumulated data on reduction process with and without recirculation system are analyzed. Sophisticated and safe recirculation system of the hydrogen has allowed decreasing specific hydrogen consumption and accelerating the reduction process. Highly positive effect of the hydrogen recirculation is proved. 20 tons of a new grade sponged iron powder has been produced. According to apparent density of the sponge iron a grade called BDP-18 is introduced to industry and its properties are characterized.

Key words: sponge iron powder, hydrogen, reduction, powder properties.

INTRODUCTION

There is reasonable contradiction between commercial and research approaches. Stability is ideal for commercial production. But wide fluctuations are paradise for researcher's studies. It is very difficult to compromise them. So, the very beginning of commissioning of a new technology is the best time for researcher. However, there are a lot of difficulties too because there are a lot of data but uncertain. Hence, in first a researcher has to treat them from clear point of view. There is a blue dust concentrate as new initial source for sponge iron powder production, there is process of hydrogen reduction. There is statistical data on reduction under hydrogen with and without recirculation of the hydrogen. The results are greatly different. Here analysis of the results is given.

TECHNOLOGICAL PROCESS AND DATA COLLECTION

Initially, all equipment of whole new technology route has to be integrated and regimes must be stabilized. Reasonably, it takes a time. In case of NMDC pilot sponge iron powder plant periodically electric power cuts off added more unpredictable problems. Anyway, 20 tons of a new grade of sponged iron powder had been manufactured during the time with daily capacity of 1 ton. Our technological route includes reduction of initial material under hydrogen recirculation in first reduction furnace following with final annealing in second annealing furnace also under hydrogen partially supplied from the recirculation system. Key stage is reduction in the gas-tight furnace under hydrogen recirculation. It is shown in Fig.1.

Initial powder is charged into the furnace through an entry lock and by conveyor band is transported through furnace muffle of hot zone, cooling zone to discharge unit with exit lock. In the discharged unit reduced and sintered powder cake is crushed into lumps and periodically is taken out from the furnace. Fresh hydrogen is supplied into entry and exit section of the furnace. Without recirculation addition amount of the hydrogen is supplied into middle zone and exhausted gases are burned out at the chimney. Under recirculation the exhausted gases are directed by the blower through several apparatus for purification and returned back into furnace instead fresh one through middle point.

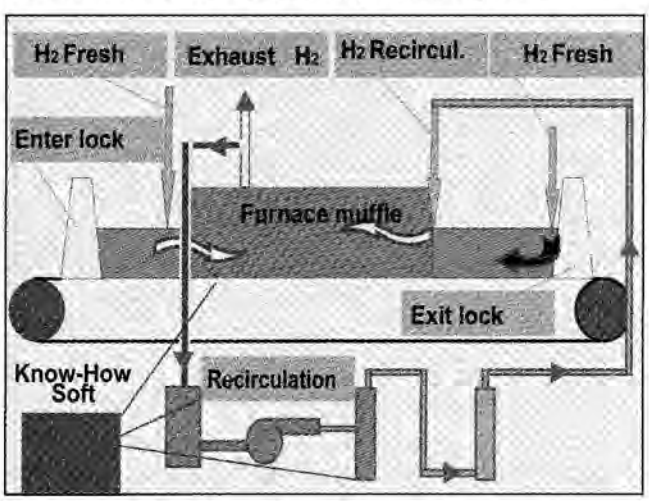

Fig. 1. Key stage of the technology: (a) scheme of H2 recirculation system,

(b) reduction Furnace

Special software program controls of recirculation process. Location of the chimney determines that within hot zone there are two hydrogen streams, from entry to the chimney in parallel with powder movement and counter flow from cooling zone to the chimney. That is to stabilize recirculation of the hydrogen. Such principle has been patented [1]. The system works stable while demands a time for start and stabilization. Details of the technological process are already reported in paper [2].

Due to particular circumstances at NMDC Pilot Sponge iron powder plant during commissioning the hard testing of the system had been taken place. It had been caused by electric power cuts-off for 3-4 consecutive times during short times, daily. That forced to trip immediately hydrogen electrolizer and stop hydrogen production for as minimum as 40 minutes for safety reason. That forced us to start and stop very often the reduction furnace and recirculation system as main consumers of the hydrogen. Due to particular features to start and stabilize the recirculation system the reduction was conducted with conventional method following by burning exhausted hydrogen at outlet chimney for a full process time. In such way there were accumulated the data on reduction process with and without recirculation of the hydrogen in actual industrial furnace.

Our initial material is blue dust fine powder concentrate. Its particles are shown in Fig 2. (Photomicrograph at Brovary Powder Plant lab, Ukraine)

Microstructure of initial material blue dust concentrate, reduced powder under recirculation and finally ready powder are given in Fig. 3–5 as photomicrographs of polish specimens, which had been prepared and analyzed at the Research&Development Laboratory of Fluidtherm Technology and published here with their permission.

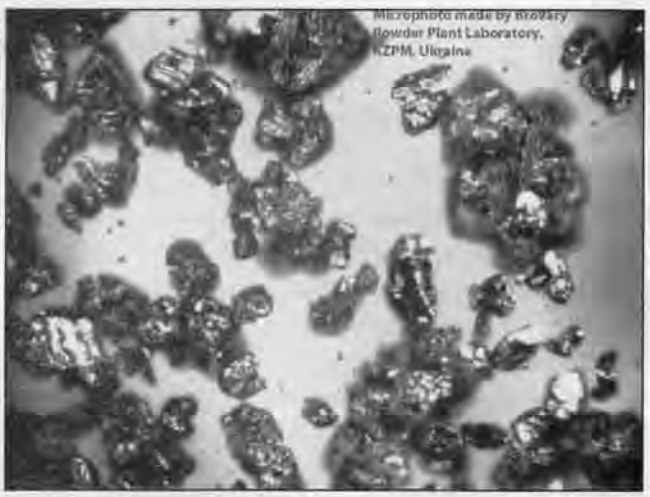

Fig.2 Blue Dust concentrate particles. Photomicrograph (Brovary Laboratory)

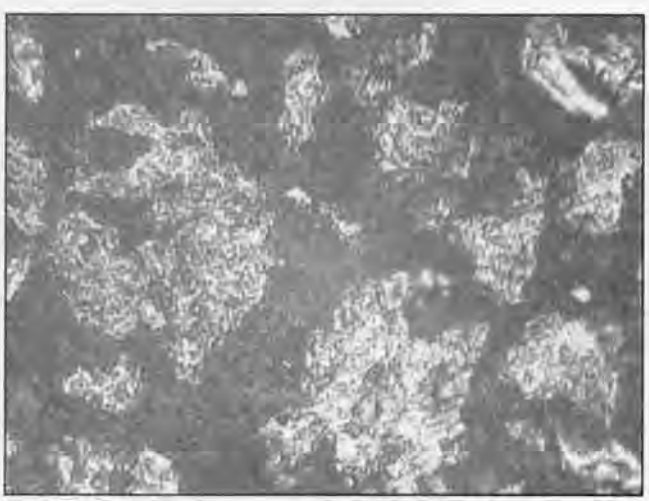

Fig. 3 Blue dust concentrate particles microstructure. Mag. 200X. Hydrogen loss 29.80% (Fluidtherm lab)

Fig. 4 Structure of powder particles, reduced under hydrogen recirculation. Mag. 200X. Hydrogen loss 2.75% (Fluidtherm lab)

Fig. 5. Structure of powder particles, after annealing under hydrogen. Mag. 200X. Hydrogen loss 0.28% (Fluidtherm lab)

Fig 2 shows complicated and irregular particles shape of the initial powder. Its microstructure (Fig.3) is porous consisting from oxides noticed in iron matrix. After reduction under the hydrogen recirculation particles microstructure becomes even more porous with remnant oxides present predominantly at the core. (Fig 4). Finally, after annealing in second furnace the particles are partially agglomerated and oxides are insignificant (Fig.5)
The selected results on oxygen contents are given in Table 1.

Table 1. Observation data on oxygen content before and after reduction for different regimes of the process

No of a group	No of sample	Initial oxygen content [O] %,	Inlet H2 m3/hr fresh	H2 m3/hr recirculated	Final oxygen content [O], %	Removed oxygen, kg/hr	Remark
A	1	19.70	44	0.00	8.83	6.439	No H_2 recirculation
	2	18.30	44	0.00	7.12	6.524	No H_2 recirculation
	3	17.09	44	0.00	3.53	7.615	No H_2 recirculation
B	4	19.66	44	0.00	4.70	8.99	No H_2 recirculation
	5	19.66	34	80	1.02	12.25	70% of time H_2 recirculation
	6	19.66	34	80	0.64	12.45	H_2 recirculation full
C	7	29.80	44	0.00	10.71	11.59	No H_2 recirculation
	8	29.80	34	80	3.42	17.27	70% of time H_2 recirculation
	9	29.80	34	80	2.73	17.60	H_2 recirculation full
D	10	24.52	44	0.00	9.97	8.76	No H_2 recirculation
	11	22.28	34	100	3.38	11.56	50% of time H_2 recirculation
	12	22.28	34	100	0.62	14.17	H_2 recirculation full
E	13	29.80	44	0.00	12.65	10.64	No H_2 recirculation
	14	29.80	34	100	3.08	17.27	50% of time H_2 recirculation
	15	29.80	34	100	1.89	17.60	H_2 recirculation full

The data are divided into 5 groups with three specimens in each. Furnace temperature was set one and the same for all cases. Charged capacity had been within 55-65 kg/hr due to different band speed or height of powder bed. Variable parameters are initial oxygen content of the charged material and re-circulated hydrogen had been applied or not.

Group A includes the specimens with different initial oxygen content reduced without re-circulated hydrogen. Refer to this group as regime A-1, A-2, A-3 and corresponding specimens.

Group B includes the specimens with practically the same initial oxygen content but reduced with different regimes of the re-circulated hydrogen. Refer as -4, B-5, B-6.

Group C includes specimens of pure blue duct concentrate reduced without re-circulated hydrogen (C-1) and under re-circulation. Refer as BC-7, C-8, C-9.

Group D includes a partially reduced powder as initial charge and increased amount of re-circulated hydrogen. Refer as D-10, D-11, D-12.

Group E is control group of blue dust charge with regime similar to the group D. It is the only regime which had been planned intently. Refer as E-13, E-14, E-15.

Oxygen contents for all specimens had been conducted in-situ at NMDC Pilot Plant by the author and repeated selectively to cross-check at Fluidtherm Technology laboratory. Method of determination is MPIF Standard No 2 "*Determination of Loss of Mass in a Reducing Atmosphere for Metal Powders (Hydrogen Loss)*"[3]

DISCUSSION ON RESULTS

It is clear from the table that the higher inlet oxygen content the higher the remnant one. Also, remnant oxygen content under recirculation of hydrogen is less than without. But there was fluctuation in charge capacity due to powder bed height or band speed, so it would be better to determine how much oxygen had been removed during particular trials. In order to show relationship between removed oxygen amount and its initial content I select and compare 5 results for specimens reduced without recirculation, namely: A-1, A-2, A-3, D-10, E-13. The plot in Fig. 6 summarizes this relationship.

The plot points are actual results, the line serves only to demonstrate a trend. Results of regime A-1 is out of general trend, probably due to our limited statistics and fluctuation in the mixed powder properties. But anyway it may be concluded that the higher oxygen content, the higher amount of oxygen is removed at least within the observation limits. According to well-know data on oxide reduction the kinetic curve is exponent. According to our studies [2] the reduction degree 88..92% (4..3% of remnant oxygen) is point of remarkable slow down of the reduction process Hence, these results are in accordance with our previous studies on the subject. The reduction process without recirculation is not complete in time.

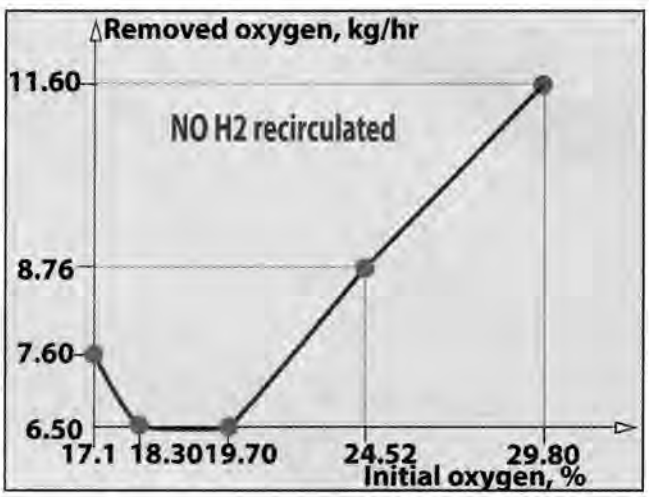

Fig. 6. Removed amount of oxygen during reduction without recirculation of hydrogen versus initial oxygen content of charged powder

16.24 m^3/hr of hydrogen is required to combine as maximum as 11.60 kg/hr of oxygen It is 36% of supplied hydrogen, which indicates value near to the equilibrium of reduction process. That means to provide higher degree of reduction we have to increase hydrogen flow through the furnace. But there is still 64% of hydrogen just burnt out. In the case it had been supplied 44 m^3/hr of hydrogen, and its specific consumption is 3.80 m^3/kg of oxygen.

With applying the hydrogen recirculation we are able to increase hydrogen flow without increasing of its actual consumption.

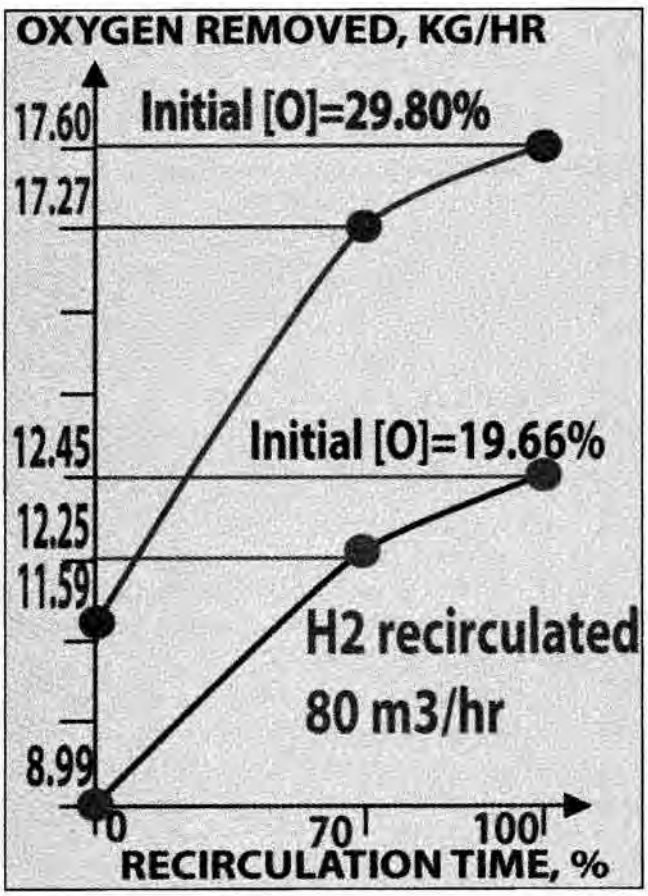

Fig. 7. Removed amount of oxygen during reduction with recirculation of hydrogen versus time of recirculation and initial oxygen content of charged powder for group B and C

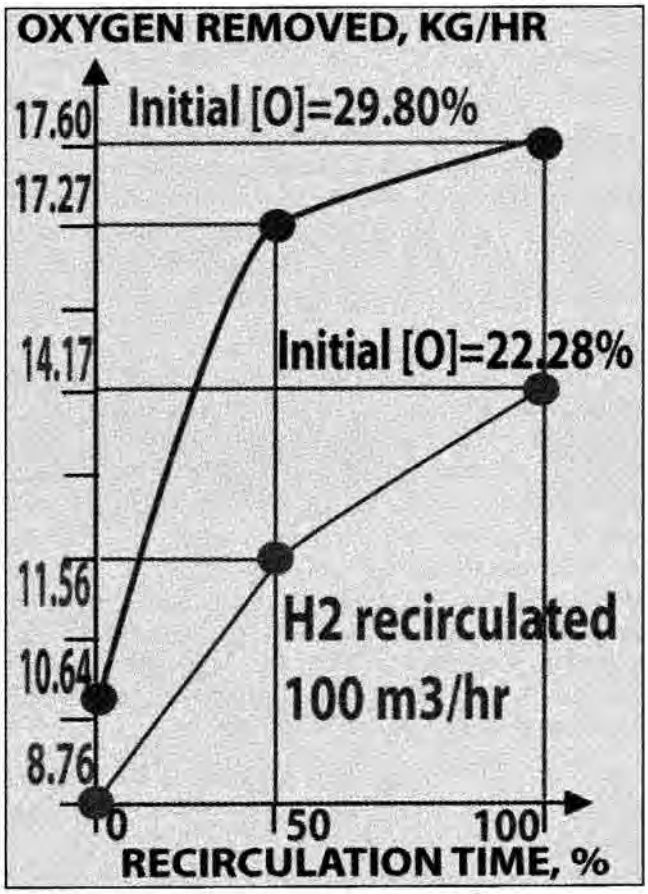

Fig. 8. Removed amount of oxygen during reduction with recirculation of hydrogen versus time of recirculation and initial oxygen content of charged powder for group D and E

Trend on removed oxygen depending on re-circulation regime for group B and C is shown in Fig. 7. Here we compare trend of removed oxygen depending on initial oxygen content and hydrogen regime. Trend on removed oxygen depending on re-circulation regime for group D and E is shown in Fig. 8. This is control comparison of trend of removed oxygen versus hydrogen regime.

Both plots show great acceleration of reduction with applying hydrogen recirculation. It is more effective for charged powder with higher oxygen content. (Compare max 12.45 kg/hg at 19.66% of initial with 14.17 kg/hr at 22.28% and 17.60 kg/hr for 29.80%) It is again in accordance with generalized kinetics of reduction process. Amount of re-circulated hydrogen is 80 m^3/hr for cases B and C and 100 m^3/hr for cases D and E. But the amount of removed oxygen, especially for blue dust as charged material is practically the same. Dynamics of reduction is very similar, so in our particular case there is no reason to increase the amount of re-circulated hydrogen any more. 24.64 m^3/hr of hydrogen is required to combine as maximum as 17.60 kg/hr of oxygen. Only 34 m^3/hr of fresh hydrogen is supplied into the furnace. So, in this case we use 72% of supplied hydrogen directly for reaction, which in twice overcome the equilibrium value of the of reduction process. And no hydrogen is burnt out in the case. So, in the case 34 m^3/hr of hydrogen had been supplied and its specific consumption is only 2.1 m^3/kg of oxygen. It is decreased in 1.8 times due to recirculation. Even more, part of re-circulated hydrogen is supplied into second annealing furnace, saving its consumption for the final operation.

So, it is considered, the regime E-15 (remnant oxygen is 1.89%) under 100 m^3/hr of re-circulated hydrogen is optimal.

CHARACTERISTICS OF BDP-18 POWDER GRADE

BDP-18 is just a working name for the new grade of sponge iron powder. Apparent density of the powder varies from 1.5 to 1.9 g/cm^3. By densification of annealed powder is possible to provide as high as 2.5 g/cm^3. So, 1.8 g/cm^3 is selected as the most frequent results. The studies and production must be continued to stabilize the properties and claim for a new grade in true sense.

Nowadays the trend is to produce mainly atomized powders. It is connected to improving of compacting processes to manufacture high dense PM parts according to strong market demands. But it is also result of deterioration of natural resources. As a rule, any iron ore, as raw material, contains impurities of silica, alumina etc. By methods of iron ore beneficiation to remove the impurities below particular level depending on initial quality of the ore is economically very expensive. So with deterioration of high quality natural iron ore source the process of reduction from iron oxides is missing its basis.

However, the demand of sponge iron powder on the market remains. It is dilemma: there is not enough of initial source of high quality iron oxides, the cost of sponged iron powder is increasing and make them very expensive for the customers and at the same time real sector of the market demands such powder for any future.

Leading powder production companies has started to search for alternative way. [5, 6] The task of the both studies is to obtain surface particles structure of atomized powder closely similar to sponged particles. The company «Hoeganaes Corporation» has developed a new grade of atomized powder ANCORSTEEL AMH with AD=2.55 g/cm^3. Comparison of its properties with conventional sponge iron powder and atomized powder grades have shown that the new developed atomized iron powder with special structure of the particle surface is very close to sponge iron powder and may replace them for many applications.

NOTE. Researcher from Kyiv E. Ch. Pioro in 1980th developed and patented technology by methods of molten cast iron atomization to manufacture "bistructural" powders. [7, 8] These powders due to special structure of particles surface have properties both as sponge iron as well atomized iron powders. By certain variation of technological process it may be possible to regulate the properties into required direction whether more atomized powder or more sponge powder. The process had been implemented at Steel Making plant of Cherepovets, Russia in 1993 with author's active participation. Now it is powerful company "SEVERSTAL" and the biggest producer of iron powder in Russia. But the raw material for process is remarkably changed from that time and "bistructural" powder is produced there no longer.

The blue dust concentrate is a new option to produce sponge iron powder. The powder produced at NMDC was tested at Brovary Powder Plant laboratory, Ukraine, by our experts. Apparent density is determined according to GOST 19440-94 (ISO-3923/1-79), compressibility according to GOST 25280-90 (ISO 3927-77), green strength – according to GOST 25282-93 (ISO 3995-85). This powder grade can also improve green strength of atomized powder without compromising of its background properties. Such studies have been done by addition of the BDP sponge iron power to the standard grade of Brovary water atomized powder PZhR 3.200.28. Atomized powder characteristics are next: AD=2.71 g/cm^3, flow ability 30 s^{-1}, compressibility 7.06 g/cm^3 at 700 MPa, green strength 24 MPa at 6.5 g/cm^3. Data on BDP-18 and its mix with atomized powder are given in table 2 and table 3.

Table 2 Characteristics of BDP sponge iron powder. AD=1.57 g/cm^3, Flow ability = 48 c^{-1}

Load, MPa	Compressibility, g/cm^3		Shrinkage, %		Green strength, MPa
	Raw	Sintered	ΔD/D	ΔH/H	
400	5.59	6.12	1.3	1.2	55
600	6.60	6.75	1.1	1.0	93
700	6.80	6.98	1.0	1.05	112
Up to 6.5 g/cm^3 density	-	-	-	-	83

In all case no lubricant added, only die set lubricated.

The sponge iron powder has low apparent density, low compressibility, but very high green strength. Due to porous structure of the particles and compact during sintering it has high shrinkage. So, it suggest its application for porous antifriction iron parts of ferrite structure with sintered density 5.0...6.5 g/cm^3 with oil impregnation or similar.

Table 3 Characteristics of mixed water atomized powder with added BDP sponge iron powder. AD=2.44 g/cm^3, Flow ability = 33 c^{-1}

Load, MPa	Compressibility, g/cm^3		Shrinkage, %		Green strength, MPa
	Raw	Sintered	ΔD/D	ΔH/H	
400	6.28	6.28	0.2	0.2	27
600	6.84	6.84	0.2	0.3	47
700	7.00	7.04	0.2	0.3	54.5
Up to 6.5 g/cm^3 density	-	-	-	-	32

In all case no lubricant added, only die set lubricated.

Addition of BDP-18 sponge iron powder to water atomized powder has greatly improved its green strength. Compare original powder green strength at 6.5 g/ cm^3 density 24 MPa and 32 MPa at the same density of the mixed powder. It is 30% of increasing. At the same time, the compressibility has practically no change. Flow ability and apparent density are also in suitable range for common compaction process. Shrinkage of the mixed powder is negligible.

This trials suggest application of BDP-18 as addition to conventional atomized iron powders to improve the strength. Also, it can be use as basic material for various powder steels produced by mechanical blending of elemental powders like Mn, Cr etc.

CONCLUSIONS

1. During commissioning of the Sponge Iron Powder Plant by the author and Fluidtherm Technology at NMDC Research Center, Hyderabad, reduction process of fine blue dust with hydrogen recirculation had been stabilized and 20 tons of a new powder grade produced.
2. Comparison and analysis of reduction process with and without hydrogen recirculation have shown remarkable advantages of recirculation in acceleration of the process and more effective usage of the hydrogen. Specific hydrogen consumption per 1 kg of oxygen decreased into 1.8 times.
3. Test of the sponge iron powder characteristics has established its comparatively low compressibility but extremely high green strength, suggesting its application for porous antifriction and complex parts as well as matrix for friction materials.
4. Addition of the new grade sponge iron powder to common water atomized powder improves its green strength significantly keeping all other properties closed to atomized powder.

REFERENCE

1. Patent No 2138748 of Russian Federation. B22F 01/09. *Furnace for decarbonizing annealing of the raw iron powder* / D. Fedorov and others, claimed 10.02.98. Published 27.09.98; - № 27. (In action till 2018).
2. Dmytro Fedorov. *Background Studies and Implementation of Iron Powder Production from Blue Dust.* – Proceeding of PM-2010, 10-14 October 2010. Florence, Italy. - Powder Manufacturing. – 8pages. CD – copy.
3. *Standard Test Methods for Metal Powders and Powder Metallurgy Products*. Edition 2007 – Published by MPIF
4. D. Fedorov *Thesis on PhD Energotechnological study and improvement of iron powder production.* - Kyiv.- Academ Periodika.- 2002. – 24 p.
5. Peter Sokolovky, Francis Hanejko. *Atomized Low Apparent Density (AD) Iron Powder for Advanced Application.* – Proceeding of PM-2010, 10-14 October 2010. Florence, Italy. - Powder Manufacturing.. – 8 pages. CD – copy.
6. Francois Shagnon. *New Iron Powder for Low Density Application.* – Proceeding of PM-2010, 10-14 October 2010. Florence, Italy. - Powder Manufacturing.– 8pages. CD – copy.
7. Lipukhin Yu. V., Danilov L.I, Pioro E. Ch. SU Patent No 4344220. *Method of iron powder production.*
8. Pioro E. Ch. *Thesis on PhD Technological process of iron powder production by atomization of cast iron.* - Kyiv: 1985. – 24 p.

EFFECT OF IRON POWDER DILUTION ON PROPERTIES OF M3/2 SINTERED COMPACTS

A.A. Manwatkar, J.B. Suryawanshi, N.B.Dhokey

Department of Metallurgical Engineering, College of Engineering, Pune, India

Abstract

Powder Metallurgy process has been claimed to produce near net shape with an opportunity to improve the properties and reduces the processing cost of the material. The main objective of this project was to assess sintered properties by dilution of M3/2 HSS with iron powder. Mixes of varying composition were prepared i.e. M3/2 (base), 10, 20, 30 and 40% by wt. iron powder. These blended mixes were compacted at 600 MPa and then sintered at 1140°C in hydrogen atmosphere in tubular sintering furnace and followed by air and furnace cooling to realize the impact on properties. Sintering, hardening and copper infiltration was carried out in a single treatment. Few set of specimens were copper infiltrated along with sintering. The sintered density, microstructure, and bulk hardness were measured for all compositions. Another set of samples were copper infiltrated to analyze effect on properties. Add-on cryogenic treatment on material properties was analyzed. Wear rates of sintered compacts was recorded using Pin-On-Disc machine. A study with and without copper infiltrated sintered compacts and cryogenic treatment was compared as a function of varying amount of iron powder. A threshold value of iron powder content was obtained without appreciable change in properties of the resultant sintered compacts.

1. INTRODUCTION

High hardness, mechanical strength, heat resistance and wear resistance of M3/2 HSS make it an attractive material for the manufacturing of valve train components [1]. With the emergence of new material, old materials are being replaced very often. The material today would be light, strong and durable. The machining of such developed material to give required shape has now become challenge to the metal cutting industries. Over the year considerable research has led to the evolution of new varieties of tool materials in the race of higher productivity [2]. Molybdenum series high speed steels are the most popular tool steel alloys which have been widely used for manufacture of VSI of automotive engines. M3/2 tool steel is most commonly used material, which contains strong carbides forming elements. These carbides in structure enhance better wear resistance and high temperature properties of component. P/M route showed advantage than that of conventional route. Compositions can be controlled easily by close control over dimensions of the product can be easily obtained. [3, 4, 5]. The approach of this present work is related to know the effect of dilution by varying the iron powder concentration on the sintered M3/2 compacts in order to make the process of fabrication more cost effective.

2. MATERIAL AND EXPERIMENTAL DETAILS

2.1 Selection of Powders for blending

The fully pre-alloyed water atomized and vacuum annealed powder of M3/2 was obtained from Hoganas India Pune. The chemical composition of M3/2 and iron powder is given in Table 1. The Iron powder (apparent density is 2.99 g/cc) added in varying proportions viz. 10, 20, 30, and 40 wt% into M3/2 powder and blended for one hour in a double cone mixer. Electrolytic copper powder (99%) of size 2-8 micron was used for infiltration.

TABLE-1: Chemical composition of M3/2 and Iron powder.

Material	C%	Cr%	Co%	Mn%	Mo%	Si%	V%	W%	O ppm
M3/2	0.90-1.10	3.75-4.50	1.0 max	0.40 max	4.75-6.25	0.50 max	2.75-3.40	5.60-6.75	1000 max
Iron powder	<0.01	-	-	-	-	-	-	-	-

2.2 Sinter-hardening

Green compacts of 10 mm diameter and 10 mm height were die pressed at 600 MPa. These green compacts were sintered in tubular sintering furnace at 1140°C in hydrogen atmosphere and soaked for 30 minutes and then furnace cooled to 850°C followed by air cooling (A/C) to room temperature and few set of samples were furnace cooled (F/C). The overall treatment cycle is superimposed on T-T-T diagram of M3/2 as shown in Fig 1.

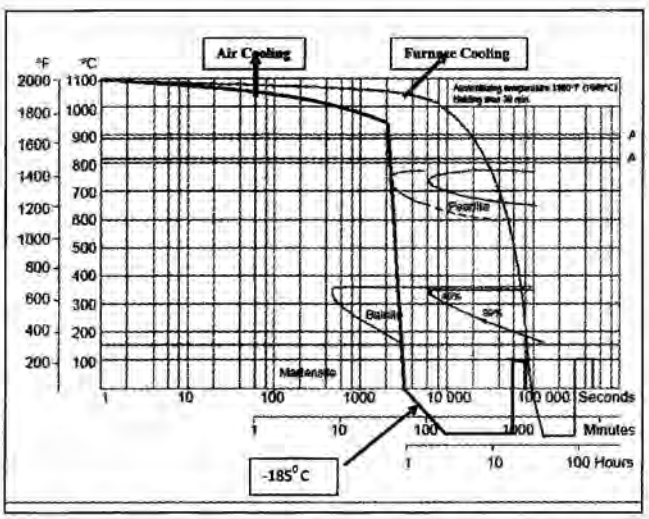

Fig.1: Heat treatment and cryotreatment cycle superimposed on TTT diagram of M3/2

2.3 Cryogenic Treatment

After sintering, samples were subjected to cryogenic treatment in Cryoprocessor (Make; Sandmar, Mumabi). Four samples of each composition were subjected to cryogenic treatment at -185°C and soaked in the bath for 16 hours. After soaking for 16 hours, the samples were warmed upto room temperature in thermocol boxes. After cryogenic treatment, soft tempering at 100°C for 1 hour was given to relieve cold stresses.

2.4 Copper infiltration

In this case, M3/2 compacts were placed on green compact of 1 mm thickness and 10 mm diameter at 1180°c in tubular hydrogen atmosphere sintering furnace. This treatment is simultaneously carried out along with Sinter-hardening.

2.5 Density measurement

The density of the sintered specimen was determined by Archimedes method. Average five readings were noted as sintered density of compact.

2.6 Hardness measurement

The bulk hardness was measured on Rockwell hardness tester using 150 kgf load. Average of three readings on three samples was recorded as measure of bulk hardness (HRC) and expressed in equivalent HRA scale of hardness using standard reference.

2.7 Dry Sliding wear test

Dry sliding wear test was performed by using a computerized Pin-on-Disc machine (Make: Magnum Engineers, Bangalore). Sintered cylindrical specimens of 10 mm diameter and 10 mm height were used to record wear loss. The wear test was carried out using a fixed normal load of 6 kg at constant sliding distance of 3000 mm. The disc rpm (568, 455, and 379) was adjusted for selected track radius (40, 50, 60).The test were carried on each samples for 21 minutes and average of wear loss was estimated.

2.8 Metallography

Sintered samples for the metallographic examination were prepared using usual techniques and etched in 2% nital. The specimens were metallographically examined by using image analyser (Make: Carl Zeiss, Germany) and Scanning electron microscope (SEM).

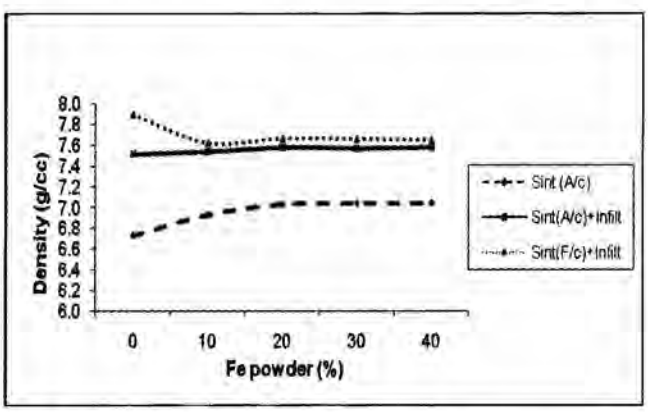

Fig 2: Variation of iron content and cooling rate on sintered density (with and without copper infiltration) of compacts

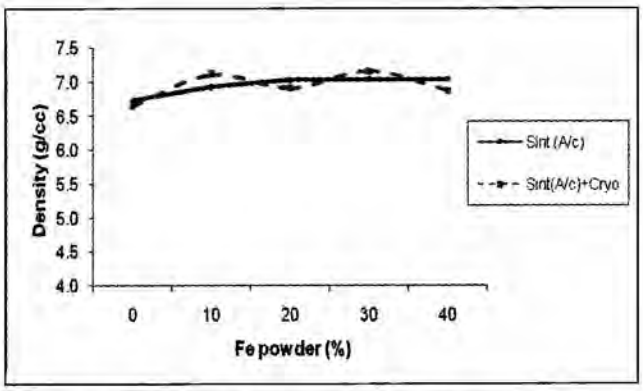

Fig 3: Variation of iron content and cryotreatment on sintered density (without copper infiltration) of Compacts.

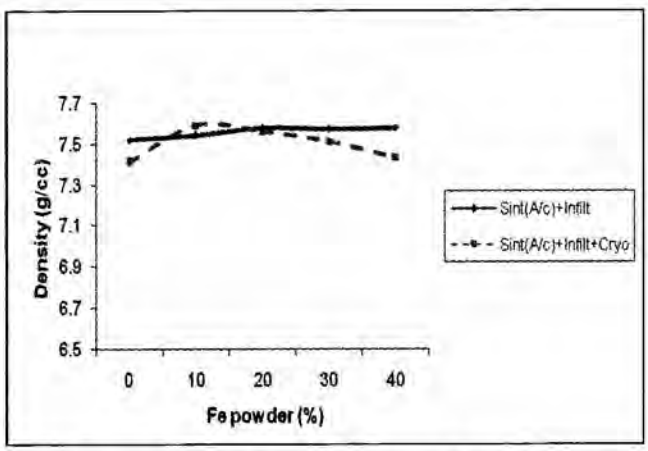

Fig 4: Variation of iron content and cryotreatment on sintered density of copper infiltrated Compacts.

1. RESULTS AND DISCUSSION

3.1 Density variation of sintered compacts

Figure 2 show that as iron powder content increases the sintered density of the compacts also increases till 20% and thereafter sintered density attains steady state plateau. However, cryotreatment has insignificant influence on density as indicated in Fig.3.Copper infiltration has a marked effect on density of compacts as indicated in Fig.4. It is believed that liquid phase of low melting eutectic consisting of iron and M3/2 HSS forms at 1140^{0}C and thus enhance wetting of particles which facilitate cross diffusion of atomic species across the particle-particle interface [3].

3.2 Microstructure analysis

Figure 5 depicts representative SEM microstructures of noncryogenically treated and cryogenically treated specimens. Figures 5 (a) specimen shows segregation of carbides all along the grain boundaries. There is less density of carbides before cryotreated specimens as depicted in Fig. 5(c, e). It is seen that cryogenically treated specimen shown in Fig. 5 (b, d, and f) reveals some level of homogeneity and relatively more population of carbides.

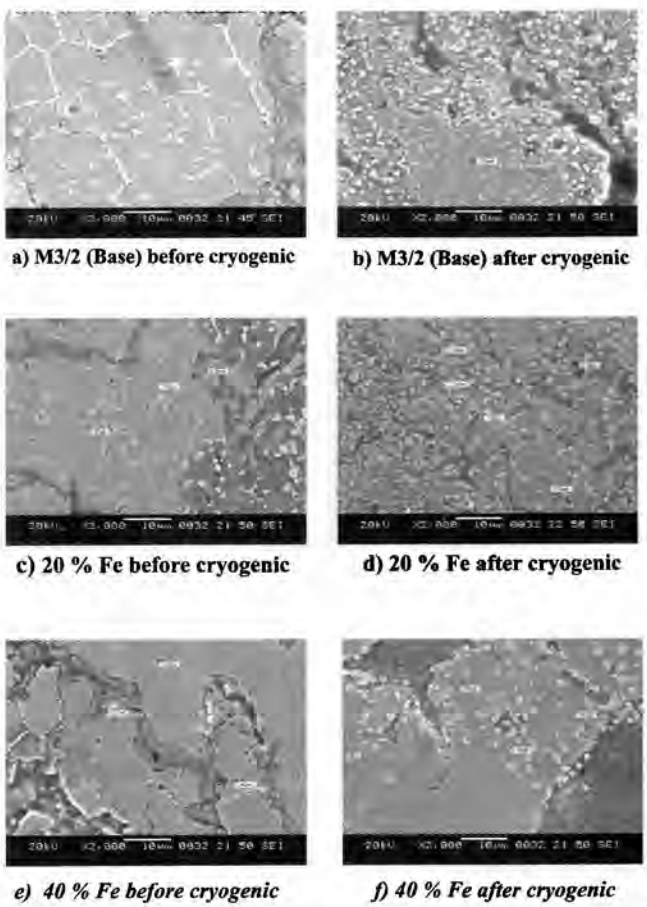

a) M3/2 (Base) before cryogenic **b) M3/2 (Base) after cryogenic**

c) 20 % Fe before cryogenic **d) 20 % Fe after cryogenic**

e) 40 % Fe before cryogenic ***f) 40 % Fe after cryogenic***

Fig 5: SEM microstructures of non-cryogenically and cryogenically treated specimens of varying amount of iron powder depicting distribution of carbides.

3.3 Hardness results

Figure 6 shows hardness goes on decreasing with iron content for plain sintered compacts in which air cooling was used whereas the hardness was maintained at highest order with gradual drop in furnace cooled

specimens. Figure 7 shows cryotreatment improves hardness of sintered specimen to some extent which might be the results of formation of fine carbides as evident in Fig. 5(d). Similar effect is seen in copper infiltrated specimens but gradual drop in hardness depicted in Fig.8. In case of Cu infiltrated samples, it has been noted that the hardness is maximum for M3/2 (base) whereas it went on decreasing for 20% and 40%. This is because of presence of both Cu and Fe.

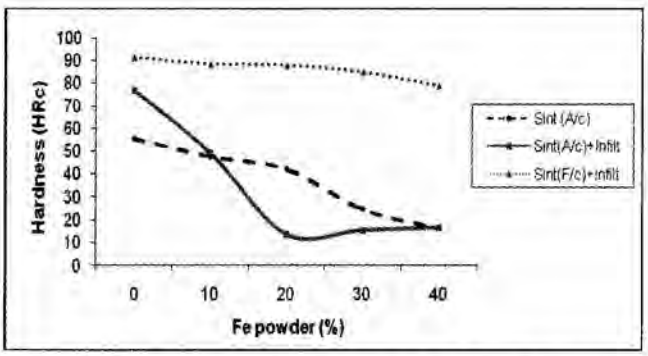

Fig. 6: Variation of iron content and cooling rate on hardness (with and without copper infiltration) of compacts

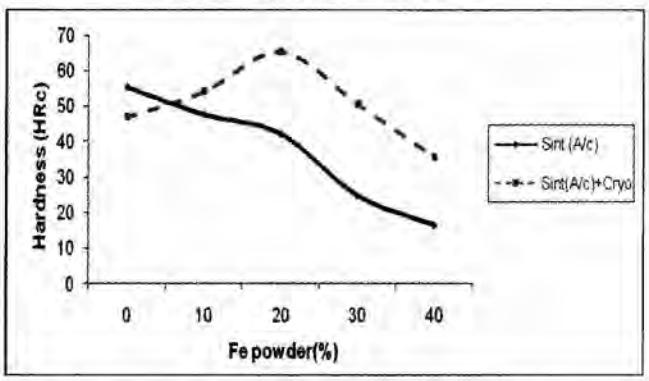

Fig. 7: Variation of iron content and cryotreatment on hardness (without copper infiltration) of compacts.

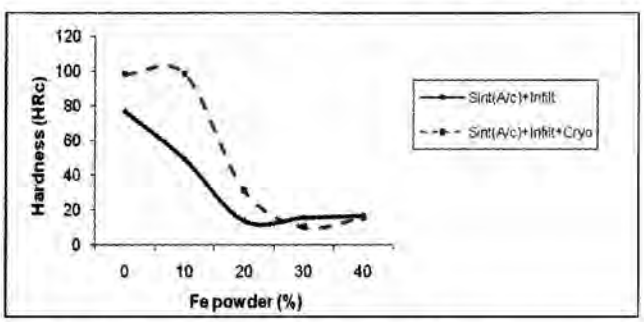

Fig 8: Variation of iron content and Cryotreatment on hardness of copper infiltrated compacts cooled in air.

3.4 Wear Analysis

Wear rate of cryogenically treated specimen shows slight reduction in wear rate as compared to plain sintered specimen as shown in Fig.9. Copper infiltration facilitate reduction in wear rate is clearly visible. The cooling from sintering temperature has a key role in enhancing the precipitation of the secondary carbides. It is revealed that furnace cooling allows fine precipitation of carbides due to more time available for diffusion of carbide forming elements than air cooling does. Wear curve can distinctly be divided into two parts a) Mild wear and b) Sever wear. Particularly, mild-severe is transition seen at 20% Fe powder due to air cooling is shifted to 30% Fe powder in furnace cooled specimen. This shift in wear transition can be attributed to more density of fine carbides precipitated in furnace cooled specimen than the air cooled. It can also be corroborated with increase in hardness in furnace cooled specimen, as indicated in Fig.6. Effect of cryogenic treatment employed for sintered specimen has also seen to decrease the wear rate till 20% Fe powder and beyond this transition point, wear rate dramatically increases, as revealed in Fig.10. When cryotreatment is coupled with sintering and copper infiltration, as characterised in Fig.11, the wear rate deteriorates considerably. However, cryotreatment does not affect wear transition point.

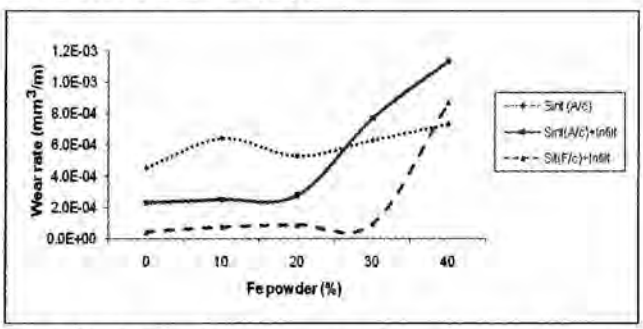

Fig. 9: Variation of iron content and cryotreatment on wear rates (with and without copper infiltration) of compacts

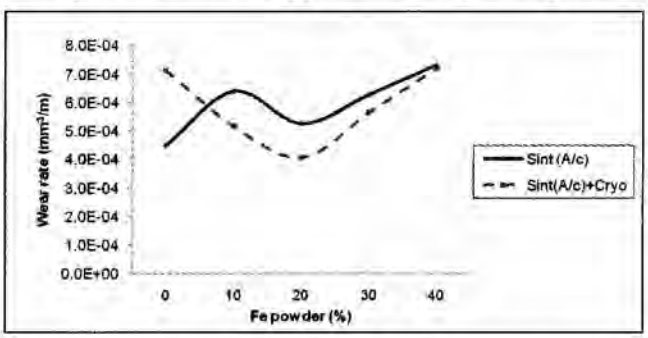

Fig 10: Variation of iron content and cryotreatment on wear rates of (without copper infiltration) compact

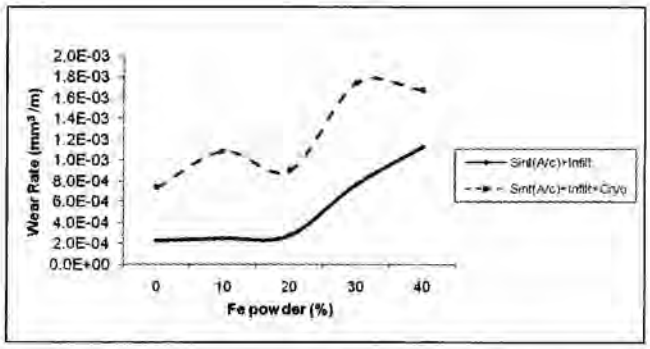

Fig 11: Variation of iron content and cryotreatment on wear rates of copper infiltrated compacts cooled in air

4. CONCLUSIONS

The forgoing discussion on results of sintered, cryogenically and copper infiltrated specimens of M3/2 blended with varying amount of iron powder provide valuable insight into the sintered properties. Based on the discussion, the following conclusion can be drawn

I. The manner of cooling of copper infiltrated specimen from sintering temperature has less effect on density of the sintered compact.

II. The cryogenically treated copper infiltrated specimen show more population of carbides than non-cryogenically treated specimen. However, little influence is seen on improvement in hardness.

III. Mild to severe transition is seen at 20% iron powder in air cooled specimen whereas same is seen at 30% of iron powder in furnace cooled specimen. However, cryotreatment does not influence wear transition point.

ACKNOWLEDGEMENT

The authors would like to thank, the Director, College of Engineering, Pune for the encouragement. Authors gratefully acknowledge the support provided by the Specialty Sintered Pvt.Ltd. Pune.

REFERENCES

[1] M.Madej , J.Lezanski, Structure and properties of Copper infiltrated HSS based composite Archives of Metallurgy and Materials, Volume 53, (2008).

[2] Hoganas: Technical data sheet M3DATA – Issue 05/07.

[3] ASM metal handbook – Volume 7 Powder Metallurgy.

[4] ASM metal handbook – Volume 4 Heat Treatment.

[5] J.Y. Haung, Y.T.Zhu, X.Z.Liao, I.J.Beyarlein: Microstructure of cryogenic treated M2 tool steel. Material Science and Engineering A 339 (2003) 241-244.

[6] Mohd Asri Selamat & Mazlan Mohamad: Supersolidus sintering and mechanical properties of water-atomized M3/2 high speed steel powder sintered under nitrogen-based atmosphere. Jurnal teknologi, 41(A) Dis.2004: 77-84 © University teknologi, Malaysia.

[7] Janusz Konstanty, Sintered HSS base composites for wear and sliding applications, Manufacturing Technology and Research (2008).

DESIGN AND DEVELOPMENT OF POWDER PROCESSED Fe-0.3 wt. %P-0.5 wt. %Al ALLOY

Deepika Sharma, Kamlesh Chandra, Prabhu Shanker Misra
Department of Metallurgical and Materials Engineering
Indian Institute Of Technology, Roorkee, India

Abstract

The present investigation deals with development of high density Fe-0.3wt%P-0.5wt%Al alloy in the form of thin sheets. Soaking it at high temperature eliminates iron-phosphide eutectic and brings entire phosphorus into solution in iron. The technology developed has eliminated the use of hydrogen atmosphere by use of carbon powder to form CO gas within the compact by reacting with oxygen of iron powder particles. The gas so formed is not allowed to escape from the compact by use of glass-based ceramic coating, applied over the compact serving as protective coating to avoid atmospheric oxygen attack over the compact held at high temperature. The alloy so formed yielded coercivity as low as 0.61 Oe, resistivity as high as 29.7 μΩcm and total loss of 2.25 W/Kg at 50Hz. Such a combination of properties may suit their application in high performance precision automotive components, energy conversion and conversation devices, magnetic relays etc.

Introduction

Soft magnetic materials play a vital role in designing electrical and electronic machines, equipments and devices. Basically it is the material and secondly the processing, which control the performance (smooth running without any humming sound) and efficiency (minimum losses in energy conversion) of a device. Soft ferromagnetic materials are generally associated with electrical (DC as well as AC) circuits where they are used to amplify the flux generated by the electric currents. The materials with high duty flux multiplier are most suited for making cores of transformers, generators, and motors. Thus, soft magnetic materials play a key role in power distribution, and make possible the conversion between electrical and mechanical energy, and provide both the transducers and the active storage material for data storage in information systems.

The sintered parts mostly as solid cores made of pure iron are now well established in the market for soft magnetic applications. These components at high sintered density possess high saturation magnetization but they exhibit low resistivity and high magnetic losses [1]. Therefore the use of pure iron powder for P/M soft magnetic components is limited only for DC applications. Increasing resistivity directly reduces the eddy current losses. As eddy current losses are directly proportional to the square of the thickness of the component [2]. Alloying primarily increases the resistivity [3]. It is found that phosphorus and aluminum increase the resistivity of iron [3].

Phosphorus activates sintering process in Fe-P alloys by the formation of low-melting eutectic phase with iron [4]. Phosphorous helps in carrying out alloy constituents into iron matrix which are otherwise sluggish or difficult to diffuse. Phosphorus increases induction and permeability, and decreases coercivity of iron [5]. Employing appropriate sintering time and temperature allotropic transformation in iron is completely avoided [6]. Hence aluminum addition contributes to grain growth and consequently improves the magnetic characteristics.

Despite these advantages, powder metallurgical parts continue to face stiff competition from their wrought counterparts unless they can show equivalent performance at a competitive cost. Density is the most important parameter in this context. As the density of powder metallurgical parts increase, physical and mechanical properties improve and at a near-full density the properties are comparable with their wrought counterparts. It is therefore realized that powder metallurgy substitution can only be possible by proper densification at reasonably low cost [7]. There are several densification processes available in the literature [7]. Conventional powder metallurgy processes enable iron powder to be compacted to 7.1 g/cc or 93% of the theoretical density. Moreover, if we follow the traditional powder metallurgical process, such as compaction and sintering, for manufacturing Fe–P-based alloys, heavy volume shrinkage will be experienced [1]. Double pressing achieves higher density but at increased cost. Existence of prior particle boundaries (PPBs) renders Hot Isostatic Pressing (HIP) unsuitable for magnetic applications. In view of this, in the present investigation, densification is carried out by cost effective hot powder preform forging technique. The process renders highest possible densification

without resorting to hydrogen as sintering atmosphere. It is essentially the process where shaping and consolidation are deformation based. This causes redistribution of segregants if at all remained at the particle surfaces (deformation can displace these from grain boundary and disintegrate them to fine particles which easily dissolve inside the ferritic grains). Such a processing route provides superior magnetic properties in comparison to existing sintering approach.

It has been possible to eliminate the use of costly hydrogen (employed as protective atmosphere during sintering of such alloys) by use of addition of carbon (in the form of graphite). This helps in number of ways, firstly as solid lubricant during cold compacting; secondly as solid state reducing agent to take care of oxygen situated at iron powder particles surfaces during high temperature processing. Carbon combines with oxygen and forms protective reducing atmosphere of CO within the compact. The CO gas is not allowed to escape from the compact by the use of tenacious and adherent glass-based ceramic coating [8]. This coating also serves as protective coating to avoid atmospheric oxygen attack over the compact held at high temperature. The overall purpose of such a protective coating is economy in processing these materials and improves their magnetic performance.

Experimental Procedure

Atomized iron powder (ASC 100. 29) with a nominal carbon 0.01% and hydrogen loss value 0.1% (size -100 mesh) and aluminum powder with size -100 mesh (C~ 0.00 wt %) were taken. Iron-phosphide powder (C- 0.01 wt %) (size -100 mesh) was prepared by reacting iron powder with ortho-phosphoric acid and a subsequent thermal treatment ($800^0C/2h/H_2$) to yield Fe_3P coating over iron powder. The powders are suitably mixed with 0.3wt% of carbon (in the form of graphite; size -100 mesh) to yield Fe-0.3 wt% C-0.3 wt% P-0.5 wt% Al alloy.

The powder mix was filled in a rectangular die and the green compacts (preform) with 7mm thickness and 25mm x 50mm size were formed. The oxidation resistant glassy coating [8] was applied on the surface of preforms like a paint with a brush to serve as protective layer resisting oxidation at high temperatures and protecting reducing gaseous atmosphere of CO produced inside the compact at high temperature by reaction of C with O_2 (of iron powder). Coated preforms were baked at 120^0C for two hours. These performs were then transferred to a furnace held at a temperature 1050^0C and soaked there for one hour. Hence entire phosphorus and aluminum are dissolved into iron to yield homogeneous ferrite phase. The hot preforms were immediately transferred to a forging die fitted in the press and were forged. Then the slabs were hot rolled at temperature 900^0C to form a sheet of 0.1mm thickness. Toroids were stamped from the sheet using a die/punch arrangement. Glassy coating was applied on the toroids and these were again annealed at 850^0C for three hours to relieve residual stresses. The dimensions of toroids were 1mm thickness, 50mm outer diameter, 40mm inner diameter with 74 primary and 6 secondary windings using Teflon coated multi strand wire.

The samples prepared this way were characterized in terms of their density, microstructure, electrical resistivity and magnetic properties. The content of carbon and oxygen was analyzed by Spectroscopic Analyzer. Density of the forged, rolled and annealed sheets was determined by Archimedes' Principal. Microstructure (etched with 2% Nital) of the rolled and annealed sheet was analyzed by using image analyzer to estimate the grain size and volume percentage of porosity in the alloy. Scanning Electron Microscopy (SEM) and X- Ray Mapping confirmed the presence of ferrite phase and showed uniform distribution of phosphorus and aluminum in iron matrix. Electrical Resistivity (ρ) was measured by four probe method. Magnetic properties were measured under a.c. mode with varying field (20Oe to 100Oe) and frequency (50 Hz to 1 Khz).

Results and Discussion

Incorporating carbon to the alloys has helped in number of ways, firstly as solid lubricant during cold compacting; secondly as solid state reducing agent to take care of oxygen situated at iron powder particles surfaces during high temperature processing. Thirdly pushing phosphorus into ferrite grain as solute and thereby discourages it to precipitate as phosphide along ferrite grain boundaries [9]. Furthermore, aluminum acts as deoxidizing agent and minimizes the formation of carbon monoxide [10]. The complete chemistry of alloys developed (spectroscopic analysis) is given in TABLE 1 along with the measured values of density (forged, rolled and annealed sheets), grain size and porosity percentage present in the sheets. It was

observed that densification has improved with the present processing technique.

TABLE 1: Density, porosity and grain size of the alloy developed in the present investigation.

Final Chemistry	Forged Density (g/cc)	Rolled and Annealed Density (g/cc)	Percentage Porosity	Grain Size (μm)
Fe-0.07C-0.1O-0.3P-0.5Al	7.03	7.43	1.97	110

The microstructure shows residual alignment of porosity due to rolling (Fig 1). Pores are elongated due to unidirectional compressive force [11]. Pore rounding and coagulation of smaller pores into bigger pores are observed in the microstructures. This may be due to the presence of phosphorous content in the alloy [12].

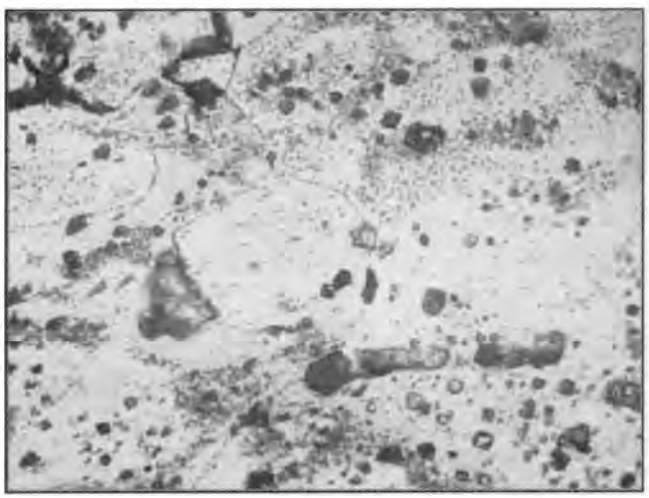

Fig 1: Microstructure of rolled and annealed alloy (etched with 2% Nital) at 200X.

Phosphorus and aluminum are both ferrite stabilizers and are added to iron below its solubility limit; therefore only alpha phase is present (Fig 2 (a)). The alloy developed in the present investigation is free of any segregation of the alloying elements along the grain boundaries. They get distributed uniformly in the entire structure (Fig. 2 (b)-(d).

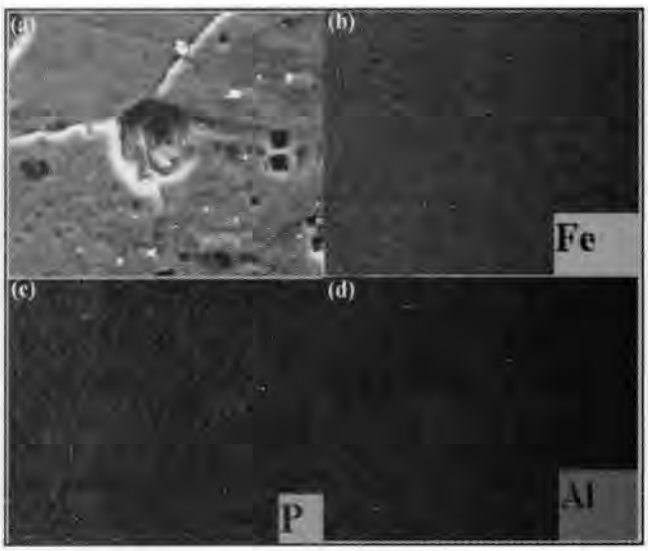

Fig 2: (a) Compositional Image (Secondary Image), X-Ray Mapping showing uniform distribution of alloying elements in Fe-0.07C-0.3O-0.3P-0.5Al alloy at 3000X. (b) Fe, (c) P and (d) Al

TABLE 2: Comparison of electrical and magnetic properties of the alloy developed in present investigation with commercially available soft magnetic material.

Composition	Electrical Resisitivity (μΩcm)	Coercivity (Oe)	Permeability	Total Magnetic Loss (W/Kg)	Saturation Magnetization (G) at 100 Oe
Fe-0.07C-0.1O-0.3P-0.5Al	29.7	0.61	8100	2.25	13436
MOH	48.0	0.46	27662	1.38	18238

The resistance of iron increases greatly due to alloying additions like P and Al [12]. TABLE 2 represents the electrical resistivity and a.c. magnetic properties of the alloy and compares with the commercially available soft magnetic material.

Coercivity of Fe-based alloys falls as we add alloying elements such as P and Al to Fe. The higher the alloying content, lower is the coercivity value [5]. The narrow hysteresis loop for Fe-0.07C-0.1O-0.3P-0.5Al alloy is shown in Fig 3.

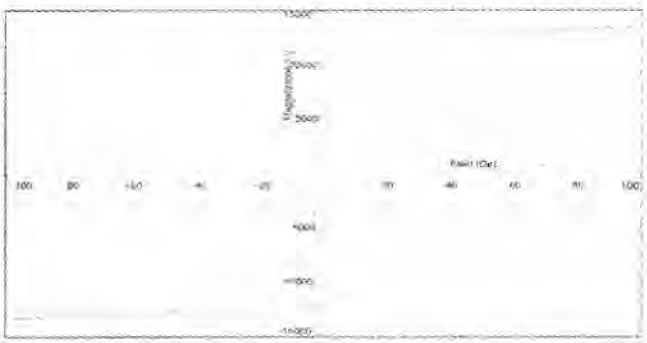

Fig 3: Hysteresis Loop of Fe-0.07C-0.10-0.3P-0.5 Al alloy

The permeability increases greatly due to alloying additions like P and Al [13]. Higher value of permeability observed was due to large grain size and low porosity. Total magnetic loss is the sum of eddy current loss and hysteresis loss [2]. Combined addition of P and Al has decreased the total magnetic loss of the alloy developed. This may be due to the fact that the alloy has simultaneously high resistivity and low coercivity values. Variation of total magnetic loss with varying frequency is shown in Fig 4.

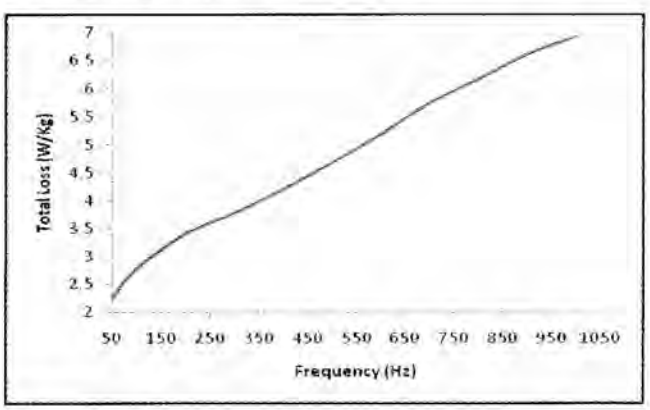

Fig 4: Variation of total magnetic loss with frequency

Saturation magnetization of iron increases when phosphorous is added up to 0.8wt % and decreases thereafter [12]. In the present investigation addition of 0.5 wt% of Al, lowers saturation magnetization at a rate corresponding to simple dilution [3]. The effect of varying field on saturation magnetization is shown in Fig 5.

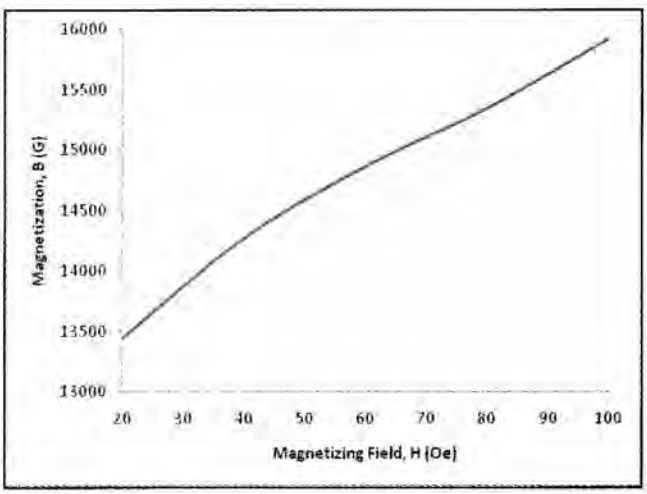

Fig 5: Effect of varying magnetic field on magnetization

Such a combination of properties is achieved by the use of hot powder preform forging technique employed in the present investigation.

Conclusions

- The technology developed showed very low coercivity and total loss values.
- Combined application of glassy ceramic coating and use of graphite as a reducing agent has lead to economy in P/M processing for soft magnetic applications.

Acknowledgements

The authors acknowledge their collaborators, Defence Research Metallurgical Laboratory, Hyderabad, India.

References

[1] K. Chandra and P.S. Misra, "Characteristics of sintered Fe-P alloys", *Proceeding National Seminar on Advances in Materials & Processing, Department of Metallurgical & Materials Engineering, IIT, Roorkee*, pp 263-268 (2001).

[2] K.S. Narasimhan, "P/M processing of soft magnetic materials", *Int. J. Powder Metall*, Vol.40, pp 25-36 (2004).

[3] C.W. Chen, *Magnetism and metallurgy of soft magnetic materials*, North Holland Publishing Company, N.Y. (1977).

[4] Technical Report, *Powders for soft magnetic sintered parts*, Hoganas AB, Brochure PM 92- 01, Sweden.

[5] K.H. Moyer, *Magnetic materials and properties for part applications*, *ASM Hand Book on Powder Metallurgy and Application*, Vol. 7, pp 1006–1019 (1998).

[6] L. Taylor, *Properties and Selection of Metals*, Metals Handbook, 8th edition, American Society for Metals, metals Park, Ohio.

[7] P. Jones, K. B. Golder, R. Lawcock and R. Shivanath, "Densification strategies for high endurance *P*/M components", *Int. J. Powder Metall*, Vol. 33, pp 37-44 (1997).

[8] P.S. Misra and K. Chandra, "High Temperature Oxidation Resistant Glassy Coating", Indian Patent application no. 153/DEL/2010 dated January 27, 2010.

[9] R. Balasubramaniam, "On the corrosion resistance of Delhi iron pillar", *Corrosion Science, Vol. 42, pp* 2103-2129 (2000).

[10] G. Krauss, *Steels: Processing, Structure, and Performance*, (2005).

[11] J. Das, K. Chandra, P.S. Misra and B. Sarma, "Novel powder metallurgy technique for development of Fe–P based soft magnetic materials", *J. Magn. Magn. Mater.*, Vol. 320, pp 906-915 (2008).

[12] B. Weglinski and J. Kaczmar, "Effect of Fe_3P Addition on Magnetic Properties of Sintered Iron", *Powder Metall.*, Vol. 23, pp 210-216 (1980).

[13] L. Anestiev, M. De. Wulf, L. Froyen, L. Dupre and J. Melkebeek, "Preparation of soft magnetic alloys $Fe_{100-x-y}Si_xP_y$ ($0<x<9$, $0<y<0.6$ wt %), using solid phase diffusion- sintering method", *J. Magn. Magn. Mater.*, Vol. 281, pp 124-134 (2004).

DEVELOPMENT OF NANOCRYSTALLINE STRUCTURE AND STUDY OF MAGENTIC PROPERTIES OF Fe-Co-B-Mo ALLOY THRUOGH MECHANICAL ALLOYING

Sreenivasa Murthy K.V., T. Srinivasa Rao and S. Kumaran

Department of Metallurgical and Materials Engineering, National Institute of Technology Tiruchirappalli, India.

Abstract

Recent technology in materials science and engineering is looking for better performance materials and processing in order to meet current fast growing competing industrial evolution. The non-equilibrium structures such as nanostructure, amorphous phase, etc., can be produced in an existing engineered alloy by adopting non-equilibrium materials processing technologies such as rapid solidification processing, mechanical alloying, etc. In the present research, equiatomic Fe-Co alloy with alloying addition was synthesized in a high energy ball milling process. Since nanostructured iron-cobalt magnetic materials offer superior soft magnetic properties than conventional soft magnetic materials, the Fe-Co system was chosen. The chosen system was synthesized in optimized process parameters such as milling speed, milling time, process control agent, environment, etc. Mechanically alloyed powders were characterized by X-Ray Diffraction (XRD), Scanning Electron Microscopy (SEM) and Vibrating Sample Magnetometer (VSM). The influence of milling parameters on average particle size in these alloys was studied by Laser Particle Size Analyzer. The effect of milling time on crystallite size and corresponding magnetic properties of nanocrystalline powders are discussed. MA led to particle refinement as well grain refinement. The minimum grain size achieved was 6.35 m for $Fe_{47}Co_{47}B_4Mo_2$ 50 hrs milled powder. Coercive value obtained was 47.98 Oe (3818 Am^{-1}) in above said system.

1. Introduction

The current curiosity on nanoparticles has been phenomenally increasing because of their interesting electronic, optical, magnetic, mechanical and chemical properties. Interest in these materials is motivated by the fact that the small grain size gives the nanoparticles unique physical and chemical properties which are totally different from those of their bulk counterparts. Owing to the importance of the iron-cobalt system in magnetic applications at high temperature, FeCo alloys which have highest magnetic induction among all the magnetic materials, as well as the high Curie temperature, are one state of art topic of the nanomagnetic research.

In general soft magnetic materials require a low coercivity and a high permeability. Therefore, a little change in the applied magnetic field causes a large change in magnetization. Simply, magnetization is a process that involves domain wall movement and domain rotation so that their magnetization is aligned in parallel. In conventional magnetic materials, grain boundaries are known to be impediments to domain wall motion, and it has been found that magnetic hardness is approximately inversely proportion to grain size for grain size exceeding 0.1-1 micron meter. However, in recent developments of nanostructured soft magnetic materials, Coercivity has been found to follow a proportional relationship to grain size for average grain diameters below the ferromagnetic exchange length L_{ex} [1].

Mechanical Alloying (MA), which is basically a powder metallurgy processing technique. This technique can be used to synthesis a variety of both equilibrium and non equilibrium materials at room temperature starting from the blended powders or prealloyed powders. The processing involves repeated cold welding, fracturing, and rewelding of powder particles in a high energy ball mill resulting in the formation of alloy phases. The non-equilibrium phases synthesized include supersaturated solid solutions, metastable crystalline and quasicrystalline phases, nanostructures, and amorphous. This technique has been extensively applied to produce nanostructured

bulk materials with a wide range of chemical compositions and crystal structures. It is now known to be versatile route for fabrication of alloys with nanocrystalline and amorphous phases. Soft magnetic nanocrystalline iron – cobalt alloys are produced by non-equilibrium materials processing technique mechanical alloying.

2. Experimental

The chosen elemental Iron, Cobalt, Molybdenum, Nickel and ferroboron powders with average particle size of 55 μm, 1 μm, 64 μm, 10 μm and 32 μm respectively were mechanically alloyed in a planetary ball mill, rotated at a speed of 260 rpm. The elemental powders of Fe, Co, B with varying proportion of Mo were mixed together and subjected to mechanical alloying. INSMART planetary ball mill was used for milling the powders. Vials were filled according to nominal composition of powders. Wet milling was performed; Toluene was used as wet medium. Vial and Grinding medium material was Stainless steel. The ball to powder ratio (BPR) has a significant effect on the time required to achieve a particular phase in the powder being milled. At high BPR lattice strain produced on powders are more significant, which drastically affects the magnetic properties of the alloy. In this experiment BPR 10:1 was used. Milling time was varied from 5 to 50 hrs. Mill was allowed to run for 20 min and then rested for next 15 mins in order to avoid temperature raise. Since alloying among powder particles occurs due to the impact forces exerted on them, it is necessary that there is enough space for the balls and the powder particles to move around freely in the milling container. Therefore, the extent of filling the vial with the powder and the ball is important. Here approximately 50% of the vial space is filled with Powder and balls. True alloying among powder particles can occur only when a balance is maintained between cold welding and fracturing of particles. Toluene which acts as Process Control Agent (PCA) to the powder mixture, balance the cold welding and fracturing of particles. During Mechanical alloying process, because of balls impact on powder particles lattice strain is induced on MA powders.

Structural evolutions during milling such as formation of intermetallics, nanocrystalline structure, amorphous structure, etc were studied with the help of X-Ray Diffraction (XRD). Magnetic properties such as Coercivity, magnetic saturation, etc were with the help of Vibrating Sample Magnetometer (VSM).

3. Results and discussion

3.1 Characterization of mechanically alloyed Fe-Co-B Mo system

3.1.1 X-Ray Diffraction Analysis

3.1.1.1 X-Ray Diffraction Analysis of $Fe_{47}Co_{47}B_4Mo_2$ sample

In XRD patterns for the sample $Fe_{47}Co_{47}B_4Mo_2$ powders with different milling time interval, as the milling time increases decrease in the intensity and broadening of iron peak is observed. This broadening is associated with the refinement of grains and lattice distortion with respect to milling hours. At the end of 50 hrs grain size of 6.35 m is observed.

3.1.1.2 X-Ray Diffraction Analysis of $Fe_{46}Co_{46}B_4Mo_4$ sample.

In XRD patterns for the sample $Fe_{46}Co_{46}B_4Mo_4$ at the end of 20 hrs, boride compound formation is observed in XRD peak. After 50 hrs of milling, grains size is 11.31 m. Lattice distortion is 1.27 % at 50 hrs of milling. $Fe_{46}Co_{46}B_4Mo_4$ Sample shows increase in crystallite size and decrease in lattice strain with respect to milling time when compared with the sample $Fe_{47}Co_{47}B_4Mo_2$.

3.1.2 Vibrating sample magnetometer analysis

3.1.2.1 VSM analysis of $Fe_{47}Co_{47}B_4Mo_2$ sample

Saturation magnetization Ms is the maximum value of induction that magnetic material can reach when subjected to a magnetic field. Cobalt is the only element which, when alloyed with Fe, brings about an increase in saturation magnetization and Curie temperature. It can be seen that Ms of as milled powders increases continuously with increasing milling time, reaching a

maximum value of 19.575 emu, at 50 hrs of milling. The increase in Ms can be attributed to the diffusion of Co into iron form Fe-Co alloy and formation of nanocrystalline [1].

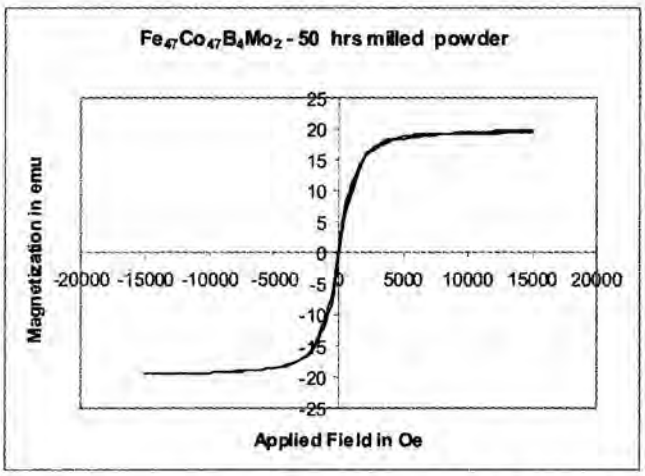

Fig. 1: Magnetic hysteresis loop of $Fe_{47}Co_{47}B_4Mo_2$ 50 hrs milled powder.

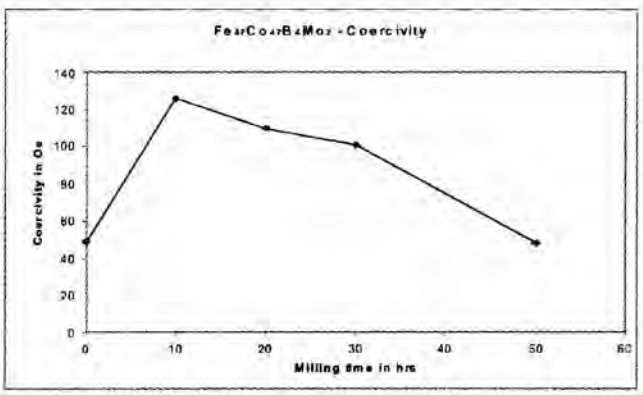

Fig. 2: Variation of Coercivity with increased milling time.

From the graph it is confirmed that coercivities of milled powders decreases with increasing milling time. At 10 hrs of milling coercive value was 125.93 Oe (10021 Am^{-1}Hard magnetic behavior), as the alloying occurred upon milling, low coercivity of 47.98 Oe(3818 Am^{-1}) was observed at the end of 50 hrs mechanical alloying.

3.1.2.2 VSM analysis of $Fe_{46}Co_{46}B_4Mo_4$ sample

Similar to Fe47Co47B4Mo2 sample, coercivities of milled powders reduced with increase in milling hours. After 50 hrs of milling, coercivity of 82 Oe (6525 Am^{-1}) is found. It has been confirmed from the XRD pattern of $Fe_{46}Co_{46}B_4Mo_4$ sample, Cobalt boride, Co_3B compound formed in MA powders. The borides are non magnetic in nature which affects the magnetic properties such as saturation magnetization. Fig. 4 shows variation of coercivity with milling time [2&3]

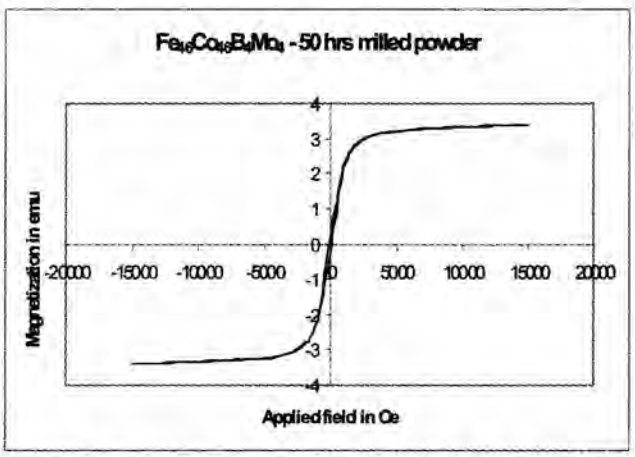

Fig. 3: Magnetic hysteresis loop of $Fe_{46}Co_{46}B_4Mo_4$ 50 hrs milled powder.

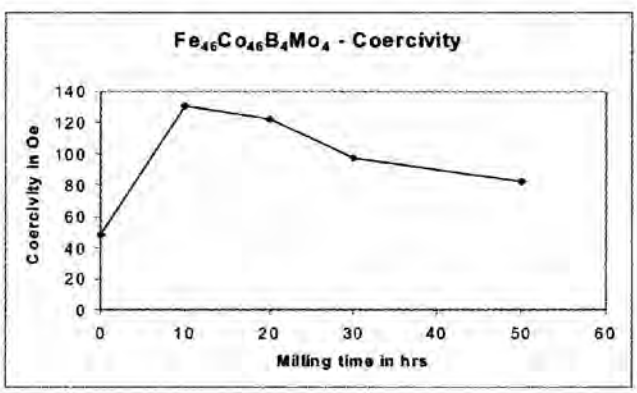

Fig. 4: Variation of coercivity with milling time.

4. Conclusions

4.1 The minimum grain size achieved was 6.35m for $Fe_{47}Co_{47}B_4Mo_2$, 50 hrs milled powder. The change in grain size is predicted to be approximately inversely proportional to the milling hours. This is mainly due to competing evens of cold welding and fracturing during MA.

4.2 Addition of boron in Fe-Co-B-Mo system has strong influence on structural transformation and particle size reduction.

4.3 VSM studies of MA powders showed decrease in coercivity value and increase in saturation magnetization with milling time. The coercivity value of $Fe_{47}Co_{47}B_4Mo_2$ system is increased at initial milling hrs (10 hrs) and further milling decreases the coercivity value. The $Fe_{47}Co_{47}B_4Mo_2$ system milled for 50 hrs resulted lower coercivity value. The minimum coercivity value obtained is 47.98Oe (3818 Am^{-1}). Maximum value of saturation magnetization is found to be 19.57 emu.

5. References

1. J. Zhu and M. Mujahid: Journal of Materials science and Technology (2005) vol. 21 No8 925-933

2. H.F. Li and R.V. Ramanujan: Journal of Metastable and Nanocrystalline Materials Vol. 23 (2005) pp187-190.

3. Happy, S.R. Mohanty, P.Lee, T.L. Tan, S.V. Springham, A. Patran, R.V. Ramanujan, R.S. Rawat: Applied Surface Science, 252(2006), pp 2806-2816

CHARACTERIZATION OF YITRIA DISPERSED MECHANICALLY ALLOYED (ODS) FERRITIC STAINLESS STEEL POWDERS

Mayur Zinzuwadia, R. Sunil Kumar, V.V. Dabhade, U. Prakash

Department of Metallurgical and Materials Engineering,
Indian Institute of Technology Roorkee, Roorkee, India

Abstract

Mechanically alloyed ferritic alloys (ODS) are potential candidate for core structural applications at elevated temperature in high energy neutron environment of fast breeder and fusion reactors. Mechanical alloying involves the severe deformation of mixtures of powder until they form the most intimate of atomic solution. The elemental powders of Fe, Cr and Y_2O_3 are mixed in proportionate quantities and mechanically alloyed for 60 hours (in several stages) in a planetary mill. MA powders at several milling intervals (10h, 20h, 30h, 40h, 50h and 60 h) are characterized by XRD, FESEM for the degree of alloying, particle morphology, crystallite size and phases. The elemental powders are also characterized for crystallite size and morphology. The effect of milling time on the alloy formation is determined.

Introduction

Oxide dispersion strengthened (ODS) ferritic steels are promising materials with a potential to be used at elevated temperatures due to the addition of extremely thermally stable oxide particle dispersion into the ferritic matrix. The characteristic feature of ODS steels is to introduce the Y_2O_3 oxide particles into the matrix, which serve as a block for mobile dislocations to improve the high-temperature strength and as a sink of point defects induced by radiation displacement to maintain superior radiation resistance [1, 2]. The development of ODS Ferritic Steels has been conducted in the field of fast breeder reactor fuel cladding application. Y_2O_3 dispersed ferritic steel possesses a unique combination of body centre cubic (BCC) structure with low co-efficient thermal of expansion, high thermal conductivity, good creep resistance and high tensile/compressive strength [3].

Mechanical alloying was originally developed to produce oxide-dispersion strengthened (ODS) nickel- and iron-base super alloys for applications in the aerospace industry. MA has now been shown to be capable of synthesizing a variety of equilibrium and non-equilibrium alloy phases starting from blended elemental or pre-alloyed powders. Mechanical alloying is a completely solid-state processing technique and therefore limitations imposed by the phase diagrams do not apply here. In the present investigation mechanical alloying of ODS ferritic stainless steel powder (Fe-10%Cr-0.3%Y_2O_3) via elemental route was carried out.

Experimental

Y_2O_3 dispersed (ODS) ferritic stainless steel was prepared by Mechanical alloying. Pure atomized Fe (99.99% and 30μm), Cr (99.99% and 40μm) and Y_2O_3(99.9% and 4 μm) powders of were mixed together having composition (Fe -10% Cr -0.3% Y_2O_3) and milled for 60 hrs in a planetary ball mill (Retsch PM 400/2). Elemental powders of Fe and Cr were mixed in a required proportion to get a final weight of 60 grams. Yttria was dispersed in ethanol for 10 min in an ultra-sonic vibrator to avoid agglomeration. This was then added to the elemental powder mixture. The powder mix was taken into the steel vessel of planetary mill along with the hardened steel balls. The initial ball to powder ratio maintained is 10:1 (by weight). The ball to powder ratio was maintained in milling by removing 15gm of milled powder and 150gm of steel balls regularly after 10, 20, 30, 40, 50 and 60 hours. The milled powders at regular intervals were characterized. The parameters of milling are given in Table 1.

TABLE 1: Mechanical Alloying Parameters

Planetary Ball mill Details (Retsch PM 400/2)	Milling Parameters
Milling Balls- Hardened steel balls	Milling Media-Toluene
Milling Jars- Hardened steel jars	Charge to Ball ratio-1:10
Jar capacity- 500 ml	Milling speed- 300 rpm Vial Speed- 600 rpm
Process Control Agent-Toluene	Total time of milling- 60 hr Weight of initial charge- 60gms

The powder was characterized for phases and elements in XRD. The powder morphology, particle distribution and particle size can be known from SEM analysis. SEM micrographs of all the powders were used for the optical counting for the particle size distribution and morphology analysis. The instrument used for SEM was LEO 435 VP. XRD analysis was also done for the powders to know the phases present. All the XRD analysis was done on Bruker AXS D8 Advance.

Results and Discussion

XRD Analysis

X-ray diffraction spectra for the Fe-10% Cr-0.3%Y_2O_3 powders with respect to milling times are shown in Fig. 5. Both Fe and Cr are body-centered cubic (BCC) structure and the difference in their lattice parameters is only 0.5% (Fe-2.8664 A^0 and Cr - 2.8839A^0) . Therefore it is very difficult to differentiate between them.

Fig 1 shows the XRD pattern of the mechanically alloyed powder at various stages. From the XRD analysis it is revealed that the XRD peak of the initial Fe-10% Cr-0.3%Y_2O_3 powder without mechanical alloying is very sharp and also the Fe and Cr peaks are not distinguishable. After 10 hr of mechanical alloying Y_2O_3 peak is disappeared. The X-ray diffraction patterns of the MA powder show that that the spectra becomes broader and peak intensities decrease, but

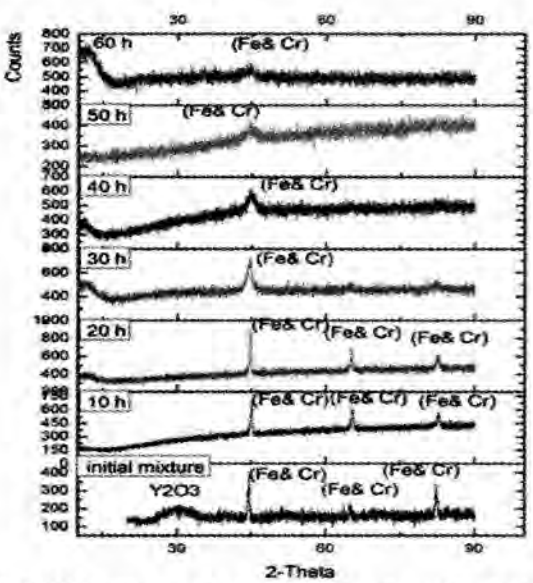

Fig 1: XRD patterns of as received and mechanically alloyed powders (0-60 hr)

positions stay at the same diffraction angles with milling time. Though the diffraction lines of the respective elements can be resolved in the starting powders, line broadening owing to the decrease in crystallite size, accumulation of strains and defects in the course of the ball milling makes it almost impossible to pursue the structural change any further.

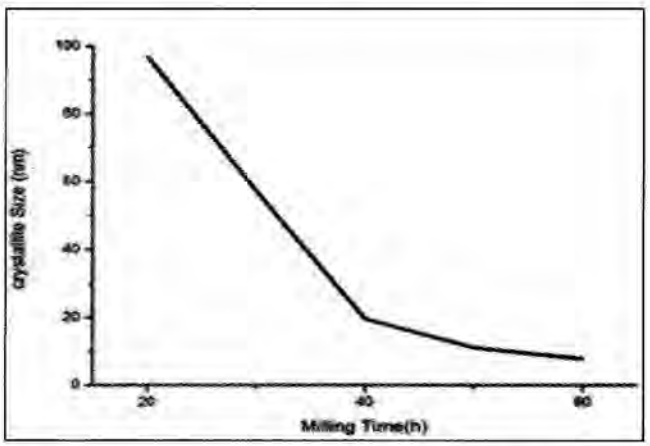

Fig 2: Crystallite size as a function of milling time

Crystallite size for particles below 100 nm is measured from the XRD patterns with the help of the Scherrer's Formula [4]:

$$\text{crystallite size} = \frac{k * \lambda}{\cos\theta * \beta_{1/2}}$$

Where, k = shape factor (0.94 for cubic systems)

λ = wavelength (Cuk_α -1.542 A^0)

β = the full- width at half maximum, and

θ = Bragg angle.

As the Mechanical alloying time increases dramatic decrease in the particle size is observed (Fig. 2). Crystallite size in the range of 7-10 nm is obtained after 60 hrs of milling. During calculation of crystallite size by scherrer's formula lattice strain was not taken in to consideration.

5.2 SEM Analysis

Fine powders of Fe and Cr were observed separately under SEM for their morphology and particle size distribution.Fe powder has somewhat spherical geometry and average particle size of the Fe powder is 25μm. The Fe

powder used is produced by atomization route. The greater sphericity of the Fe powder is due to its atomized nature.Cr powder has angular shape and average particle size of the Cr powder is 35μm. As is evident from the SEM micrographs both the powders are of different shape and have different particle sizes.

The mechanical alloying of Fe, Cr and Y_2O_3 powders was carried out to form ODS ferritic stainless steel. Both Fe, Cr are ductile in nature and Y_2O_3 is brittle in nature. In the early stages of MA the ductile components (i.e. Fe & Cr) get flattened to platelet/ pancake shapes (Fig.3 (a) & (b)). The brittle oxide (i.e.Y_2O_3) may get fragmented or comminuted. These fragmented brittle particles tend to become occluded by the ductile constituents and trapped in the ductile particles. Amount of Fe powder is more than Cr so the Cr particles may be surrounded by the Fe particles.

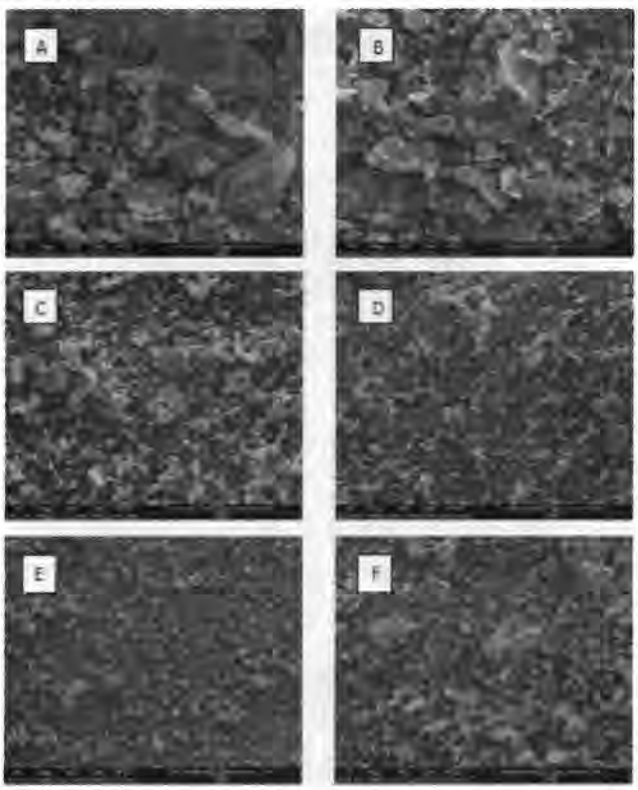

Fig 3: SEM micrographs of mechanically alloyed powder for (A) 10 hr (B) 20hr (C) 30 hr(D) 40hr(E) 50hr(F) 60hr

With continued milling, the cold welding and fracturing events continue to take place leading to microstructural refinement (Fig.-3 (c) and (d)). The combination of severe cold-work and possible heating from the kinetic energy of balls aids diffusion and as diffusion distances decrease continually by the finer mixing of constituents, solute elements dissolve, areas of solid solution grow in composite powders and metastable phases may precipitate [5]. Alloy formation (either stable or metastable phases) may occur due to the effect of these factors. With continued milling, the microstructure gets further refined. It is also noticed that after 50 hr of Mechanical alloying uniform particle size distribution is observed (Fig 3(e)). With the additional mechanical alloying up to 60 hrs agglomeration of fine particles is taking place which is clearly seen from (Fig.3 (f)). It is expected that the brittle particles get uniformly dispersed, if they are insoluble, in the ductile matrix after such long hours of milling [6]. It is difficult to differentiate between 111 peaks from mechanically alloyed powder with those from 409L Ferritic stainless steels which contain 11-12%Cr. It is, however, likely that after 50 hours of mechanical alloying Ferritic stainless steel powders are obtained from the initial elemental powders.

Conclusions:

- From the XRD analysis it is revealed that as the milling time increases the peak broadening is taking place owing to the decrease in crystallite size, accumulation of strains and defects in the course of the ball milling.
- The result of the study show that Fe-10%Cr-0.3%Y_2O_3 Nano-crystalline powders can be produced by mechanically alloying of elemental powder Fe and Cr at times longer than 50 hrs.
- Increasing MA time to 50 hours led to a dramatic decrease in the particle size of Fe-10%Cr- 0.3%Y_2O_3 and Crystallite size in the range of 7-10 nm. Further milling leads to increased particle agglomeration.

Referance:

1. Shigeharu Ukai, Masayuki Fujiwara, "Perspective of ODS alloys application in nuclear environments", journal of nuclear materials, Vol. 307-311, Part 1, , PP. 749-757(2002)
2. A. Hishinuma, A. Kohyama, R.L. Klueh, D.S. Gelles, W.Dietz, K. Ehrlich,"Low-activation ferritic and martensitic steels for fusion application" ,Journal of Nuclear Materials, Vol. 233-237, Part 1,PP 138-147 (1996)
3. R.L. Klueh, D.R. Harries," High-chromium ferritic and martensitic steels for nuclear applications", ASTM Stockno.: MONO 3 (2001).
4. B.D.Cullity, Elements of X-Ray Differaction, Addison-Wesley Publishing Company (1956).
5. Sundaresan, R. and Froes, F. H., "Mechanical alloying", J.Metals,39,pp 22-27(1987).
6. C. Suryanarayana, Mechanical alloying and milling,Marcel and Dekker Publication,(2004)

BORIDING OF Fe AND Fe-2Cu-2Ni-0.2C (wt %) ALLOY PRODUCED BY POWDER METALLURGY ROUTE

Tikam Singh and A. N. Tiwari

Department Of Metallurgical Engineering and Materials science
Indian Institute of Technology Bombay, Powai, Mumbai, India

Abstract

Boriding is a thermo-chemical process involving the diffusion of boron into the surface of selected metal alloys resulting in a reaction zone of metal borides. This generates very high surface hardness which cannot be achieved by other thermo-chemical process like carburizing and nitriding. Boriding is highly effective in enhancing wear resistance of components for tribological application.

Boriding has been applied to a variety of wrought steel parts but boriding of powder metallurgy products has received less attention. This research investigates boriding of (i) Directly hot forged P/M Fe and (ii) Sintered Fe-2Cu-2Ni-0.2C (wt%) alloy. Boriding has been conducted for 5 hours at 950°C using liquid and pack boriding process. Two compositions of liquid boriding baths were used containing Borax, Boric acid, Ferro-silicon, Al, B_4C, NaF and KF. Pack boriding was also conducted using two different composition containing Borax, B_4C, SiC, KBF_4.

It was found that the boriding layer consisting of Fe_2B monophase layer only. The thickness of the boriding layer is the range of 104 to 180μm depending on the boriding sources. The Vickers microhardness of boriding layers varies from 1073 to 1288 kg/mm^2. The minimum improvement in the micro-hardness has been found to be 5 to 12 times respectively for the sintered Fe alloy and the preform hot forged Fe. Abrasive wear has been studied under dry sliding conditions against 400 grit using pin-on-disc type tribometer. Boriding has been found to increase wear resistance significantly in spite of the porosity in the P/M steels.

1. INTRODUCTION

Boriding is a thermochemical treatment which can develop hardness in the range of 1200 – 2000 VHN as compared to hardness in the range of 600 – 1000 VHN for carburising and 700 – 850 VHN for nitriding of plain carbon steels. Boron atoms can diffuse into ferrous alloys due to their relatively small size and very mobile nature. They can dissolve in iron interstitially, but can react with it to form FeB and Fe_2B compounds. Depending on the boron potential of medium and chemical composition of base materials, single or duplex layer may be formed [1]. Amongst different types of wear, abrasive wear in dry condition is the severest mode. Hence, in this study P/M steels having different porosity levels have been subjected to dry abrasive wear against SiC paper. This was done to illustrate that the boriding is an effective treatment to enhance wear resistance in P/M steels in spite of their inherent porosity.

In the present investigation, P/M Fe preform forged and P/M Fe-2Cu-2Ni-0.2C sintered samples were borided using two techniques viz. Liquid Boriding and Pack Boriding. A comparative study of the depth of boriding, microhardness and abrasive wear rate of the samples was carried out. The main aim of this study was to find a suitable boriding composition which is easy to clean and develops thick borided region possessing good hardness and abrasive wear resistance.

2. EXPERIMENTAL PROCEDURE

For conducting boriding experiments, two types of P/M materials were used viz. preform hot forged Fe (produced from sponge iron powder) and sintered Fe-2Cu-2Ni-0.2C (wt%) alloy. The source of powders and their particle size are given in TABLE 1. The preform hot forged Fe was prepared at I.I.T. Roorkee using the route given in the Fig. 1. The sintered samples of Fe-2Cu-2Ni-0.2C were manufactured at Sintbush India Pvt. Ltd. Mumbai. The details of sintering route are given in Fig 2. The properties of P/M materials in as received condition are shown in TABLE 2.

Two types of boriding treatment have been conducted, liquid and pack boriding using four different types of boriding compositions enlisted in TABLE 3. Pack boriding formulations incorporate boron sources

TABLE 1: Powder specifications

Powder	Source (grade)	Size (μm)
Fe (Sponge iron powder)	Höganäs (SCI 100.26)	20 – 180
Fe (water atomized)	Höganäs (AHC 100.29)	45 – 150
Cu	P.P. Patel & Co., Solapur	37 – 100
Ni	Micrometals Technology Nashik (M-EF)	1.4
Graphite	Graphite India, Kolkata	45

TABLE 2: Properties of unborided samples

Type of P/M Sample	Hardness (Hv,50g) kg/mm^2	Density (g/cm^3)	Porosity (%)
Fe Preform Hot Forged	96	7.42	5.71
Fe-2Cu-2Ni-0.2C (wt%), Sintered	256	7.10	9.67

TABLE 3: Boriding compositions

Type of Boriding	Code of Boriding Media	Composition(wt%)								
		Borax	Boric Acid	B_4C	KBF_4	FeSi	Al	SiC	NaF	KF
Liquid	LB-1	46.67	16.25	-	-	35.0	-	-	2.28	-
	LB-2	84.0	-	5.0	-	-	10.0	-	-	1.0
Pack	PB-1	5.0	-	5.0	5.0	-	-	85.0	-	-
	PB-2	5.0	-	10.0	5.0	-	-	80.0	-	-

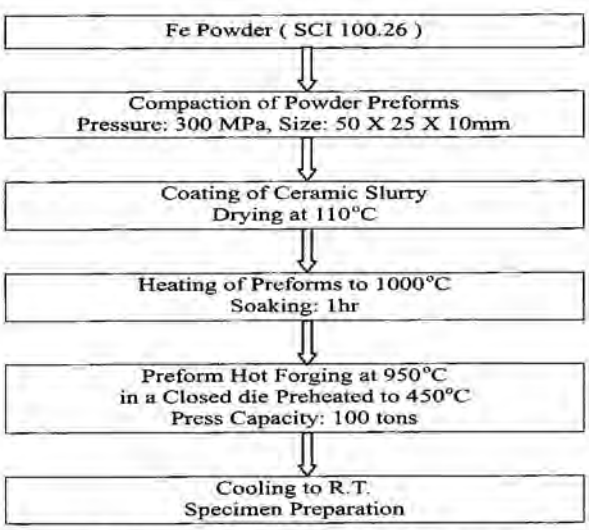

Fig. 1: Powder preform forging route

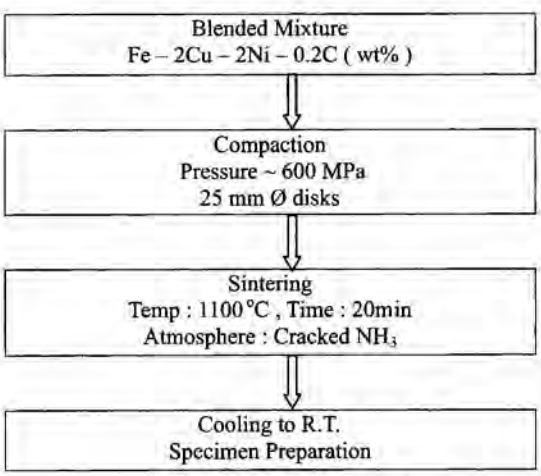

Fig. 2: Sintering route

(Borax, Boric acid and B_4C), dilutent (SiC) and activators (KBF_4, NaF, KF). Liquid boriding baths consist of boron sources (Borax, Boric acid and B_4C), reducers (Al. FeSi) and activators (KBF_4, NaF, KF). Boron sources are used for providing boron atoms for boriding treatment and activators are mainly used to accelerate the reaction, and increase the thickness of the boriding layers. Dilutents (i.e. SiC) do not take part in the reaction. However, SiC controls the boron chemical potential and prevents caking of the boriding agent [1].

Before boriding treatment, test specimens of size 15x8x7 mm^3 were polished up to 1200 grit SiC paper followed by cloth polishing using alumina slurry. For boriding treatment the samples were degreased and placed inside a stainless steel crucible containing boriding medium. The sealed crucible was introduced into electric muffle furnace and the treatment was carried out at 950°C for 5hr followed by air cooling. In the case of liquid boriding excess salts sticking to the samples were cleaned by immersing in boiling water. In pack boriding samples could be easily cleaned using a brush. Boriding samples were mounted in a cold setting compound, sectioned using Struers Accutom-2, metallographically polished and etched with 2% nital solution.

The thickness of boriding region was determined by optical microscope using OLYMPUS GX51. The XRD analysis was performed using PANalytical's X'Pert Pro Materials Research Diffractometer using Cu-K_α radiation. Vickers microhardness of the samples was measured at a load of 50g using Leco Microhardness tester LM300AT. Dry sliding abrasive wear was evaluated using pin-on-disc machine[2]. Silicon carbide (SiC) papers (400-500 grit) have been earlier used for conducting two-body abrasive wear testing of hard coating and borided steels [3-4]. Hence, in the present work 400 grit SiC paper (Carborundum Universal LTD. Chennai) has been used as counter abrasive. The test parameters are given in the TABLE 4. Minimum 3 tests were conducted to obtain average specific wear rate (WR). Specific wear rate (WR) was calculated using the equation:

$$WR = \frac{\Delta m}{SL}$$

where, Δm = change in mass (mg)
S = sliding distance (m)
L = normal load (N)

$$\text{Coefficient of friction } (\mu) = \frac{friction\ force}{normal\ force}$$

SEM images of worn surfaces of boriding samples were observed using Hitachi S-3400 N Scanning electron microscope.

3. RESULTS and DISCUSSION

Optical microstructures of the cross sections of the borided Fe and Fe-2Cu-2Ni-0.2C are given in the Fig. 3 and 4 respectively. Borided layers have been demarcated by 'B' and it can be clearly seen that the layer consist of single phase and the interfaces with the substrate have saw-tooth morphology. However, in the case of preform forged Fe saw-tooth morphology is vary pronounced while in the case of sintered Fe-2Cu-Ni-0.2C alloy saw-tooth morphology has been suppressed. The average thicknesses of borided layers are given in the TABLE 5. Under the same conditions, sintered Fe-2Cu-2Ni-0.2C alloy exhibits lower thickness than the preform forged Fe. The suppression of saw-tooth morphology and decrease in thickness may be attributed to the presence of the alloying elements in the sintered samples [5-7]. Optical micrographs (Fig. 3 and 4) also show the presence of porosity in the P/M samples. However, porosity is less and pore size is small in preform forged Fe as compared to the sintered Fe alloy. This can be explained due to the effective densification by the preform forging route. Borided zone also shows porosity but it is much less as compared to the underlying substrate.

In order to identify the composition of the borided layer XRD technique was used and results are shown in Fig. 5 and 6. All diffraction peaks could be assigned to Fe_2B (tetragonal phase) using JCPDS files. In general, boriding of steels leads to the formation FeB (16% boron) and Fe_2B (9% boron). It has been reported that Fe_2B layer is more desirable than FeB because of lower brittleness and less tendency for cracking. The tendency for cracking in FeB is higher than in Fe_2B because of thermal expansion coefficient of FeB is about 3 times greater than that of Fe_2B($\alpha_{FeB} = 23 \times 10^{-6}$/°C, $\alpha_{Fe2B} = 7.85 \times 10^{-6}$/°C)[8-9]. In the present study all the boriding media have given only Fe_2B mono phase layer due to the lower boriding potential.

TABLE 4: Abrasive wear test parameters

Parameter/Condition	Value
Configuration of the test	Pin-on-disc
Counter surface	SiC Abrasive paper (400 grit)
Normal Load	16.806 N
Sliding Speed	0.6 m/s
Sliding Distance	2.6m
Temperature	22-26°C
Relative Humidity	50-55%

Vickers microhardness of unborided and borided specimens of P/M Fe and P/M Fe-2Cu-2Ni-0.2C are given in TABLE 6 and 7 respectively. Unborided sintered Fe alloy shows the microhardness of 256 as compare to 96(kg/mm^2) in preform forged Fe due to the presence of alloying elements Cu, Ni & C. It can be noticed that the improvement in the microhardness due to boriding treatment is about 12 and 5 times respectively for the preform forged Fe and sintered Fe alloy. From Fig. 7 it is obvious that boriding medium PB-2 gives highest hardness compared to all other compositions.

Steady state values of abrasive specific wear rate (WR) and friction co-efficient (μ) for the preform forged Fe and sintered Fe-2Cu-2Ni-0.2C alloy in both unborided and borided conditions are given in TABLE 6 and 7 respectively. These tables also present wear resistance [$(WR)^{-1}$] and relative wear resistance (RWR). RWR is defined as WR of the substrate material divided by WR of the borided substrate. RWR gives a direct comparison in the abrasive wear performance of the borided layer with respect to the substrate steel. It can be seen that the boriding improves abrasive wear resistance at least 3.5 times in the preform forged Fe while 1.4 times in the Fe-2Cu-2Ni-0.2C sintered alloy. Unborided samples shows high friction due to the presence of porosity, because pores interlock with a SiC abrasive grain during sliding but after boriding, friction drops down significantly because of very high hardness and low porosity in the borided layer[10]. Fig. 8 shows the correlation between abrasive wear resistance [$(WR)^{-1}$] and microhardness. The data points have been fitted into straight lines by linear regression analysis. Fig. 8 also shows that the wear resistance of forged and borided Fe is higher than that of sintered and borided Fe alloy for a given microhardness value. This means that the dependence of wear resistance on porosity is stronger than that of microhardness on porosity.

SEM images of the worn surfaces of unborided and borided P/M steels are illustrated in Fig. 9 to 11. A close examination of wear tracks in these figures reveals the following:

I. The worn surfaces are essentially composed of microgrooves running along the sliding direction.

   The presence of microchips can also be seen. This implies that dominant the mechanism of abrasive wear is micro-cutting.

ii. The surface damage in the unborided samples (Fig.9) is more severe as compared to theborided samples(Fig. 9 and 10).

iii. Worn surfaces show pitting due to the porosity in the borided layer.

TABLE 5: Effect of P/M ferrous substrates on boriding process

Boriding Composition Code	Thickness (t) of Borided Layer		% decrease in thickness $\Delta t/t_f * 100$
	Preformed Hot Forged Fe (t_f, μm)	Sintered Fe-2Cu-2Ni-0.2C (t_s, μm)	
LB – 1	163	109	33.1
LB – 2	165	163	1.2
PB – 1	171	104	39.2
PB – 2	174	134	23.0

TABLE 6: Microhardness and abrasive wear rate of unborided and borided Fe (Preform forged)

Boriding Code	Vickers microhardness of the Borided Layer (kg/mm^2)	Abrasive wear Rate (μg/m N)	$(WR)^{-1}$ [m N/g * 10^3]	Relative Wear Resistance (RWR)	μ (friction coefficient)
Unborided	96	122.18	8.18	1.00	1.01
LB-1	1210	33.81	29.57	3.61	0.79
LB-2	1251	33.21	30.11	3.68	0.76
PB-1	1163	35.13	28.46	3.48	0.76
PB-2	1287	29.37	34.05	4.16	0.67

TABLE 7: Microhardness and abrasive wear rate of unborided and borided Fe-2Cu-2Ni-0.2C (sintered).

Boriding Code	Vickers mirohardness of the Borided Layer (kg/mm^2)	Abrasive wear Rate (μg/m N)	$(WR)^{-1}$ [m N/g * 10^3]	Relative Wear Resistance (RWR)	μ (friction coefficient)
Unborided	256	113.90	8.77	1.00	1.05
LB-1	1212	67.18	14.88	1.70	0.82
LB-2	1241	63.18	15.82	1.80	0.74
PB-1	1073	79.13	12.63	1.44	0.80
PB-2	1266	59.77	16.73	1.90	0.82

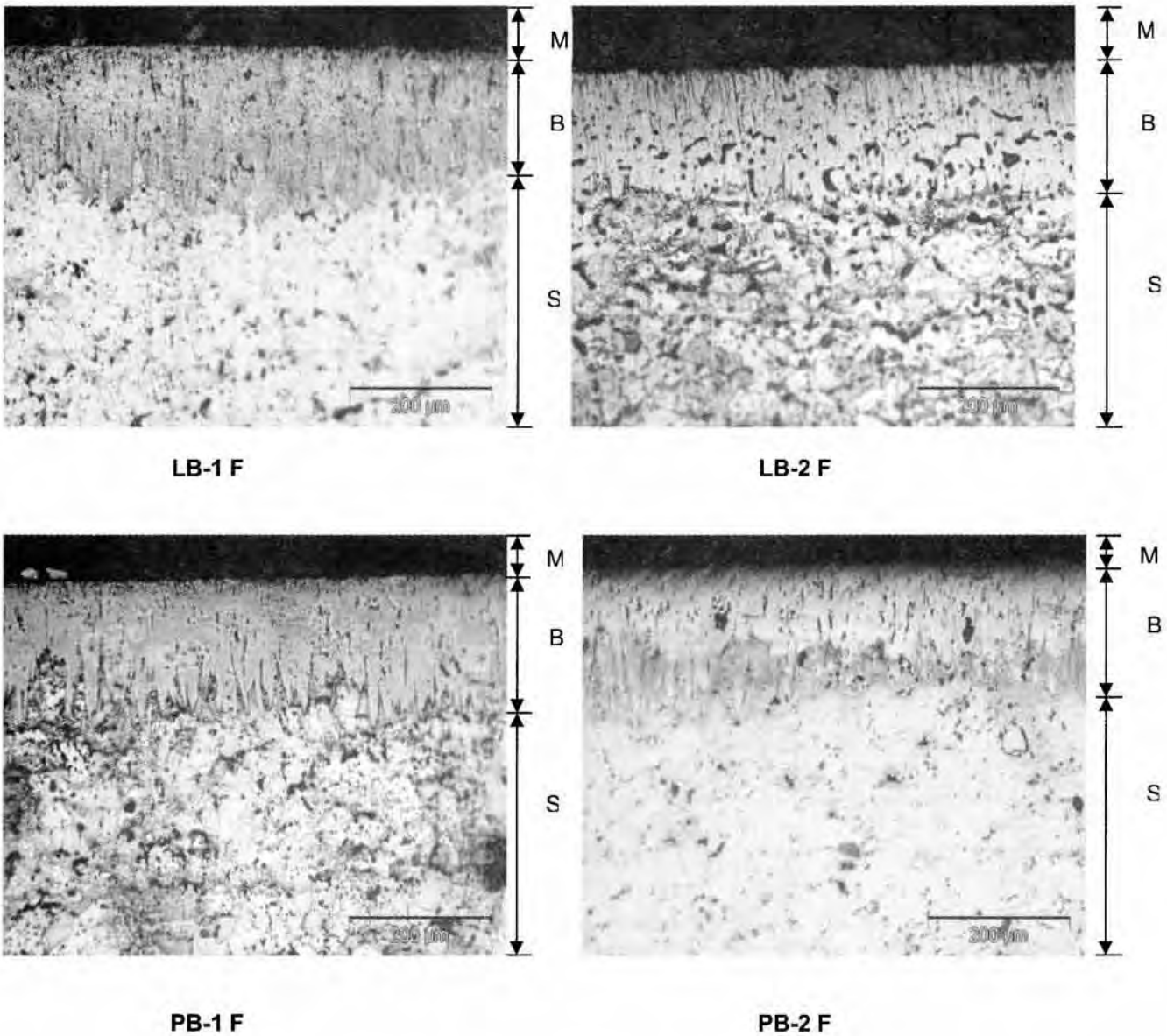

Fig. 3: Microstructure of borided Fe (preform forged).

[M = Mounting; B = Boriding layer; S = Substrate]

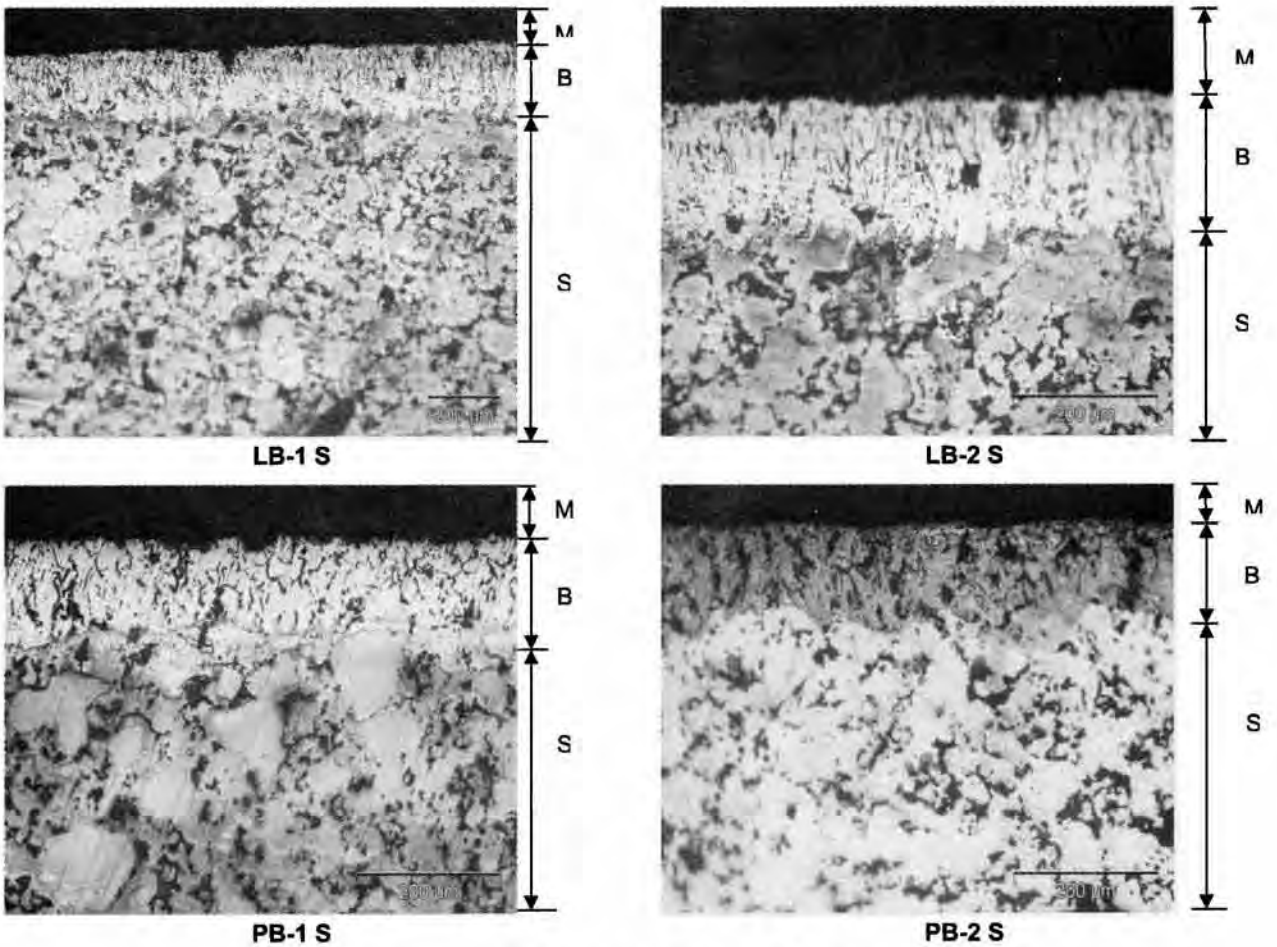

Fig. 4: Microstructure of borided Fe-2Cu-2Ni-0.2C sintered alloy.

[M = Mounting; B = Boriding layer; S = Substrate]

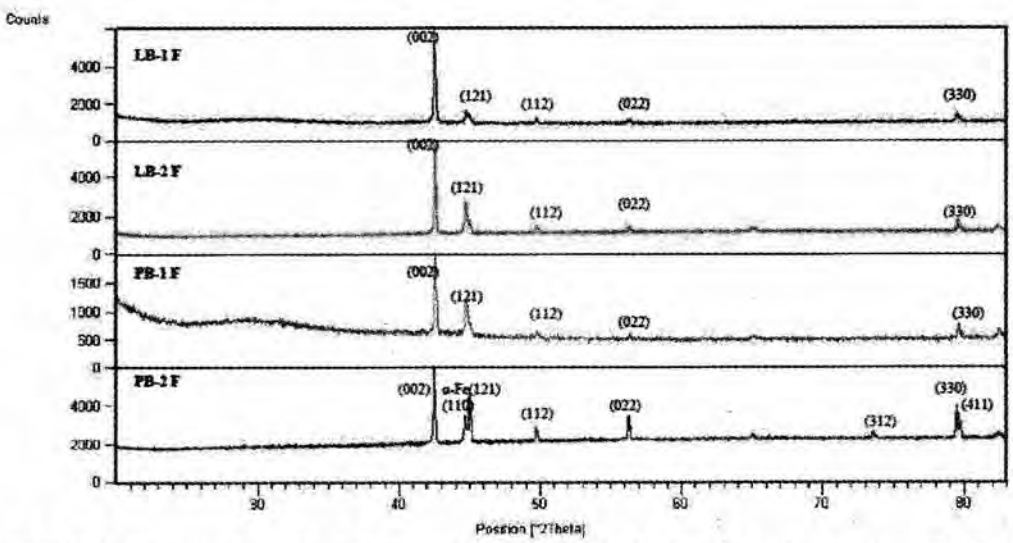

Fig. 5: XRD patterns of borided Fe (preform forged). (indexed peaks are from Fe_2B phase)

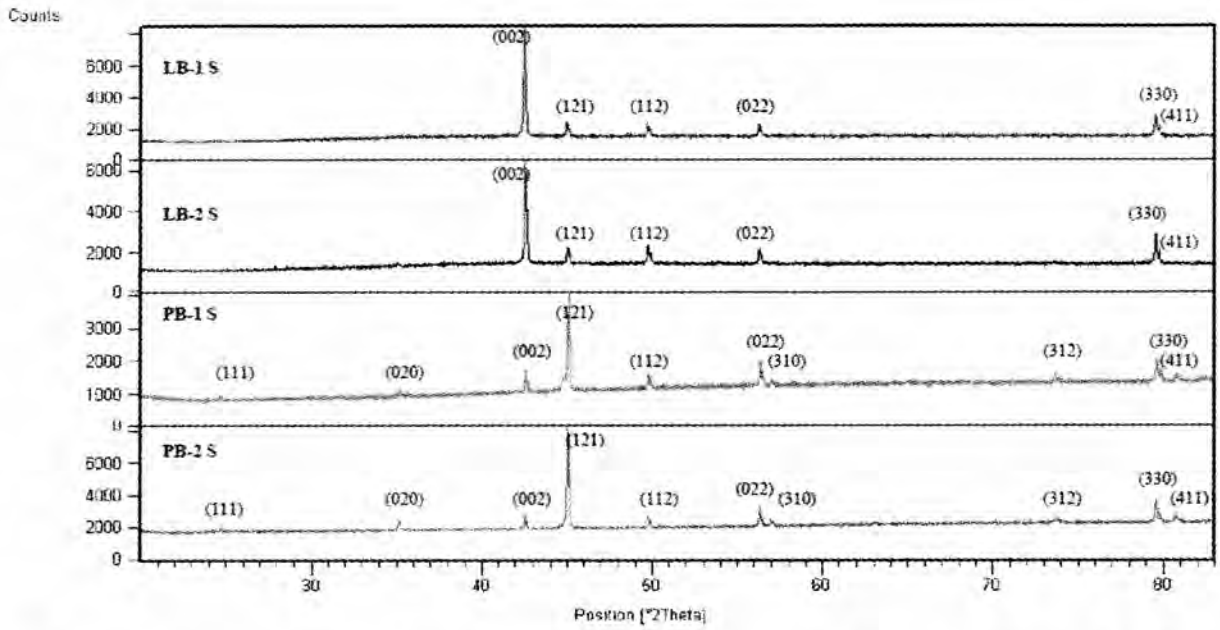

Fig. 6: XRD patterns of borided Fe-2Cu-2Ni-0.2C sintered alloy. (indexed peaks are from Fe_2B phase)

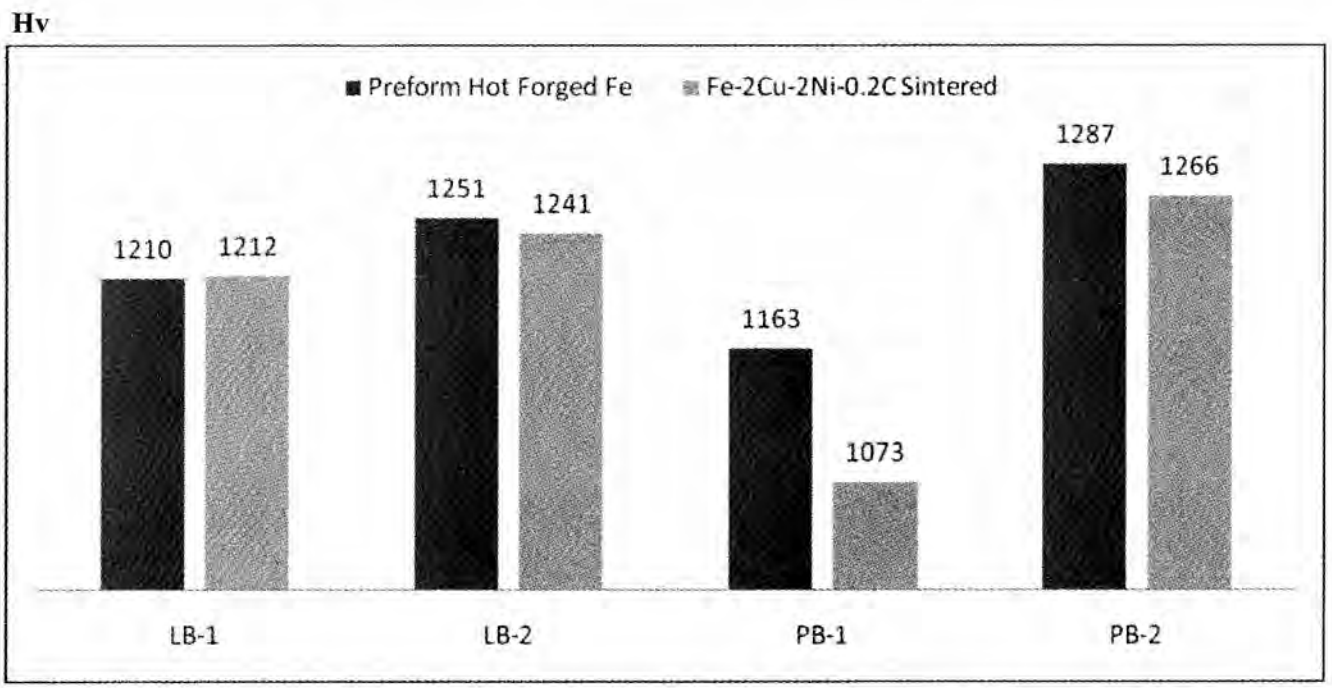

Fig.7: Comparison between Vicker microhardness of borided samples of Fe preform forged and sintered Fe-2Cu-2Ni-0.2C.

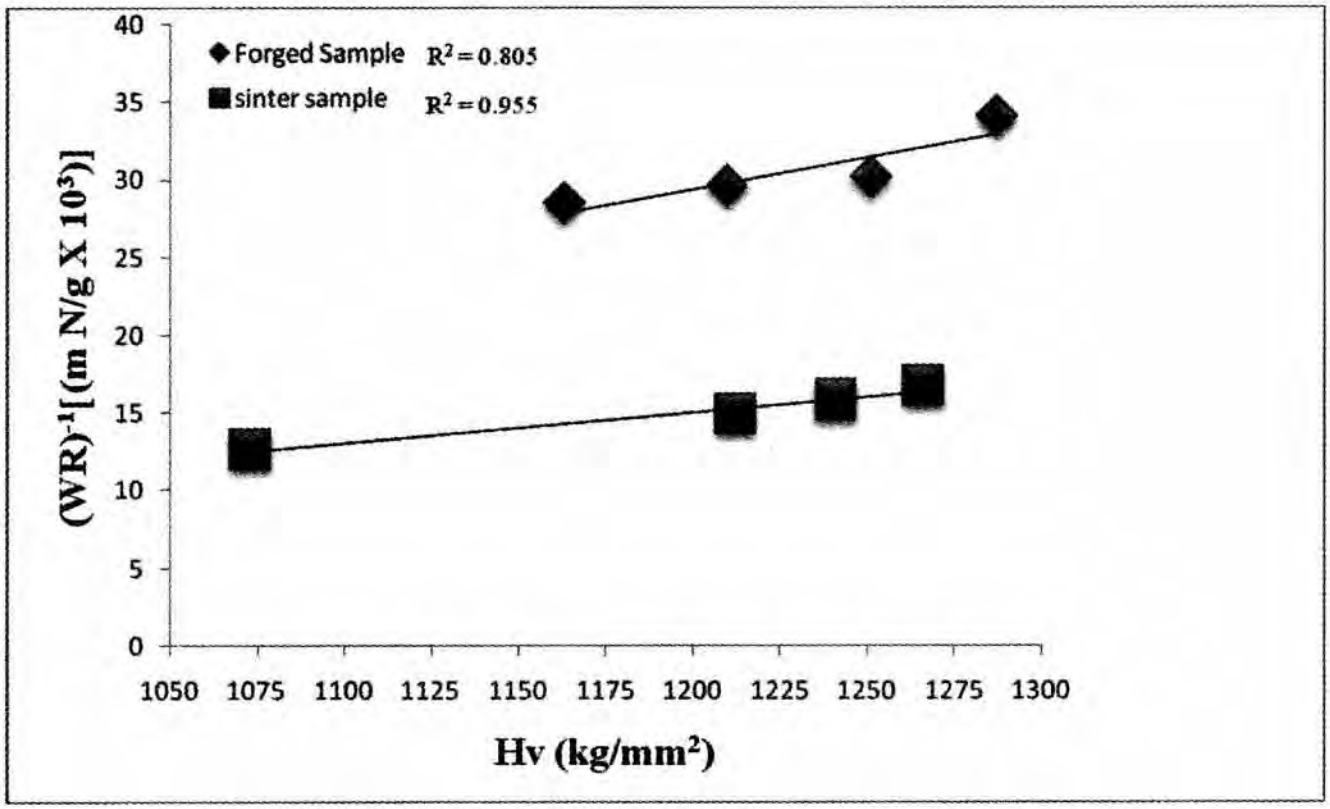

Fig. 8: Relation between inverse wear rate and microhardness of borided samples.

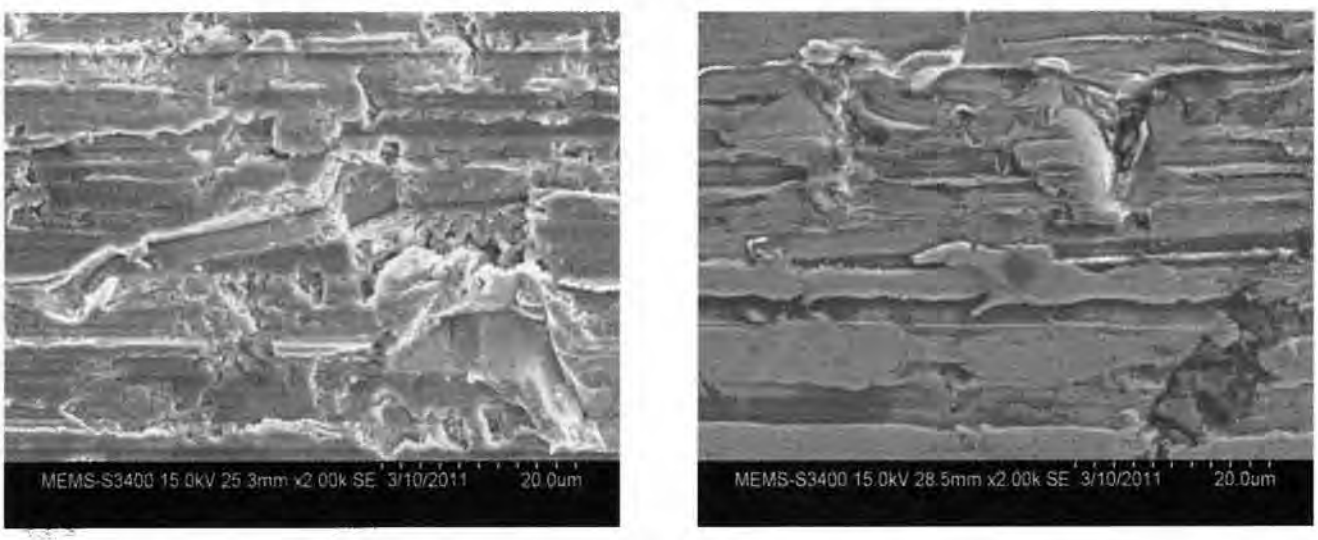

Fig.9: SEM images of worn surfaces of unborided P/M Fe perform forged & Fe-2Cu-2Ni-0.2C sintered alloy.

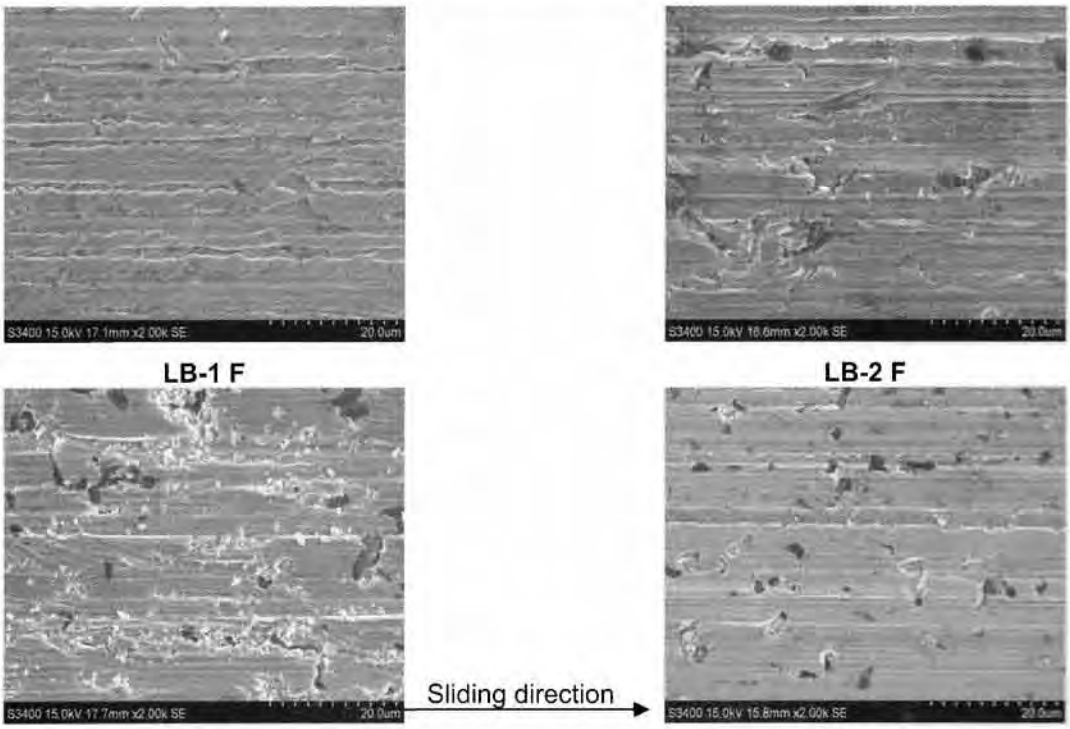

Fig. 10: SEM images of worn surfaces of borided Fe (preform forged).

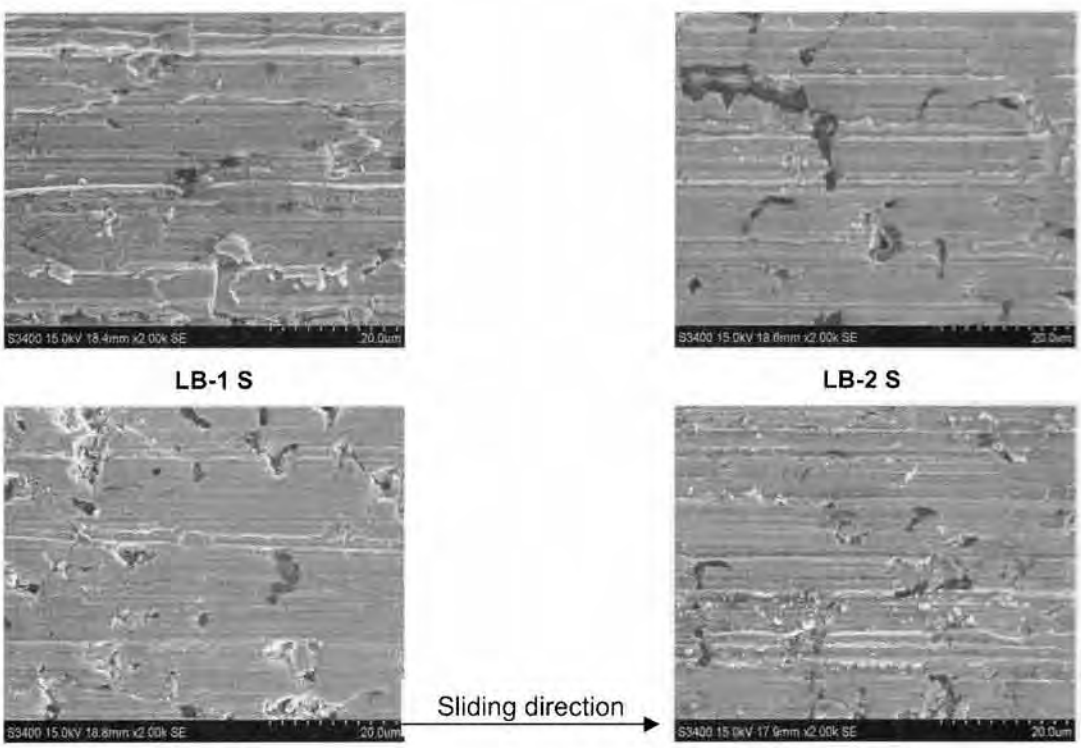

Fig. 11: SEM images of worn surfaces of borided Fe-2Cu-2Ni-0.2C sintered alloy.

4. CONCLUSIONS

Two types of liquid (LB-1 & LB-2) and pack (PB-1 & PB-2) boriding compositions have been successfully used at 950°C for 5 hr for boriding P/M Fe steels. The following conclusions can be drawn:

1. Boriding composition containing B_4C are more effective in increasing the depth of boriding.
2. As compared to the preform forged Fe, sintered Fe-2Cu-2Ni-0.2C shows lower boriding depth under similar boriding conditions. This may be due to the presence of alloying elements.
3. The borided layer consists of only Fe_2B single phase, which is a desirable feature.
4. Vickers microhardness of the borided region is found to be in the range of 1073-1287 kg/mm^2. Boriding in PB-2 has resulted in the highest hardness of 1287 and 1267 kg/mm^2 for preform forged Fe and sintered steel respectively.
5. The abrasive wear resistance can be improved at least 3.5 times in the preform forged Fe P/M material while 1.4 times in the Fe-2Cu-2Ni-0.2C sintered alloy.
6. Abrasive wear resistance has been found to be linearly proportional to Vickers microhardness.
7. Considering ease of post cleaning, microhardness and wear resistance, PB-2 composition gives the best performance.

Acknowledgement

Authors are grateful to Prof. Kamalesh Chandra of IIT Roorkee, Mr. P. N. S. Sivan managing Director of Sintbush India Pvt. Ltd. Mumbai and Dr. Murli Gopal Krishnamoorty, Novoken Innovations Mumbai for providing P/M ferrous samples. Thanks are also due to Ms. Neelam Bhoir for assistance in microscopy.

5. REFERENCES

1. A. K. Sinha, Boriding(Boronizing),Heat Treatment, ASM Handbook, 4, ASM International, Materials Park, Ohio, USA, p. 437 (1991).
2. ASTM G 99-05, Standard Test Method for Wear Testing with a Pin-on-Disk Apparatus (2010).
3. H. J. Kim, S. Grossi, Y. G. Kweon, "Wear Performance of Metamorphic Alloy Coatings", Wear, Vol. 232, pp 51-60 (1999).
4. M. Ulutan, M. M. Yildirim, O. N. Celik, S. Buytoz, "Tribological Properties of Borided AISI 4140 Steel with Powder Pack-Boriding Method", Tribol Lett, Vol. 38, pp 231-239 (2010).
5. L. S. Lyakhovich, L. G. Voroshnin, G. G. Panich, "Boriding of steels in Fused Media", Metallovedenie i Termicheskaya Obrabotka Metallov, Vol. 5, pp. 74-78 (1969).
6. S. C. Singhal, "A Hard Diffusion Boride Coating for Ferrous Materials", Thin Solid Films, Vol. 45, pp 321-329 (1977).
7. Z. –S. Jiang, L. –X. Zhang, L. –G. LI, X. –R. PEI, T. –F. LI, "Structure of Boride Layers and the Transition Zone Produced by Boronization", J. Heat Treating, Vol. 2, pp 337-343 (1982).
8. Vipin Jain, G. Sundararajan, "Influence of the Pack Thickness of the Boronizing Mixture on the Boriding of Steel", Surface and Coatings Technology, Vol. 149, pp 21-26 (2002).
9. T. W. Spence, M. M. Makhlouf, "Characterization of the Operative Mechanism in Potassium Fluoborate Activated Pack Boriding of Steels", J. of Materials Processing Technology, Vol. 168, pp 127-136 (2005).
10. X. Dong, J. Hu, Z. Huang, H. Wang, R. Gao, Z. Guo, " Microstructure and Properties of Boronizing Layer of Fe-based Powder Metallurgy Compacts Prepared by Boronizing and Sintering Simultaneously", Science of Sintering, Vol. 41, pp 199-207 (2009).

ALUMINA DISPERSION - STRENGTHENED COPPER - NICKEL MATRIX NANOCOMPOSITES BY HIGH- ENERGY MILLING

Bharati Rehani, P.B. Joshi, Dharti Patel and Swati Desai

Metallurgical and Materials Engineering Dept., Faculty of Technology and Engineering,
M.S. University of Baroda, Vadodara, India

Abstract:

A study was undertaken on synthesis and characterization of high- energy milled alumina dispersed copper-nickel alloy matrix nanocomposite materials. The system selected during this investigation was 67wt.% Cu- 30wt.% Ni- 3wt.% Al_2O_3 with two different sizes of alumina particles viz. micron size and nano size, as the reinforcing phase. The powder mix was subjected to milling in a planetary ball mill for 9 h and was characterized by x-ray diffraction and scanning electron microscopy for their phase identification and morphological study. The nanocomposite powders were converted into bulk solids by press-sinter-repress route. The effect of variation in the morphology and particle size of alumina on the properties of the bulk solid compacts like microstructure; microhardness and compressive strength have been examined. The study revealed that the hardness and compressive strength of the nanocomposite material depends on the nature of the dispersoid.

Introduction:

Copper-nickel alloys are known for their excellent resistance to sea-water corrosion, good strength at moderately elevated temperature, good toughness at subzero temperature, good weldablility and good fabricability and hence these alloys are widely used for marine application, heat exchanger tubes, in water desalination plant, as well as resistance welding electrodes, etc [1,2]. Though these alloys have good mechanical properties, further improvements in the properties like strength and hardness can be achieved by dispersion strengthening of copper-nickel alloy matrix [3]. Fine and uniform dispersion of the dispersoid particles with smaller interparticle distances lead to greater degree of dispersion strengthening [4]. The dispersion strengthened composites developed using the oxide, carbide or nitride ultrafine / nano size particles as the reinforcing phase have been reported in the literature [5-11].

Mechanical alloying (MA) or high- energy milling has emerged as a proven top- down approach for synthesis of nanocomposite powders and the nanostructurted materials there from. The process was originally developed by J.S. Benjamin in late 1960s as a method for production of oxide dispersion strengthened superalloys [12].

It is a high- energy ball milling process comprising repeated fracturing and rewelding of composite powder particles. The process leads to an intimate dispersion of the second phase particles within the soft and ductile metal / alloy matrix. The crystallite size of the powder particles gets reduced to nanometric size (i.e. less than 100 nm) during MA.

In the present work an attempt has been made to synthesize alumina dispersion strengthened copper-nickel matrix nanocomposite materials by high- energy milling route followed by its conversion to bulk solids by classical powder metallurgy route. Two different forms of dispersoids were used, namely micron size and nano size alumina powder. The bulk solid compacts were finally evaluated for their density, microhardness, microstructure and behavior under compressive loading conditions. It has been found that the performance of the nanocomposite materials developed under this investigation strongly depends on the size of the dispersoid particles.

Experimental procedure:

The material composition selected for this investigation was 67wt% Cu- 30 wt% Ni- 3wt% Al_2O_3. The commercially available AR grade high purity copper (< 45 μm), nickel powder(< 10 μm) and the micron size alumina powder (< 100 μm) were used as the starting materials. Whereas, the alumina nanopowder was synthesized by microwave synthesis route using aluminum nitrate and urea as reactants having 1:2.5 as the relative mole ratio. The synthesis was carried out at a temperature of 500 °C and the resultant alumina powder was washed in distilled water and oven dried at 130 °C to remove any impurities.

The stoichiometric amount of alumina (micron or nano size) was mixed with copper and nickel powder and

blended in a cylindrical blender for 30 min at 130 rpm using a roller mill. The blended powders were then subjected to high- energy milling in a 250 ml capacity twin-bowl type planetary ball mill. The milling was carried out in toluene medium in a tungsten carbide lined stainless steel vial using tungsten carbide balls of 10 mm and 16 mm diameters as grinding media. The mill was operated at a speed of 300 rpm with ball to charge ratio of 15:1 for a total milling duration of 9 h and finally the powders were subjected to characterization using SEM (model JEOL JSM-5610 LV) and XRD (D8 Advance, Bruker AXS GMBH, Germany). The milled powders were annealed at a temperature of 400 °C for 60 min in vacuum at 10^{-2} torr.

The bulk solid compacts of 10mm dia. x 2mm height were prepared from the synthesized powders by subjecting them to compaction in single- action die compaction mode on a 100 ton capacity hydraulic press at 680 MPa pressure. The green compacts were sintered at 930 °C temperature for 1 h under a vacuum of 10^{-2} torr. The sintered compacts were repressed at a pressure of 1133 MPa using the same die set to produce high density compacts and were evaluated for their density, microstructure and microhardness (at 65 g load).

The compression of a short cylinder between anvils is a proven method to measure the flow stress in a material and its resistance to plastic deformation [13].The response of the copper-nickel-alumina bulk solid nanocomposites to plastic deformation was examined by subjecting a set of as- sintered compacts to compressive loading in the range of 500 to 6000 kg in steps of 500 kg each using the hydraulic press. The dimensions of the compacts after each loading were measured and based on this data the true stress versus true strain curve and log true stress versus log true strain curve were plotted.

Results and Discussion:

Figure 1 shows the SEM micrographs for the starting raw materials. Figure 1(a) shows the SEM micrograph for elemental copper powder having the dendritic or fern-like appearance. The SEM micrograph for nickel powder shown in Fig. 1(b) displays more or less rounded and spongy morphology of the powder particles with relatively finer size. Figure 1(c) and 1(d) show the SEM micrographs for micron size and nano size alumina powders. The micron size alumina powder is having flaky shape with average particle size of the order of ~100 μm whereas the nanosize alumina powder is much finer in size and shows high degree of tendency to agglomeration.

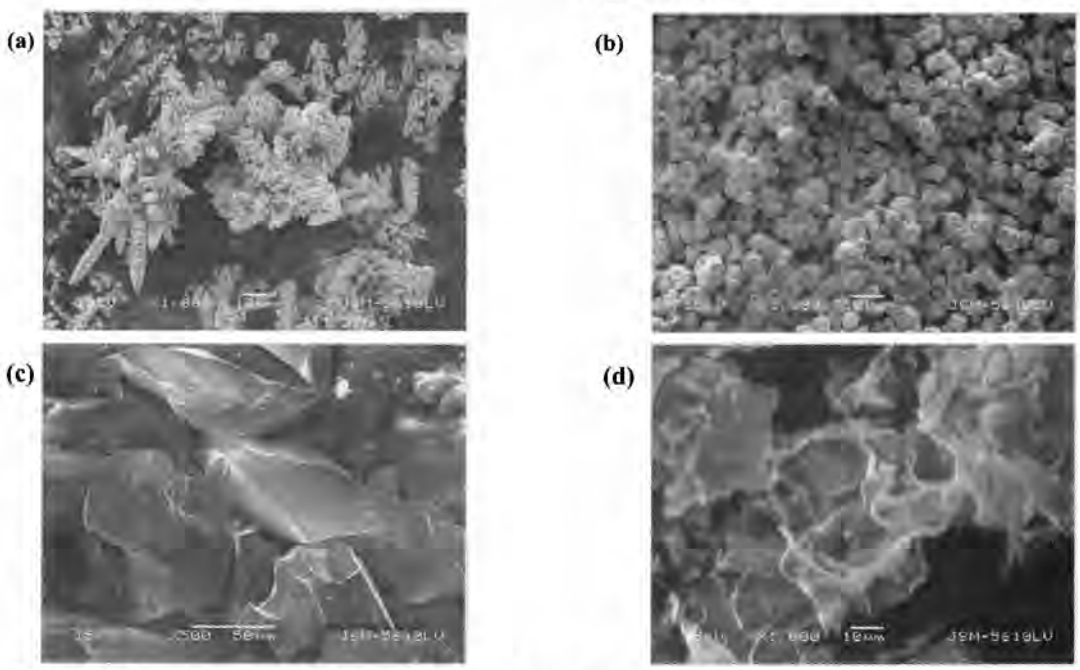

Fig. 1 SEM micrographs for the starting raw materials viz. (a) copper powder, (b) nickel powder, (c) micron size alumina powder and (d) nano size alumina powder

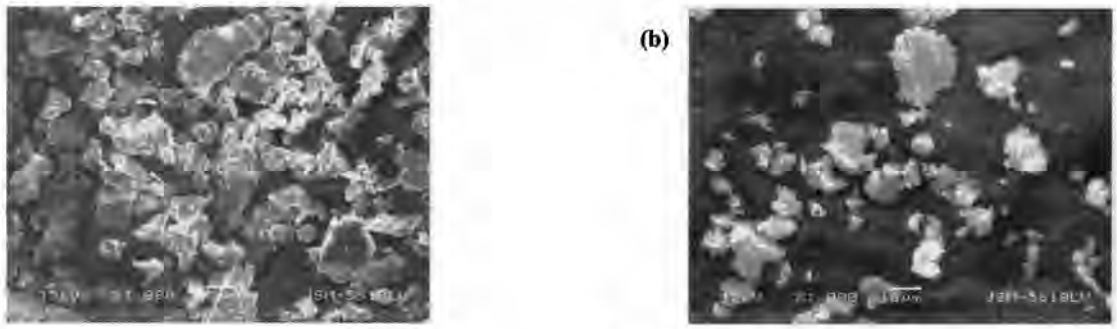

Fig. 2 SEM micrograph of high- energy milled (a) 67wt% Cu-30wt% Ni-3wt% Al_2O_3 (micron size) powder and, (b) 67wt% Cu-30wt% Ni-3wt% Al_2O_3 (nano size) powder

The corresponding SEM micrographs for high-energy milled 67wt% Cu - 30wt% Ni - 3wt% Al_2O_3 (micron size) powder and high-energy milled 67wt% Cu - 30wt% Ni - 3wt% Al_2O_3 (nano size) powder samples are shown in Fig. 2(a) and 2(b). A significant reduction in particle size is observed in both the cases.

Figure 3 shows the XRD profiles for 67wt% Cu- 30wt% Ni- 3wt% Al_2O_3 as-blended powder and 9 h milled powder samples. According to these profiles as a result of prolonged milling the diffraction peaks for Ni merge completely into the corresponding neighboring peaks for Cu and new peaks corresponding to the formation Cu-Ni alloy are seen in the XRD profile, thus confirming an alloying between copper and nickel due to high-energy milling. The minor peaks of α-Al_2O_3 which are noticeable in the XRD profile for as-blended powder are by and large disappearing now. This means that the alumina particles have uniformly dispersed within the Cu-Ni alloy matrix.

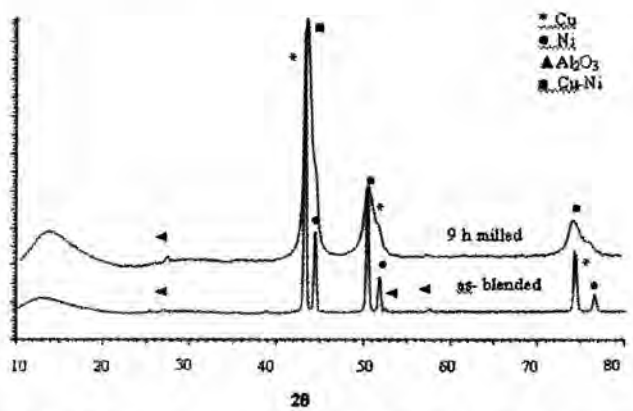

Fig. 3 XRD profiles for 67wt% Cu- 30wt% Ni- 3wt% Al_2O_3 powder in (a) as- blended and (b) 9 h milled condition

Table 1 gives the data on density, microhardness and behavior of the compacts under compressive loading for various compacts prepared from three different high-energy milled powders viz. *70wt% Cu- 30wt% Ni (without alumina), 67wt% Cu-30wt% Ni and 3wt% micron size Al_2O_3* and *67wt% Cu- 30wt% Ni- 3wt% nanosize Al_2O_3* powder. As per this table it is possible to attain a density level of 95% of theoretical density and above in all the three cases. As regards the microhardness it is apparent that dispersion of alumina leads to improvement in the microhardness of Cu-Ni alloy matrix. An increment in microhardness to the tune of 10% (compared to compacts prepared from high-energy milled Cu-Ni powders) is observed when micron size alumina is used as a dispersoid, whereas more than 20% rise in microhardness is obtained when nano size alumina powder is used as dispersoid. This clearly shows that the degree of dispersion strengthening attainable using nano size dispersoid particles is much higher as compared to that with micron size dispersoids. This can be attributed to the fact that the finer the size of the dispersoid and shorter the interparticle distance greater is the extent of dispersion strengthening [13].

TABLE 1 : Data on properties of Copper-Nickel-Alumina nanocomposites

Material description	Density g/cc (T.D. %)	Micro-hardness Hv (65g load)	Yield strength MPa	Strain hardening coefficient (n)	Strength Coefficient (K) MPa
70wt% Cu-30wt% Ni (without alumina)	8.7 (97.4)	171	110	0.39	293
70wt% Cu-30wt% Ni-3wt% Al_2O_3(micron size)	8.3 (96.0)	189	216	0.31	409
67wt% Cu-30wt% Ni-3wt% Al_2O_3 (nanosize)	8.2 (95.0)	211	520	0.14	619

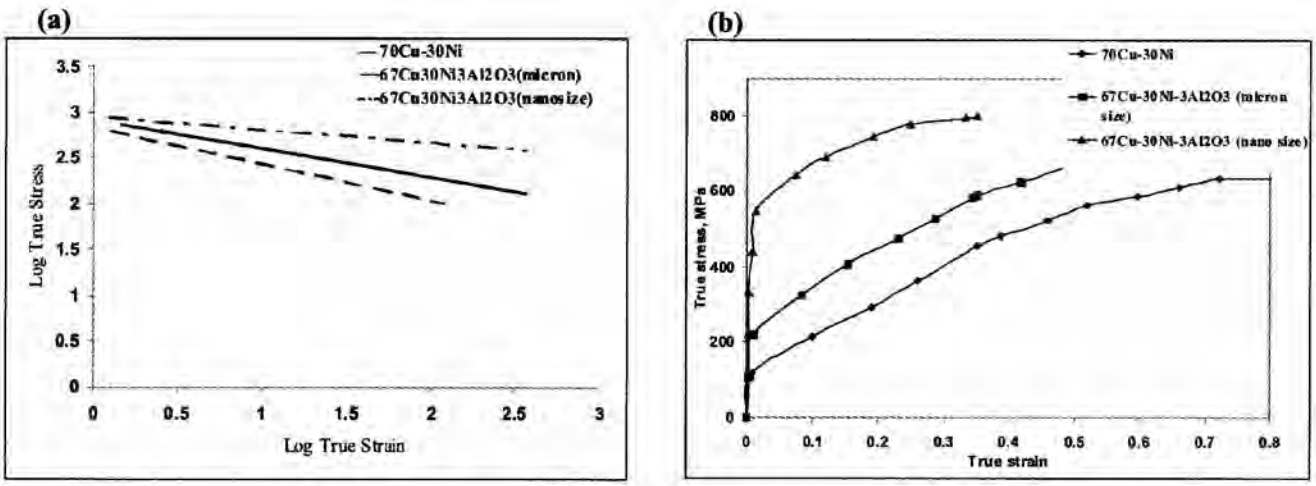

Figure 4: Multiple plots of (a) true stress versus true strain and (b) log true stress versus log true strain for Copper-Nickel-Alumina bulk solids

Data obtained from compression test is reported graphically in Fig.4 (a) and (b). From Fig. 4 (a) it is apparent that as we move from sintered compacts of high-energy milled 70wt% Cu-30wt% Ni powder to 67wt% Cu-30wt% Ni-3wt% Al_2O_3 (nano size) powder, the resistance of the materials to the plastic deformation increases. This is evident from the corresponding increase in the yield stress values (expressed as 0.2% proof stress) of the respective samples. The highest resistance to plastic deformation is offered by the compacts prepared from 67wt% Cu-30wt% Ni-3wt% Al_2O_3 (nano size) powder. The overall improvement in the yield strength due to dispersion of alumina nano particles in Cu-Ni matrix is of the order of 375% as compared to Cu-Ni matrix without any dispersoid.

Figure 4 (b) shows the multiple plots of log true stress versus log true strain for three different materials indicates that the strain hardening exponent gradually decreases from 0.39 to 0.14. Thus a significant amount of strain hardening is achieved by going for dispersion of nano size alumina particles in high- energy milled copper-nickel matrix. A similar trend is observed in the values for the strength co-efficient 'K' for three different materials. Dispersion strengthening with nano size alumina particles leads to more than 100%

(a) (b) (c)

Figures 5(a) to (c): Microstructures of Copper-Nickel-Alumina nanocomposite bulk solid compacts

increase in the strength co-efficient as compared to that for Cu-Ni matrix without any dispersoid.

Figures 5(a) to (c) show the microstructures of bulk solid compacts prepared from three different powders, viz. as-blended 67wt%Cu-30wt%Ni-3wt%Al_2O_3, high-energy milled 67wt%Cu-30wt%Ni-3wt%Al_2O_3 (micron size) and high-energy milled 67wt%Cu-30wt%Ni-3wt%Al_2O_3 (nano size) powders, respectively. A much finer and uniform dispersion of the alumina dispersoid particles in Cu-Ni matrix is observed for the compacts prepared from high-energy milled powders as shown in Fig.(b) and (c); irrespective of the fact that whether the initial alumina dispersoid particles used were of micron size or nano size.

Conclusion:

The study reveals that it is possible to strengthen the soft and ductile matrix of copper by (a) alloying of copper with nickel resulting in solid solution strengthening, (b) by the refinement of the grain size by high-energy milling for Cu-Ni alloy matrix resulting in strengthening due to grain refinement and (c) dispersion strengthening of Cu-Ni alloy matrix by fine and uniform dispersion of Al_2O_3 particles of either of micron size or nano size. Finally, it may be concluded that a remarkable improvement in the performance of material in terms of microstructure, microhardness and behaviour under compressive loading condition is attainable with the use of nanosize alumina particles as dispersoid.

References:

1. "Copper-Nickel Alloys - Properties and Applications", Copper-Development Association (CDA) Publication, www.copperinfo.co.uk, TN 30, pp1-40 (1982).

2. G.O.Carlson, "General Applications and Properties of Copper-Nickel Alloys', Product Data Bulletin 90/10 and 70/30 Cu-Ni , www.electralloy.com, pp 17-31, (2010)

3. X.M.Ding, N.Merk, B. Ilschner, "Mechnaical behaviour of metal-matrix composite deposits", Journal of Materials Science, Vol.33, No. 3, pp 803-809 (1998).

4. "Dispersion Strengthened Materials" in Metals Hand Book, Powder Metallurgy , Vol. 7, American Society for Metals, Metals Park, Ohio, pp 710-711 (1988).

5. D. L. Zhang, A. Mukhtar, C Kong and P Munroe , " Synthesis and Thermal Stability of Cu-(2.5-10)vol.%Al_2O_3 Nanocomposite Powders by High-Energy Mechanical Milling " , Journal of Physics: Conference Series, Vol.144, pp 1-6 (2009).

6. J. P. Stobrawa and Z. M. Rdzawski ,rsion Strengthened Nanocrystalline Copper", Journel of Achievements in Materials and Manufacturing Engineering, Vol.24, No. 2, pp 35-42 (2007).

7. Z. Andic, M Korac, M. Tasic, K.Raic and Z. Kamberovic, "The Synthesis of Ultrafine and Nanocomposite Powders Based on Copper, Silver and Alumina", Kovove Mater., Vol. 44, pp145–150 (2006).

8. V. Rajkovic , O. Eric, D. Bozic , M. Mitkov and E. Romhanji , "Characterization of Dispersion Strengthened Copper with 3wt%Al2O3 by Mechanical Alloying ", Science of Sintering,Vol.36, pp 205-211 (2004).

9. Zhan Yongzhong, Zhang Gouding, 'The effect of interfacial modifying on the mechanical and wear properties of SiCp/Cu composites', Materials Letters, Vol.57, pp 4583-4591 (2003).

10. M. Kambley and N. B. Dhokey, "Study of Ultrafine Alumina Reinforced Copper Composite", Transaction of Powder Metallurgy Association of India,Vol.34, pp 45-48 (2008).

11. Feisel, D.H., 'Development of a nickel-base material dispersion hardened by alumina for 1600 F to 2000 F service', A Report of Westinghouse Electric Corp Pittsburgh, PA, 06 Dec (1960).

12. J.S. Benjamin, Sci. Amer., Vol. 234, No. 5, pp 40-48 (1976).

13. R. Ebrahimi and N. Pardis , "Determination of Strain Hardening Exponent using Double Compression test ", Materials Science and Engineering ,Vol. 51, No.8, pp 56-60 (2009).

DEVLOPEMENT OF AN ALTERNATE AND ECONOMIC SINTERING PROCESS FOR MANUFACTURING OF CuCr CONTACT MATERIALS

S. K. Jena, T. Rakesh, S.Rayudu, J. Nemade, V.Singal*
AMPTC, CG Global R&D Centre, Crompton Greaves Ltd., Mumbai, India

Abstract

The quality of sintered product depends on the sintering temperature, hold time, sintering atmosphere, gas flow rate, gas circulation, etc. For increased productivity, total cycle time is one of the important parameters for the sintering process. Infiltration process (I/F) is a common method used for the manufacturing CuCr50 contact materials that produces contacts of nearly 100% theoretical density but commercially posses a lot of quality issues. The infiltration process is characterized with long sintering time and high machining losses. Thus Liquid Phase Sintering (LPS) process was developed for sintering CuCr50 contacts to replace the I/F process. The properties of the contact materials produced by LPS process at different sintering temperatures and times were investigated and compared with those produced by I/F process. It is observed that the desired properties of contact materials for VI application could be also being achieved through LPS process.

Introduction

In power delivery engineering, powder metallurgy (PM) based CuCr contacts have been widely accepted and used in the majority of commercial, medium-voltage, high-current vacuum circuit breakers (VCB) [1]. Copper-Chromium alloys are of great interest for electrical, electronic and automobile industrial applications because of their excellent electrical and thermal conductivity, high strength and ductility [2], and good anti-welding properties [3].

Copper is used in the manufacture of electrical cable, magnet wire, contact materials etc. due to its high electrical and thermal conductivity coupled with good corrosion resistance [4]. Chromium is added to contact materials to increase the make–break properties, strength properties of the contact materials [5,6]. Since chromium and copper don't form a solid solution at higher chromium contents, hence the most preferred mode for manufacture of the contact material is Powder Metallurgy based. A typical 50-50 Cu-Cr contact material would be made using the Infiltration Process.

The Infiltration (I/F) process is a two staged process. In the first stage a skeleton of chromium rich Cu-Cr loose compact is sintered. In the second stage the skeleton is infiltrated by copper by keeping it in contact with calculated amount of copper, both being at above the melting point of copper. The quality of sintered product depends on the sintering cycle, viz., peak sintering temperature, hold time at that temperature, and sintering conditions, viz., sintering atmosphere, gas flow rate, gas circulation, etc. Thus being a double step process the total cycle time is large and this results in decreased productivity.

On the other hand Liquid Phase Sintering (LPS) process is a single stage process and is used industrially for the manufacture of 70-30 Cu-Cr contact material. The cycle time for the LPS process is about half that of the I/F process. Furthermore, the higher distortion during the infiltration process does not allow its use for near-net shape manufacturing. An attempt was thus made to increase the productivity of contact making process by reducing the cycle time through changing the sintering process from I/F to LPS process. The properties of the CuCr contact tips made by the two processes are comparatively evaluated.

Experimental

The raw materials used for the experimentation were copper powder (–325 mesh size) and chromium powders (–325 mesh). Both the powders were produced by electrolytic technique.

For LPS process Cu and Cr powders were mixed in 50:50 proportions in a V-cone blender for about 15 minutes. The mix was then subjected to iso-static compaction to get a green density of 90% theoretical density (TD). The compacts were then vacuum sintered at temperature above melting point of copper i.e. in the liquid phase region.

For the I/F process the Cu and Cr were taken in the ratio of about 28:72 wt. %. This mixture was blended in V-cone blender. The powder after blending was subjected to compaction in order to form a skeleton of about 60% TD. The skeleton was then sintered in liquid phase region to obtain 70% TD. The sintered skeleton of the Cu–Cr material was then infiltrated in liquid phase region with calculated amount of Cu corresponding to

the remaining 30 %TD. The final composition of the contact results to 50:50 Cu-Cr.

The density of the sintered compacts was measured by Archimedes principle as per ASTM B311-93(2002)e1 and bulk hardness was measured by Rockwell hardness test as per ASTM E18- 07e1. The electrical conductivity of all the sintered samples was investigated by eddy current method in SIGMATEST D 2.068, FOERSTER instrument. The conductivity was measured in terms of Percent International Annealed Copper Standard (% IACS) according to ASTM E1004-02. Gas content in the sintered compacts was measured by inert gas fusion principle using Leco (model TC400) oxygen-nitrogen analyzer.

The microstructural analysis was done for 45 samples. The analysis included measurement of roundness, corner radius and size of small particles on the microstructure. The measurements were plotted in the Minitab software.

Results and Discussion

Figures 1, 2 and 3 show box plots comparison between hardness, electrical conductivity and density for both the I/F and the LPS processed samples respectively.

It can be seen from Fig.1 that the sintered CuCr contacts show higher hardness obtained by the LPS process compared to the I/F process. This may be due to higher dissolved chromium in copper for LPS process as compared to I/F process. For LPS process, the chromium is in contact with solid and liquid copper for a longer duration where considerable high solubilities of Cr in Cu for the Cu-Cr system are observed. Thus greater amount of Cr is dissolved in the Cu matrix giving higher hardness to LPS processed samples compared to I/F process.

In concurrent with the above discussion, the difference in conductivity values (Fig. 2) can be explained. The higher amount of dissolved Cr in Cu in LPS processed samples (more "impure" copper) is also responsible for their lower conductivity values when compared to I/F process.

Though the wetting characteristics of liquid Cu with Cr are almost similar, yet higher densities were observed in I/F sintered contacts compared to LPS process (Fig. 3). This may be due to the favorable pore spectrum observed in skeletons of I/F compared to green compact of LPS. The favorable pore spectrums arise from initial green densities maintained in green compacts of respective process. Due to the high porosities maintained in the skeleton of I/F process for impregnation of large volume of infiltrant leads to increased capillary action, thus increased driving force for initial stages of sintering leading to increased densification rates. Thus densification of I/F processed samples is more when compared to LPS process.

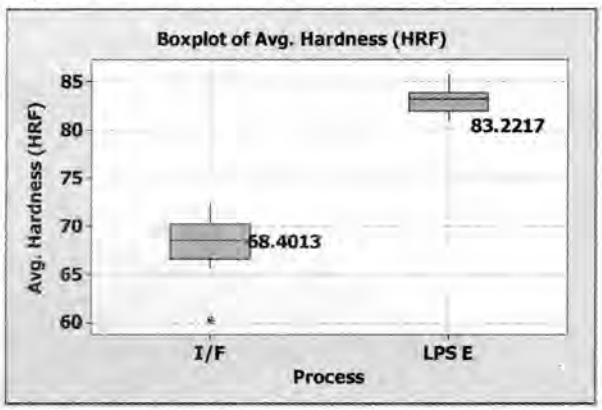

Fig. 1: Box plot comparison of hardness

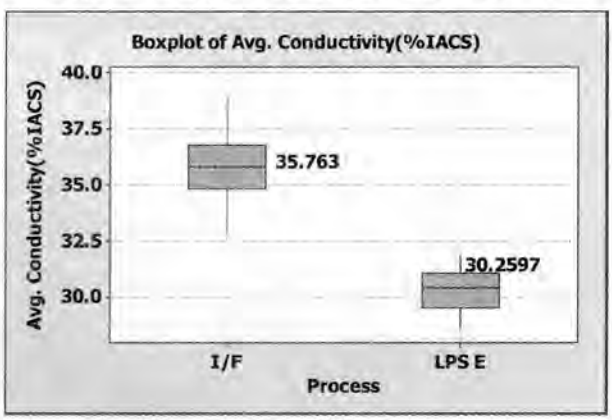

Fig. 2: Box plot comparison of electrical conductivity

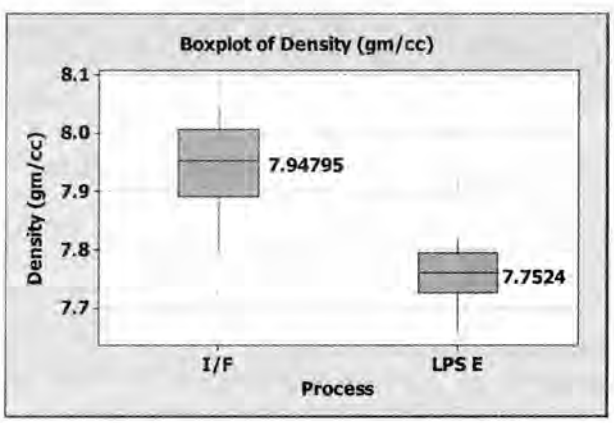

Fig 3: Box plot comparison of density

Microstructure

Similar looking microstructures were observed for infiltration and LPS contacts (Fig. 4). Homogeneous distribution of chromium in copper matrix is observed in both the cases. Finer chromium particle size is observed in LPS contact. The desired chromium particle shape for vacuum interrupter application is rounded chromium particle in Cu matrix is observed in both the process.

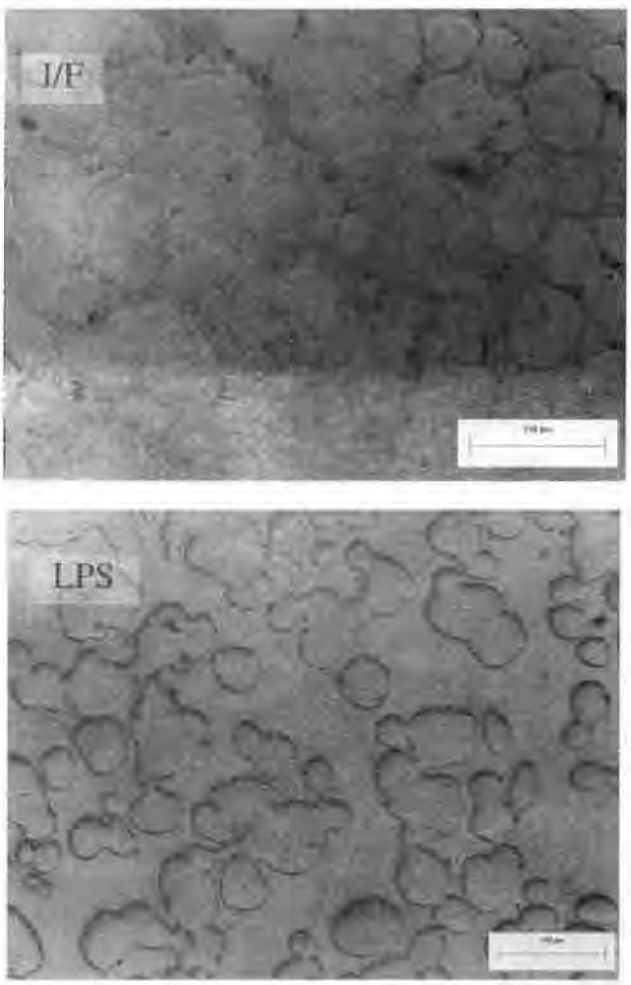

Fig 4: Comparison of microstructure of LPS and infiltration process at 200x

From the quantitative microstructural study of the I/F and LPS cycle, there is no much difference observed in case of roundness and sharp corners (Fig. 5 and Fig. 6). The roundness of infiltration process is 8.35 with large variability and LPS processes have 8.33 with very less variability.

From the microstructural box plot analysis of infiltration (I/F) and LPS process, the higher values are better for the contact materials. The roundness and sharp corners of I/F and LPS process was observed to be nearly similar. Variation is observed in case of small particles in sintered contacts of LPS and I/F process. It may be explained again by the higher dissolved Cr in Cu of sintered contacts in LPS process compared to I/F process.

The higher solubility of Cr in Cu for LPS process results in more amount of dissolved Cr in Cu in the liquid phase region. During solidification, the solubility of Cr in Cu drastically drops (Fig. 8) resulting in precipitation of more number of small Cr particles in Cu matrix. Thus higher numbers of small Cr particles were observed in the contacts made by LPS process when compared to I/F process.

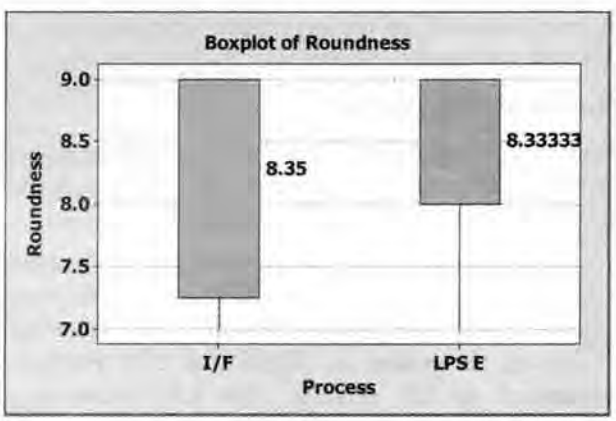

Fig 5: Box plot comparison of roundness of Cr particles

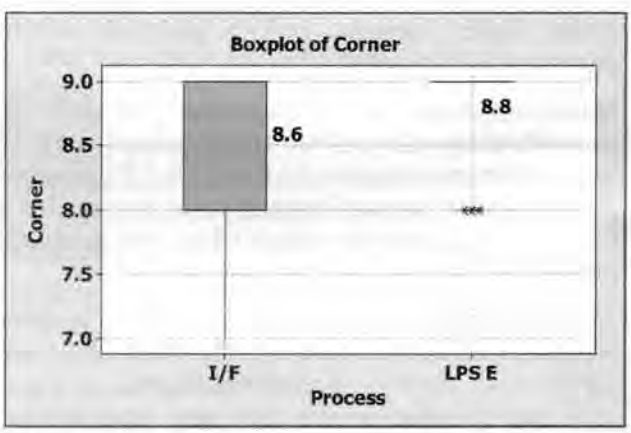

Fig 6: Box plot comparison of sharp corners observed on Cr particles in the microstructure

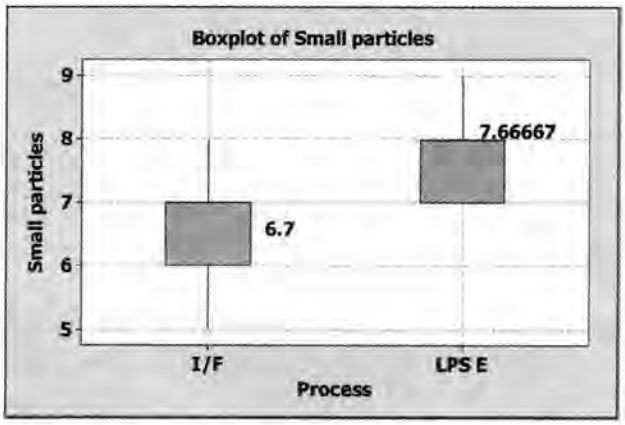

Fig 7: Box plot comparison of number of small Cr particles in the microstructure

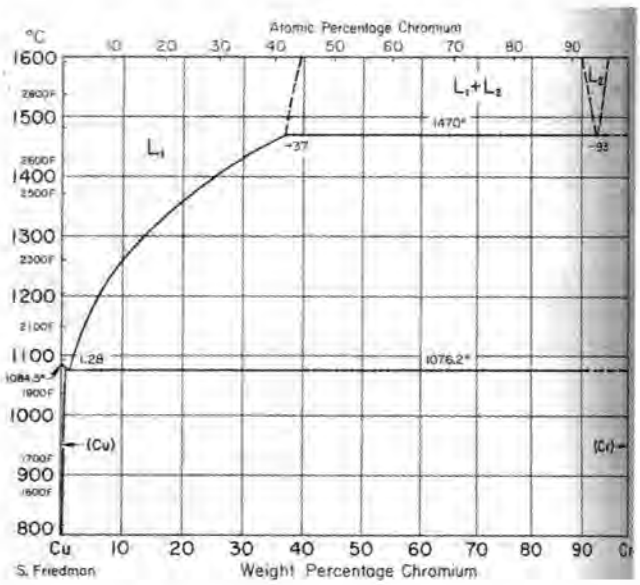

Fig 8: Equilibrium diagram of CuCr system [7]

Conclusion

An alternate LPS process was developed to replace I/F in order to increase the productivity by reducing the sintering cycle time. In order to compare the materials made by the two processes, samples were analyzed for hardness, electrical conductivity and density. Their microstructure was evaluated and compared based on the roundness of Cr particles, number of small particles present in the microstructure and the extent of sharp corners the Cr particles possess.

After comparison and analysis of the gathered data it could be concluded that LPS process attains more hardness compared to the I/F process. The conductivity of samples obtained by I/F process is more than those obtained by the LPS process. These two findings can be explained based on the amount of dissolved Cr obtained in Cu due to the difference in processing conditions. Also the density of samples obtained by LPS process is lesser than those obtained by I/F process.

The microstructures of I/F and LPS processes are similar looking. The number of small particles in an I/F structure is less when compared to LPS structure. The extent of sharp corners and roundness of Cr particles is of similar nature.

Although the electrical conductivity and density of LPS samples are inferior to I/F process, they were in the acceptable range. It can thus be concluded that the I/F process can be replaced by LPS process and advantage of increased productivity can be availed.

Reference

1. Paul G. Slade, "Advances in material development for high power, vacuum interrupter contacts", IEEE Transactions on Components, Packaging, and Manufacturing Technology, Part A, Vol.17 pp 96-106 (1994).
2. K. P. Cooper, J. D. Ayers, J. C. Malzahn Kampe, C. R. Feng and I. E. Locci, "Microstructural evolution and thermal stability in rapidly solidified high-chromium-containing copper alloys", Mater.Sci. Eng., Vol. A142 pp 221-233 (1991).
3. Ballat, J., König, D., "Insulation characteristics and welding behavior of vacuum switch contacts made from various Cu–Cr alloys", IEEE Transactions on Electrical Insulation, Vol. 28, pp. 628–634, (1993).
4. ASM hand book, Properties and selection: Nonferrous alloys and special purpose materials, Vol- 2 (1990).
5. Wangpei Li, Robert L. Thomas, and R. Kirkland Smith, "Effects of Cr Content on the Interruption Ability of CuCr Contact Materials" IEEE Transactions on plasma science, Vol. 29, No. 5, (2001).
6. ASM hand book, powder metal technologies and Applications, Vol. 7, (1998).
7. ASM metals Hand Book, Metallography, Structures and Phase diagrams, Vol 8 (1973).

DEVELOPMENT AND WEAR STUDIES OF P/M PROCESSED IRON BASED BRAKE PADS USED FOR HEAVY DUTY AIRCRAFT APPLICATIONS.

M. Asif., K Chandra, P.S.Misra*
Metallurgical and Materials Engineering Department, Indian Institute of Technology, Roorkee, India

Abstract

Development and Wear study of friction materials used for manufacturing of P/M Processed iron based brake pads employed in aircraft, by newly developed P/M technique based on hot powder pre-form forging are studied. The friction and wear characteristics of these friction materials were analyzed by using initial laboratory Pin on disc wear test; the results include measurement of COF, wear (gm), noise (db) and temperature rise. The characteristics of friction materials are also monitored by hardness and density measurements. On the basis of these initial tests, two samples are selected for friction test on Sub-scale brake dynamometer at low Kinetic energy (17300kgf). It has been observed that the pads made through this technology are superior in performance in comparison with the pads made by sintering technology. COF is stable, and is within the range of Aeronautic standard. Furthermore, the chemistry employed in the present technology is much simpler. This paper deals with detailed characterization of brake pads suitable for Military aircrafts applications.

Keywords: Wear; Powder Metallurgy; brake pad; Aircraft

1. INTRODUCTION:

Majority of modern day aircraft brakes comprises of metallo-ceramic friction materials which are used in the form of brake pads or disc. These friction materials are complex, multi-components, metal-matrix composites, manufactured by advanced powder metallurgy technology (P/M) [1].

Powder metallurgy (P/M) processing is a net or near net shaped production technology which eradicates the need of most of the secondary operations. Automotive and highway vehicle applications dominate the ferrous P/M structural parts market [2]. However, there are many other fields where ferrous P/M parts are used such as lawn, garden structural parts, hand tools, hobby applications, and household appliances, lock hardware, industrial motors controls, hydraulic applications etc., and satisfy close dimensional tolerance requirements for parts even with complex geometries [3].

Friction materials are used to induce friction in applications such as in brakes & clutches where de-acceleration is desired. When a brake is applied, it activates a system that places the friction material against a rotating disc or drum that slows down/stops the vehicle. [4]

The friction materials so produced have much more wear resistant, better friction and wear properties for superior performance, more thermal shock resistance, more fatigue strength, shear strength, compressive strength. An iron based metallo ceramic friction material has been successfully developed by powder metallurgy technique for the brakes of heavy military transport aircraft. The friction material composition was carefully design after an in-depth analysis of air craft brake design specification requirements and derivation of optimum level of material properties desired for these requirements. Experiments were then conducted to establish the P/M processing route and optimize the compositions and process parameters.

Iron, as the friction material matrix is chosen due of its stability under higher temperatures (1100°C) and can be applied under heavy dry operating conditions because of its high melting point and other improved properties which include strength, hardness, ductility, heat resistance and stability etc. [5]. Further, during braking, surface/oxides films on its surface are responsible for better frictional properties. Due to these reasons, iron as base materials have been chosen in the present investigation.

2.0 EXPERIMENTAL PROCEDURE:

Brake pads made in the present investigation consist of two major parts namely friction layer and backing plate which are formed simultaneously, such that these two layers do not separate out during operation. Joining of these two layers by sintering is usually difficult because of widely varying chemistry and processing involved. So the present investigation relies on manufacturing of these two parts simultaneously employing different chemistry of powders but having similar constituents. This results in better joint quality between them. Table 1 provides details of chemistry of backing plate whereas Table 2 provides chemistry of friction layers. Three compositions along with the backing plate namely, FA07, FA08 and FA09 were prepared, and sequence of manufacture is as described below:-

Powder processing

1. For backing plate:

Powder mixture for backing plate as per Table1, is subjected to mechanical alloying in the Attritor Mill with a ball to charge ratio in the range of 10:1 and duration of Mechanical alloying is 2hours and rotational speed of mill is 200 rpm.

Powder mixture for friction layer as per the chemistry given in Table 2 is prepared as per the following sequence.

2. For Friction Materials

- SiC powder is mechanically alloyed with sulphide / sulphate powders and of graphite powder (having size range 0-120micron) as shown in Table 3. The parameters of mechanically alloying are:

- Attritor speed (200rpm), Ball to charge ratio (10:1), Duration (60mins.). This will ensure coating of soft powders on hard SiC powder.

- Entire amount of iron and other powders as per the chosen chemistry is mechanically alloyed with graphite powder in Attritor Mill as mentioned above.

- The two powder mixtures so prepared are then mechanically mixed with each other

2.2 Powder Compacting

Powder compaction takes place in a suitably designed die in accordance with the given shape of disc brake pad for example, suitable for military transport such as AN-32 aircraft. Requisite quantity of backing plate powder mixture is first filled to a uniform height. Thereafter, friction layer powder mixture in requisite quantity is filled in the die. The filling of these layers of powder is done on fixed weight basis as per the design say in Fig.2 and densities of respective layers. Both the layers of powder mixture are simultaneously pressed in a Screw forging press with the help of upper and lower punches at a pressure in the range of 150 to 450MPa. The compact so pressed is ejected out of the die. The die is suitably lubricated employing graphite /Zinc stearate in the suspension of methyl alcohol/ethyl alcohol/acetone prior to filling for easy ejection without cracking of green compact.

2.3 Preform Coating

The green compact so produced is coated with an indigenously developed ceramic coating to protect it from oxidation when subjected to heating. The coating is baked to remove moisture from it at a temp of 120 °C for 2 hrs in an oven [6].

2.4 Heating

The coated green compacts are heated in a furnace. The operating temperature of the furnace is 1050°C for iron based brake pads, holding time 1 hr.

2.5 Hot powder Preform Forging

The hot powder preform samples are taken out from the furnace and quickly transferred into the hot die duly lubricated with graphite and fitted in the forging press. The forging is done at a speed of 500mm/s. The preform is fully consolidates to its near theoretical density on forging. The forged component is later on ejected out of the die.

2.6 Annealing

The forged pads are subjected to high temperature resistant ceramic/ glassy coating again and, then annealed at a temperature of 710°C for 5 hours to adjust hardness of friction layer to < 100 BHN.

On cooling the coating peels off by itself and residual coating if any is removed by minor surface finishing operations.

TABLE 1 Chemistry of back plate Materials

S.No	C %	Cu %	P %	SiC %	Fe %
B1(FA07)	0.3	1.5	0.3	-	Balance
B2(FA08-FA09)	0.1	2.5	-	1	Balance

TABLE 2 Chemistry of Friction Materials

Symbol	Chemistry (wt%)		
	Metallic Constituents	Ceramic Constituents	Lubricants
FA07	Fe-67.6, Cu-10	SiC-7, Cr-0.4	Graphite-8,Sb_2S_3-1, $BaSO_4$-4, Al_2O_3- 2
FA08	Fe-70.7, Cu-10	SiC-7, , Cr-0.3	Graphite-6,$BaSO_4$-4, Al_2O_3- 2
FA09	Fe-67.9, Cu-10 Sn-1	SiC-7,Cr-0.6	Graphite-7, Sb_2S_3-1, $BaSO_4$-4, Al_2O_3- 1.5

TABLE 3 Sizes of powders employed

S.No.	Powder	Size range	Source
1	Iron powder	-120μm	Hoganas Industries Ltd.
2	Copper powder	-120μm	Electrolytic
3	Graphite	-200 to +150μm	Natural Crystalline Grade
4	Ferro-phosphorus	-45μm	Commercial grade
5	Tin powder	-75μm	Atomized
6	Silicon Carbide	-180 to +150μm	Chemical grade
7	Barium Sulphate/ Antimony Trisulpide	-45μm	Chemical grade

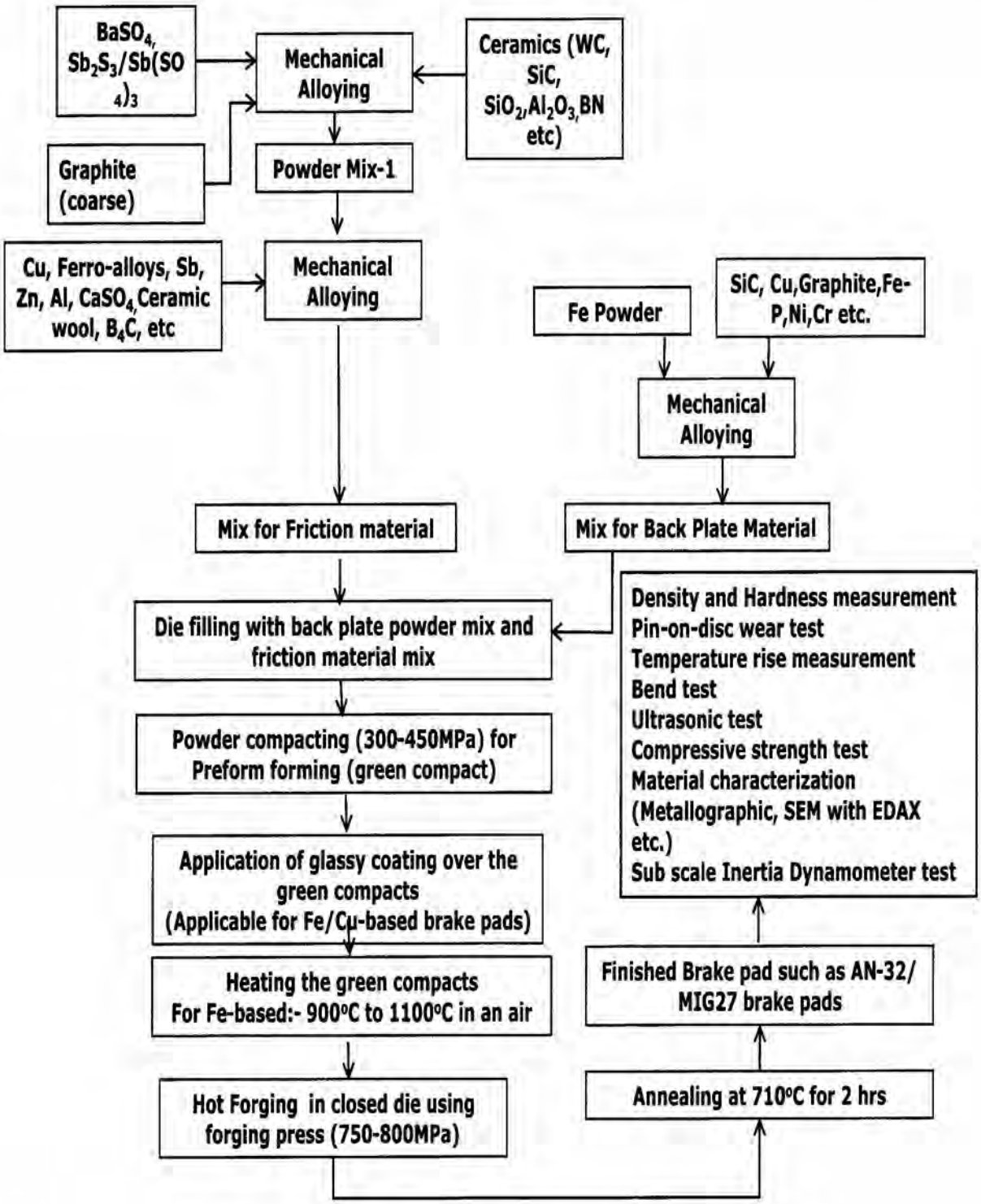

Fig.1. Process Flow sheet for manufacturing of iron based brake pad.

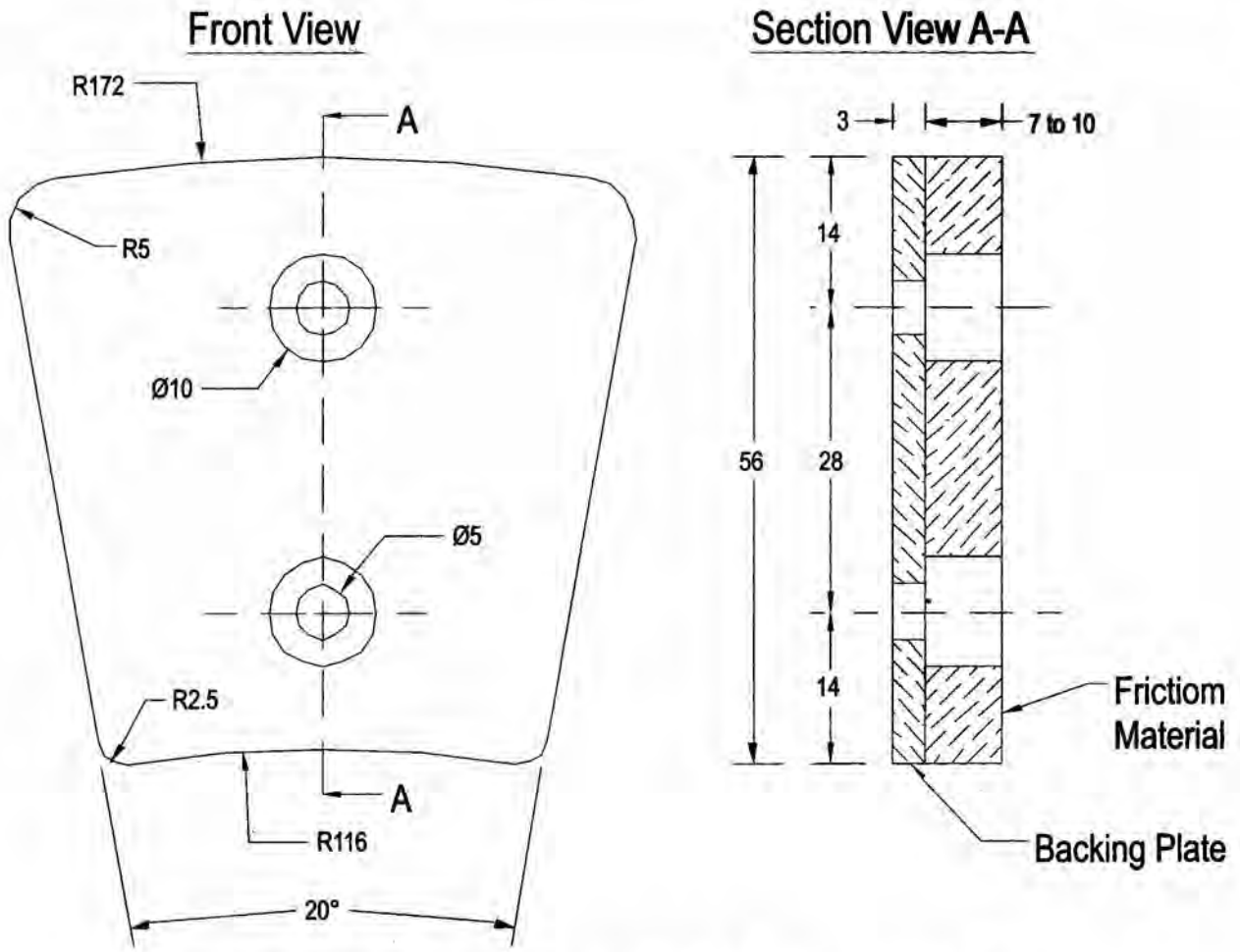

Fig.2. Design of Brake Pad as developed in the present investigation.

3. Results and Discussions

3.1 Characterization of Friction materials/pads

The brake pads so produced with built-in powder based backing plates (as in Fig.2) are characterized for physical, and functional properties namely density, hardness etc. Also pin-on-disc wear test, sub-scale brake inertia dynamometer tests are carried out.

3.1.1 Density and Hardness Test.

Density and Hardness of Friction Materials are summarized in Table 4. Both these parameters depend on forging and annealing treatments. These also depend upon, chemistry formulation of friction materials. The technology developed in the present investigation is capable of developing these parameters in wide ranges which is not possible in sintering technology. It is amply clear that the processing technique employed in the present investigation is superior with regard to density and hardness combination in comparison with the compacting and pressure sintering technology. Although hardness obtained in these brake pads are similar to the conventional brake materials, higher density levels achieved are likely to show improved performance.

TABLE4. Density and Hardness of Iron based brake friction elements

Samples	FA07	FA08	FA09
Density P (gm/ cm^2)	5.8	6.3	6.2
Hardness (BHN)	95	90	93

3.1.2 Pin-on-disc wear test:

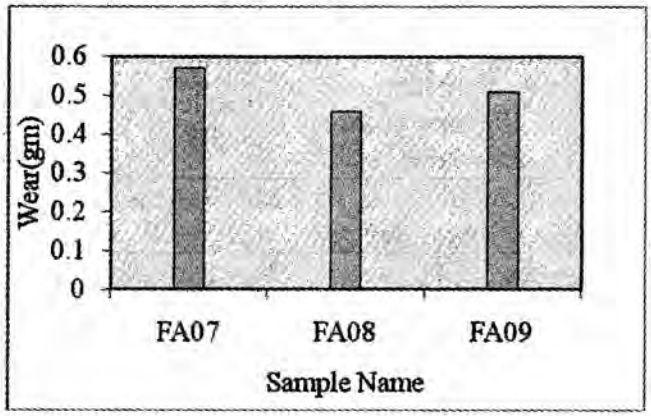

(a). Wear (gm) for friction materials.

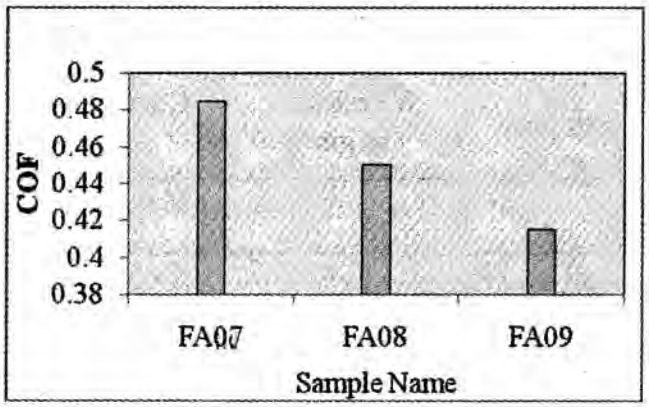

(b) Coefficient of Friction for frictions materials.

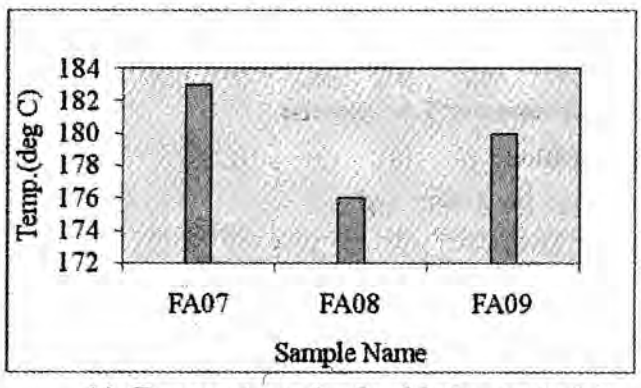

(c). Temperature rise for friction materials.

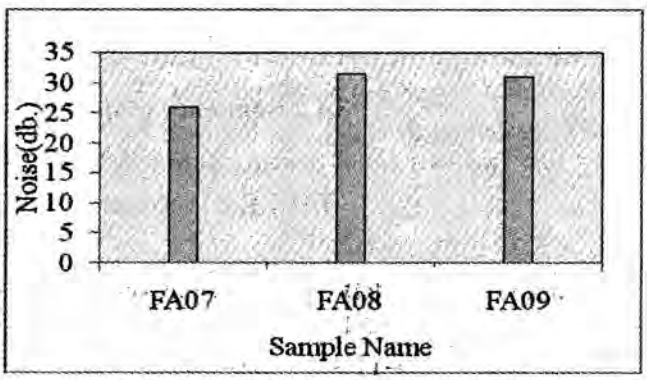

(d). Noise level for friction materials.

Figure 3. (a). Wear(gm) for friction materials, (b) Coefficient of Friction for frictions materials, (c).Temperature rise for friction materials, (d). Noise level (db) for friction materials.

The purpose of Pin-on disc wear test is to qualitatively assess material related performance of iron based brake pads. The pin on disc tests were performed on the square pin size of 7mmx7mm with sliding speed of 9m/s and applied load of 8 kg. Table 5 provides the summary results of these samples. It may be inferred from these graphs that the wear is very low as per the aeronautic standard range in all samples; this is due to the role of wear resistant constituents and lubricants. In all the compositions the presence of wear resistant materials, like silicon carbide, first increase COF and lubricants improve the engagement. Combined effect of these two types of constituents optimizes the net wear loss. The noise level during the test is not significantly altered in all the cases. This is because of the fact that the noise level is related to net metal content of the brake elements which in our case varies from 80% to 85%. The noise level shown in Table 5 is in the range of 26-31dB. Fig.3. (a) to Fig.3 (d) depicts pin-on-disc test results graphically.

However, preference of our compositions on the basis of low wear is in the following order:-

FA08 > FA09 > FA07

On the basis of preliminary wear test, the samples were qualified for sub–scale inertia dynamometer test. The wear test results of three iron powder based samples are summarized in Table5. It includes weight loss (gm), coefficient of friction, and temperature rise and noise level (db).

TABLE 5. Pin-On-Disc Wear Test results (Contact area of pin: 7×7 mm², sliding speed 9m/s and applied load 8 kg).

Samples	Wear loss, in gm	Coefficient of Friction, (COF)			Max Temperature rise	Noise level, dB		
		Max	Min	Avg	°C	Max	Min	Avg.
FA07	0.57	0.51	0.46	0.485	183	28	24	26
FA08	0.46	0.47	0.43	0.45	176	35	28	31.5
FA09	0.51	0.43	0.40	0.415	180	33	29	31

3.1.2.Summary of the Sub-scale Dynamometer Test Results:

AN-32 Rotor application:

TABLE 6. Aeronautic standard range for AN-32 Aircraft:

Sample	RD revl.	RD time, sec.	COF	Average Wear (gm)
AN-32 Rotor manual	50-110	6-12	0.18-0.40	1 4max.

TABLE 7. Test results for AN-32 Rotor application:
Test parameters: Brake Force=150kgf; KE=17300kgfm; Speed=1000rpm; Sample pad area=25.8cm²

Sample	50 Cys.	RD revl.	RD time, sec.	COF	Average Wear (gm)
FA07	Max	78	9.3	0.37	8.5
	Min	56	6.8	0.28	
	Avg	66	7.9	0.33	
FA08	Max	80	9.6	0.36	10.5
	Min	57	6.8	0.27	
	Avg	69	8.3	0.31	
FA09	Max	74	8.8	0.35	11
	Min	57	6.8	0.28	
	Avg	63	7.6	0.32	

4. Conclusion:

The brake pad developed in the present investigation by hot powder preform forging has an excellent properties required for heavy duty brake applications. Strong bonding between friction layer and backing layer during actual trial. The wear in terms of gram of developed brake pads is lower than standard wear in gram. RD time range for developed brake pads lies in the standard RD time range for heavy duty applications. Coefficient of friction for developed brake pads is stable, resulting in low vibration and judder. Good correlation between pin on disc test results and sub-scale dynamometer test results.

Based on the test carried out, the product is suitable for heavy duty application such as AN-32 Military transport aircraft.

5. Refrences:

1. Dutta D., Mohan G., Chatterjee B., Krishnadas Nair C.G 'Development of sintered metalloceramic friction material for the wheel brakes of a military transport aircraft', Published in, 'Composites: Science and Technology (ISBN 81-224-1251-3)' edited by R.C. Prasad, P. Ramakrishan, New Age International (P) Ltd., New Delhi, pp 94-114 (2002).
2. Anandakrishnan V., Sivasankaran S., Prasad K, Panday K.S., "Influence of carbon content on workability behavior of Powder metallurgy steel", Transaction of PMAI,Vol.35, pp26-27 (December 2009)
3. Asif M., Chandra K., Misra P. S., 2010, "Microstructure and Mechanical Properties of P/M Processed steel used in brake pads for heavy duty applications by hot powder preform technique." Paper presented in 'Third International Conference on Recent Advances in Composite Materials, ICRACM-2010' held at Limoges, France, held on December 13-15, 2010, will be published in Material science and Engineering- A, Elsevier journal,
4. Anderson, A.E., "Friction and wear of automotive brakes", ASME Handbook. - Friction Lubrication and Wear Technology, ASM International, the Materials Information Society, 18, pp. 569-577 (1992).
5. Lenin S. D. "Development of friction materials through powder metallurgy", Ph. D. Thesis, Indian Institute of Technology Roorkee India. (2008).
6. Misra P. S., Chandra K. "Development of High Temperature Oxidations Resistant Glassy Coating" Indian Patent, application No. 153/DEL/2010 dated (Jan. 27, 2010).

FLOW THROUGH CONICAL CONVERGING DIE OF SINTERED PREFORM

[1]Abhay Kumar Sharma, [2]R.K.Ranjan, [3]K.S.Kasna, [4]V.K.Bajpai

[1-2]Mech. Engg. Department, GGITS Jabalpur,India

[3-4]Mech. Engg. Dept., NIT Krukshetra (Institute of National Importance), India

Abstract

The forming of sintered metal-powder performs is currently arousing interest in many parts of the world as an economic method of producing components from metal powders. This paper reports on an investigation into the various aspects of extrusion of powder preforms, which have been compacted and sintered from atomized powder. An attempt has been made for the determination of the die pressures developed during the extrusion of powder preform by using an upper bound approach. The concept of a spherical velocity field is introduced and dealt with in great detail as well as the power required. Experiments were conducted on aluminium and copper metal powder performs to validate the theoretical results. The results so obtained are discussed critically to illustrate the interaction of various process parameters involved and are presented graphically.

Keywords. Preforms, sintering, conical converging die, inter facial friction law.

1. Introduction

During the last few years metal-powder components have assumed an important position in industry, as they are being used successfully in a wide range of applications. Both the mechanical and the metallurgical properties of the metal powder components compare favorably with those of wrought materials [1]. Bulk processing of metal powder preforms is a convenient method of reducing or eliminating the porosity from conventional powder metallurgy products. The process is attractive because it avoids a large number of operations, high scrap losses and high energy consumption associated with conventional manufacturing processes such as casting, machining etc. In this new technology sintered porous powder preforms are used as starting materials. Metal powder products manufactured by this new technology are comparable and in some cases even superior to those of cast and wrought products. Although a considerable amount of work has been reported recently as to the various technological aspects of the industrial processing of metal powder performs [2-4], no systematic attempt has been made so far to study the processing load and deformation characteristics during flow through conical converging dies. The paper reports on an investigation into the various aspects of extrusion of powder preforms, which have been compacted and sintered from atomized powder. An attempt has been made for the determination of the die pressures developed during the extrusion of powder preform by using an upper bound approach. The concept of a spherical velocity field is introduced and dealt with in great detail as well as the power required. The results so obtained are discussed critically to illustrate the interaction of various process parameters involved and are presented graphically. It is expected that the present work will be of great importance for the assessment of relative extrusion stress developed during the flow through conical converging dies of metal powder preforms.

2. Interfacial Friction Law

During the forming of metal-powder preforms the compressive force gradually increases the relative density, which later is directly proportional to the real area of contact. The relative density gradually approaches the apparent relative density (Fig.1) this approach probably being asymptotic [5]. During the sinter forging process it is very important to keep special consideration on the interfacial friction, as this will determine the success or failure of the operation [6]. The relative velocity between the work piece material and the die surface, together with high interfacial pressure and or deformation modes, create a condition of composite friction which is due to adhesion and sliding [7]. The shear equation becomes $t = m[p + r_d f_a]$

The first term p being due to sliding and second term $\mu p_0 \phi_0$ being due to adhesion, which later arises from change of the relative density of the preform during the process. The pattern of the metal flow during the forging of a preform is such that there exist two zones, an inner one where no relative movement between work piece and die occurs (the sticking zone) and an outer zone where sliding occurs. Therefore, the appropriate friction law for this particular condition is:

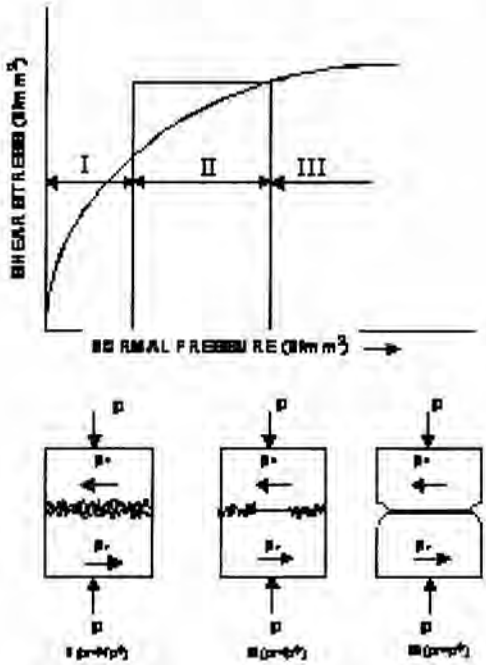

Figure 1. Three regimes of density variation.

$$t = m\left[p + r_0 f_0\left(1 - \frac{r}{nR}\right)\right] \qquad (1)$$

where r denotes the sticking zone radius and which may be approximated by the relation given by Rooks [8] and n>>1.

3. Plastic Deformation of Sintered Preforms

In an investigation of the plastic deformation of sintered metal powder preforms it is clear that a change in volume occurs due to porosity. A preform with a high relative density yields at a relatively high stress whereas a low relative density preform yields at a relatively low stress. Even hydrostatic stress can cause the sintered metal powder preforms to yield, as the yield surface is closed on the hydrostatic stress axis. Tabata and Masaki [9] proposed the following yield criterion for porous metal powder preforms:

$$r^k = \sqrt{3J_2} \pm 3h\sigma_m \qquad (2)$$

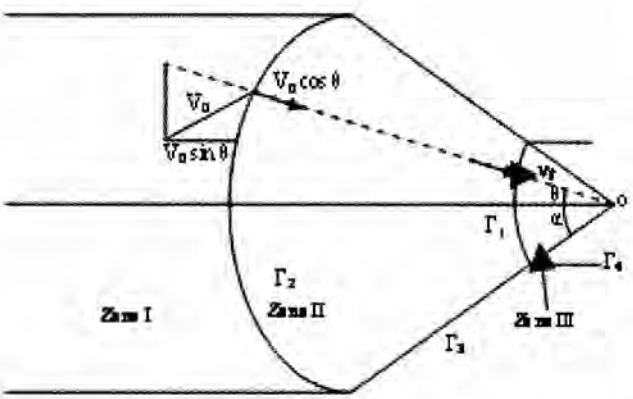

Figure 2. The spherical velocity field.

The negative sign is taken for $\sigma_m \leq 0$ and the positive sign is taken for $\sigma_m \leq 0$. The values of and k were determined experimentally from simple compression and tension tests of sintered copper powder performs [9] as

$$h = 0.54(1 - r)^{-2} \quad \text{for} \quad \sigma_m \leq 0$$

$$h = 0.55(1 - r)^{0.83} \quad \text{for} \quad \sigma_m > 0 \text{ and } k=2$$

For the axisymmetric condition the yield criterion reduces to

$$\sigma_1 - \sigma_2 = \frac{r^k \sigma_0}{(1-2h)} + \frac{(1+h)}{(1-2h)}\sigma_2 - \sigma_2 = l \text{ (Appendix A)} \quad (3)$$

4. Spherical Velocity Field

The preform is divided into three regions in which the velocity fields are continuous (Fig. 2). In zone I and zone III, the velocity is uniform and has only an axial component. In zone I, the velocity is v_0, and in zone III the velocity is v_f.

Because of mass constancy $v_0 = r\, v_f \left(\frac{r_f}{r_0}\right)^2$ (4)

In zone I, deformation has not yet begun. It consists of the incoming rod, which is separated from the deforming zone II by the surface Γ_2. Surface Γ_2 is spherical, of radius r_0 with the origin at the apex 0 of the cone of the die. Zone II is the zone of deformation bounded by the surface of the die, with a cone of an included angle 2α and two concentric spherical surfaces Γ_1 and Γ_2. The surface Γ_2 is the spherical boundary between zone I and II. The spherical surface Γ_1 of radius r_f, with the origin at the apex 0 of the cone, separates zone II from the emerging product of zone III. In zone II, the velocity is directed towards the apex 0 of the cone, with cylindrical symmetry. In the spherical co-ordinate system (r,θ,φ) the velocity components are-

$$U_r = -\frac{v_f r_f^2 \cos\theta}{r^{1/K}}; \qquad U_\theta = 0;\ U_\varphi = 0 \qquad \text{with } K = \frac{(1-2h)}{2(1+h)} \quad (5)$$

5. Strain Rate

$$\dot{\varepsilon}_r = \frac{v_f r_f^2 \cos\theta}{K r^{(1/K)+1}}; \quad \dot{\varepsilon}_\theta = -\frac{v_f r_f^2 \cos\theta}{K r^{(1/K)+1}}; \quad \dot{\varepsilon}_\varphi = -\frac{v_f r_f^2 \cos\theta}{K r^{(1/K)+1}}; \quad \dot{\varepsilon}_{r\theta} = \frac{v_f r_f^2 \sin\theta}{2 r^{(1/K)+1}} \quad (6)$$

The above strain rates must satisfy the compressibility equation of powder perform [9]-

$$\left(\dot{\varepsilon}_r + \dot{\varepsilon}_\theta + \dot{\varepsilon}_\varphi\right) = \sqrt{2}h \sqrt{\left(\dot{\varepsilon}_r - \dot{\varepsilon}_\theta\right)^2 + \left(\dot{\varepsilon}_\theta - \dot{\varepsilon}_\varphi\right)^2 + \left(\dot{\varepsilon}_\varphi - \dot{\varepsilon}_r\right)^2} \quad (7)$$

This equation may be rewritten as according to our problem-

$$\dot{\varepsilon}_r + \frac{2(1+h)}{(1-2h)}\frac{U_r}{r} = 0 \quad (8)$$

6. Internal Power of Deformation

According to Oyane & Tabata [10], the internal work done is given by-

$$W_i = \frac{2}{\sqrt{3}} r^k s_0 \int_v \left[\frac{1}{2} \left(e_r^2 + e_\theta^2 + e_z^2 + 2e_{r\theta}^2 \right) \right]^{\frac{1}{2}} dV \quad \text{and} \quad dV = 2\pi r \sin\theta . r d\theta . dr \tag{9}$$

$$= \frac{\sqrt{2}\pi r^k s_0 \sqrt{1+2K^2}\, v_f r_f^2 \left(r_0^{2-1/K} - r_f^{2-1/K} \right)}{\sqrt{3}(2K-1)} \left[1 - \cos\alpha \sqrt{1 - \frac{2+3K^2}{2(1+2K^2)} \sin^2\alpha} + \frac{1 - \frac{2+3K^2}{2(1+2K^2)}}{\sqrt{\frac{2+3K^2}{2(1+2K^2)}}} \ln \frac{1 + \frac{2+3K^2}{2(1+2K^2)}}{\sqrt{\frac{2+3K^2}{2(1+2K^2)}} + \sqrt{1 - \frac{2+3K^2}{2(1+2K^2)} \sin^2\alpha}} \right]$$

Since $\frac{r_0}{r_f} = \frac{R_0}{R_f}$ and $r_f = \frac{R_f}{\sin\alpha}$; it follows that-

$$W_i = \frac{\sqrt{2}\pi r^k s_0 \sqrt{1+2k^2}\, v_f r_f^{(4-1/K)}}{\sqrt{3}(2K-1)} \left[\left(\frac{R_o}{R_f} \right)^{2-\frac{1}{K}} - 1 \right] f(\alpha)$$

$$f(\alpha) = \frac{1}{\sin^{(4-1/K)}\alpha} \left[1 - \cos\alpha \sqrt{1 - \frac{2+3K^2}{2(1+2K^2)} \sin^2\alpha} + \frac{1 - \frac{2+3K^2}{2(1+2K^2)}}{\sqrt{\frac{2+3K^2}{2(1+2K^2)}}} \ln \frac{1 + \frac{2+3K^2}{2(1+2K^2)}}{\sqrt{\frac{2+3K^2}{2(1+2K^2)}} + \sqrt{1 - \frac{2+3K^2}{2(1+2K^2)} \sin^2\alpha}} \right]$$

For very small , f () converges to unity and the above equation reduces to-

$$W_i = \frac{\sqrt{2}p\, r^k s_0 \sqrt{1+2K^2}\, v_f r_f^{(4-1/K)}}{\sqrt{3}(2K-1)} \left[\left(\frac{R_o}{R_f} \right)^{2-\frac{1}{K}} - 1 \right] f(a) \qquad (10)$$

7. Velocity Discontinuities

Along Γ_1- $Dv = v_f \sin q$ Along Γ_2- $Dv = v_0 \sin q$

Along Γ_3- $Dv = \frac{v_f r_f^2 \cos a}{r^{1/K}} \gg \frac{v_f R_f^2 \cos a}{R^{1/K}}$ Along Γ_4- $Dv = v_f$ (11)

8. Frictional power Losses

In Cylindrical Portion

Consider the equilibrium of the small element (Fig.3)-

$$(s_x + d s_x) p R_0^2 - s_x p R_0^2 - 2mpp R_0 dx = 0 \qquad (12)$$

For cylindrical state of stress, the principal stresses are σ_r, $\sigma\theta$ and σ_z. Hence, equation (3) becomes

$$s_r - s_q = \frac{r^k s_0}{(1-2h)} + \frac{(1+h)}{(1-2h)} s_q - s_q = l$$

as the yielding of the material during this process takes place at a particular maximum value of . Hence λ is a constant for this process (Appendix A) when $\sigma_r = \sigma_x$, and $= \sigma_\theta - p$. The von Mises yield criterion reduces to-

$$s_x + p = -l \; ; \quad \text{i.e.} \; p = -(s_x + l) \qquad (13)$$

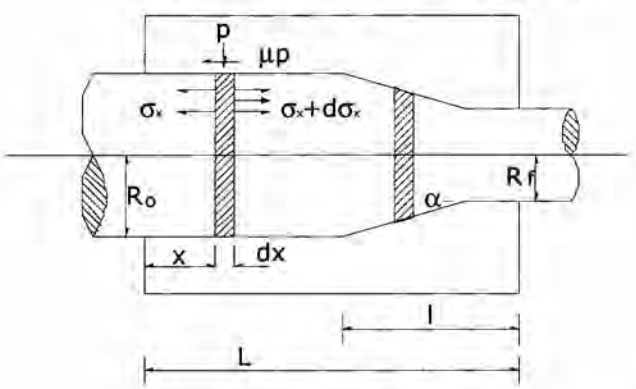

Figure 3. Free-body equilibrium

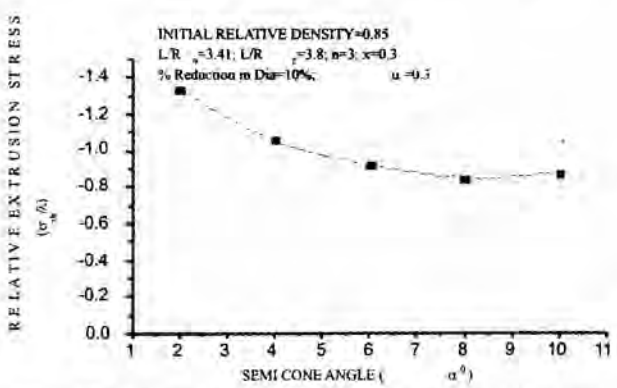

Fig. 4 Effect of semi cone angle (α) on relative extrusion pressure

$$\therefore \frac{R_0}{2} d\sigma_x = \pi p dx = -\mu(\sigma_x + l)dx$$

$$\therefore \frac{d\sigma_x}{(l+\sigma_x)} = -2\frac{\mu}{R_0}dx \quad \text{and by integration,} \quad \ln(l+\sigma_x) = -2\frac{\mu}{R_0}x + C$$

Using the boundary condition, $\sigma_x = \sigma_{xb}$ at x = 0, $C = \ln(l+\sigma_{xb})$

After putting the value of C in the above equation, we get,

$$\sigma_x = l\left[\left(1+\frac{\sigma_{xb}}{l}\right)\exp\left(-2\mu\frac{x}{R_0}\right) - 1\right] \tag{14}$$

Now, $$p = -(l+\sigma_x) = -l\left[\left(1+\frac{\sigma_{xb}}{l}\right)\exp\left(-2\frac{\mu}{R_0}x\right)\right]$$

$$W_f = \int_s \tau |\Delta v| ds \tag{15}$$

$$W_f = 2\pi v_f R_f^2 \frac{\mu}{R_0}\int_{x=0}^{L-l} p dx \;;\; \therefore -2\pi v_f R_f^2 \frac{\mu}{R_0} l\left(1+\frac{\sigma_{xb}}{l}\right)\int_{x=0}^{L-l}\exp\left(-2\frac{\mu x}{R_0}\right)dx$$

After integrating and substituting, $l = (R_0 - R_f)\cot\alpha$

$$W_f = \pi v_f R_f^2 l\left[\left(1+\frac{\sigma_{xb}}{l}\right)\left\{\exp\left(2\mu\left[\frac{L}{R_0} - \left(1-\frac{R_f}{R_0}\right)\cot\alpha\right]\right) - 1\right\}\right] \tag{16}$$

In Conical Portion

The die and a differential element are shown in Fig. 3. Considering the equilibrium of the forces in x-direction which is the direction of principal stress,

$$D d\sigma_x + 2\sigma_x dD + 2dD\left(p + \frac{\tau}{\sin\alpha}\right) = 0$$

or, $$D d\sigma_x + 2\sigma_x dD + 2dD\left\langle p + \left(\frac{\mu}{\tan\alpha}\right)\left\{p + \tau_0 f_0\left[1 - \left(\frac{r}{R_b}\right)^{\frac{1}{n}}\right]\right\}\right\rangle$$

After simplifying of the above equation, we get,

$$Dd\sigma_x + 2dD\left\langle (\sigma_x + p) + B\left[p + \tau_0 f_0\left\{1 - \left(\frac{D}{D_b}\right)^{\frac{1}{n}}\right\}\right]\right\rangle = 0; \qquad \text{where } B = \frac{m}{\tan\alpha} \tag{17}$$

Equation (17) reduces to,

$$Dd\sigma_x + 2dD\left\langle l(1+B) - B\left[\sigma_x - \tau_0 f_0\left\{1 - \left(\frac{D}{D_b}\right)^{\frac{1}{n}}\right\}\right]\right\rangle = 0 \tag{18}$$

Integrating and simplifying the equation (18),

$$\sigma_x = \frac{2B\tau_0 f_0}{n(D/D_b)}\cdot\frac{1}{(1-2B)} + \frac{1}{2B}\left[2l(1+B) + 2B\tau_0 f_0\right] + C D^{2B} \tag{19}$$

Using the boundary condition at entry for this case is, $\sigma_x = \sigma_{xf}$ at $D = D_f$

Using this value in equation (19)-

$$C = D_f^{-2B}\left[\sigma_{xf} - \frac{1}{B}\left\{(1+B) + B\tau_0 f_0\right\} - \frac{2B\tau_0 f_0}{(1-2B)n}\right] \tag{20}$$

Substituting the value of C in equation (19) and after simplification without considering front pressure, we can get,

$$\frac{\sigma_x}{l} = \frac{1+B}{B}\left[1 - \left(\frac{D}{D_f}\right)^{2B}\right] + \frac{\tau_0 f_0}{l}\left[1 - \left(\frac{D}{D_f}\right)^{2B}\right]\left\{1 + \frac{2B}{n(1-2B)}\frac{D_f}{D_b}\right\} + \frac{2B}{n(1-2B)}\frac{D}{D_b} \tag{21}$$

Now from equation (15), we can get,

$$W_f = \frac{2\pi\nu_f R_f^2 \cot\alpha\, l\, K R_f^{(2-1/K)}}{(2K-1)}\left[\left(\frac{R_0}{R_f}\right)^{(2-1/K)} - 1\right]\left[1 - \frac{1+B}{B}\left\{1 - \left(\frac{R_0}{R_f}\right)^{2B}\right\}\frac{2K-1}{2BK+2K-1} + \frac{\tau_0 f_0}{l}\left\{1 - \left(\frac{R_0}{R_f}\right)^{2B}\frac{2K-1}{2BK+2K-1}\right\}\left\{1 + \frac{2B}{n(1-2B)}\frac{R_f}{R_0}\right\} + \frac{2B}{(1-2B)}\left\{1 - \frac{R_f}{R_0}\left(\frac{2K-1}{3K-1}\right)\right\}\right] \tag{22}$$

9. Relative Extrusion Pressure

For plastic deformation of a metal powder the external power $\dot{J}$ supplied by the ram is given as-

$$\dot{J} = \dot{W}_i + \dot{W}_f + \dot{W}_a + \dot{W}_t \qquad (23)$$

The first term on the right hand side denotes the rate of internal energy dissipation W_i, the second term denotes the frictional shear energy losses W_f, the third term denotes the energy dissipation due to inertia forces W_a, and the last term covers power supplied by predetermined body tractions W_t. In this case a force due to inertia is negligibly small and no external surface traction is stipulated. Therefore, $W_a = W_t = 0$.

Now the external power $\dot{J}$ supplied by the press through the platen is -

$$\dot{J} = \grave{o} F_i U_i \, ds = = W_i + W_f \qquad (24)$$

$$\text{and} \quad \dot{J} = -pr\, v_f R_f^2 S_{xb} \qquad (25)$$

10. Results and Discussion

During the process of deformation of a metal powder preform, it is seen that initially the densification of particles takes place and thus the density of the preform increases gradually. The applied stress contributes more towards densification and less towards deformation. After attaining sufficient density the densification and deformation take place simultaneously. The applied stress now contributes more towards deformation and less towards densification. However, the extent of each of them depends upon the reduction ratio and the initial relative density of the preform. When a further deformation stress is applied, the stress-free portion is completely deformed and replaced by densified material. The latter starts to emerge from the die orifice, while the elastically deformed part of the preform crosses the back boundaries of the plastic deformation zone and starts a process of densification, and this continues until the whole preform is deformed. Fig. 4 shows the effect of semi cone angle (α) of the die. It is found that with the increase of semi cone angle (α) of the die, the deformation stress decreases. Fig. 5 shows the variation of theoretical relative extrusion stress with semi cone angle considering different values of coefficient of friction. The relative extrusion stress increases with increasing the coefficient of friction between preform and die wall. Fig. 6 shows the variation of relative extrusion stress containing theoretical as well as experimental results on aluminium preforms having an initial relative density of 0.85, proving the close agreement between theoretical and experimental results. Fig. 7 shows the variation of deformation compressive load with percentage reduction in diameter for copper powder preforms having an initial relative density of 0.85. The deformation load increases with percentage reduction in the diameter of the preform. Initially a large amount of compressive load is consumed in densification of the preform and hence shows a linear variation with large slope. After attaining sufficient densification, the preform gets deformed plastically and the curve runs nearly asymptotically into a steady state. It has been seen that the slope of the curve for different lengths of the metal powder preform is nearly the same. Initially, the difference between the deformation loads is the same. The difference becomes more significant as the punch is displaced more forward. It is due to the change in the length of the preform, and therefore it is due to the change in the friction force between preform and die wall. At the end of the process, the difference between the forces is negligible. As seen from the Fig. 8 and 9, the deformation load increases rapidly at the start of the operation. After some movement of the punch, the load decreases with a constant slope. Fig. 10 shows the variation of average relative density with reduction ratio for deformation of aluminium powder performs through conical converging dies. The result shows a tendency for the relative density at slow speed to be slightly higher than at high speed. This is due to the effect of inertia and frictional forces acting during the process.

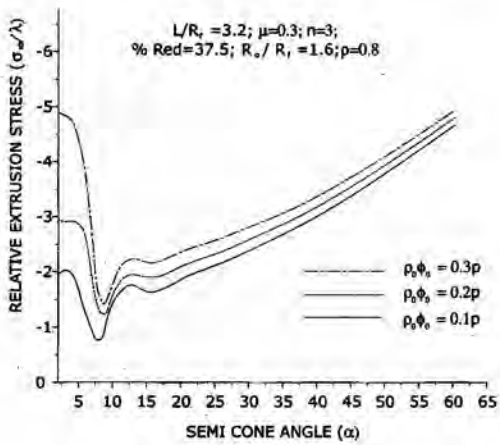

Fig. 5 Variation of theoretical relative extrusion stress with semi cone angle

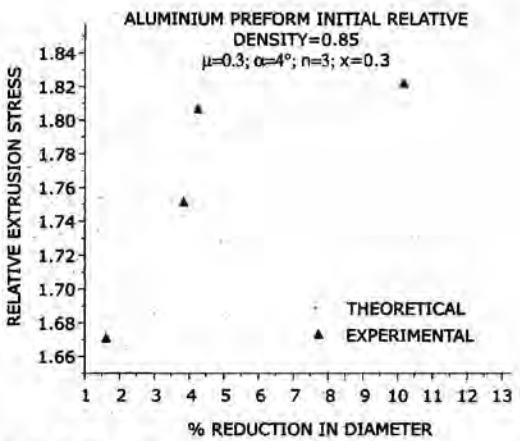

Fig. 6 Variation of relative extrusion stress with percentage reduction in diameter of the Al preform

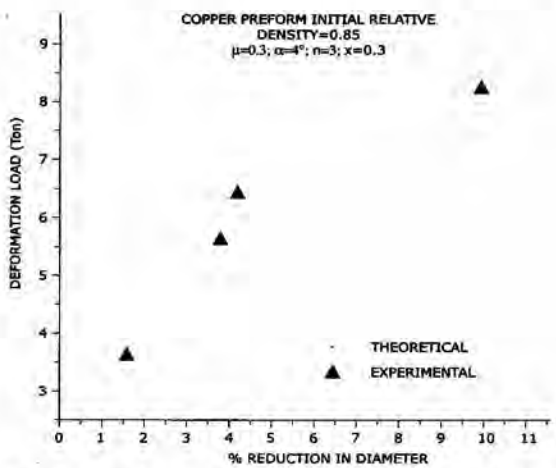

Fig. 7 Variation of relative extrusion stress with percentage reduction in diameter of the Al preform

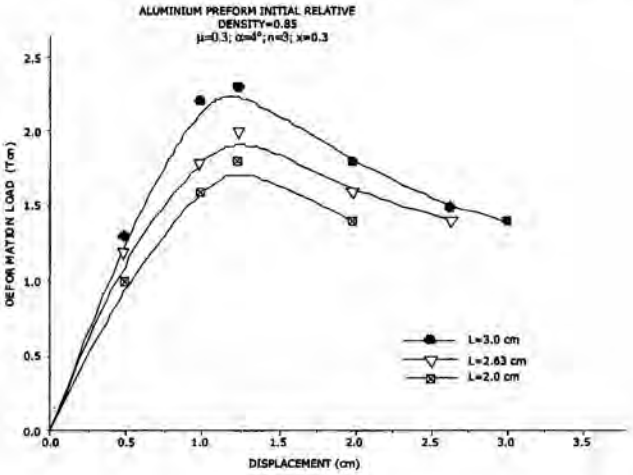

Fig.8 Load displacement curve of Al preform of length (a) 2.0cm (b)2.63cm (c) 3.0 cm

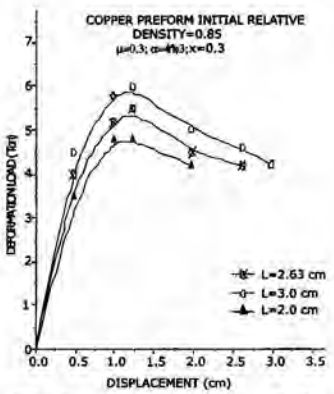

Fig.9 Load displacement curve of Cu preform of length (a) 2.0cm (b)2.63cm (c) 3.0 cm

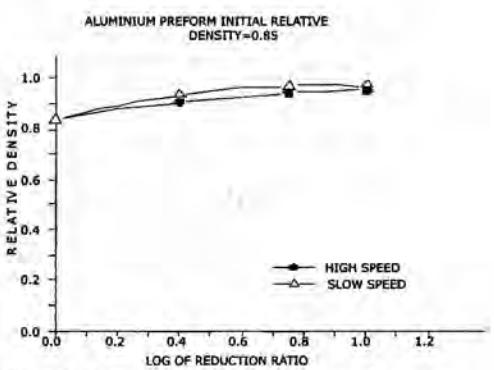

Fig. 10 Variation of relative density (deformed portion) with reduction ratio

11. Conclusion

The relative extrusion stress shows minima at a particular semi cone angle of the die, so it can be used as a criterion for the forming through conical dies. A lower value of coefficient of friction requires a low value of relative extrusion stress, i.e. it favors the forming operation. A higher initial relative density of the preform needs a lower value of relative extrusion stress. For small semi cone angle, the geometry of the preform has not too much effect on the relative extrusion stress. So all the above conclusions certainly would be helpful for the forming operation through conical converging dies.

List of symbol

τ = Shear stress
μ = Coefficient of friction
k = Constant equal to 2 in yield criterion
n = A constant quantity much greater than 1
λ = Flow stress of metal powder preform
r, θ, ϕ = Spherical coordinates
ρ = Relative density of the preform
ρ_a, ρ_r = Densities of apparent and real contact areas
σ_m = Mean yield stress
σ_0 = Yield stress of the non-work hardening matrix metal
$\dot{\varepsilon}$ $\dot{\varepsilon}_\theta$ $\dot{\varepsilon}_\phi$ = Principal strain increment
η = Constant and a function of ρ only
p = ram pressure
r = Radius of the sticking zone
J = Second invariant of deviatoric stress
r_0 = Initial radius of the rod
r_f = Final radius of the rod
V_0 = Velocity of incoming flow
V_f = Velocity of exiting flow
Δv = Velocity discontinuity
V = Volume of deformation zone
α = S emi cone angle of the die
Γ_l = Surface of velocity discontinuity
σ_{xb} = Extrusion stress

Appendix A

Of course, the value of σ_2 (-p) varies over the surface of the work piece. For a particular compression condition the value of σ_2 (-p) is constant when yielding starts. Hence the value of is constant during a particular compression condition, although the value of λ varies slightly during successive reduction of the work piece due to the variation of p in each compression condition. It requires an accurate determination of the variation of λ and/or σ_2 (-p) at the die- work piece interface during each reduction. But this consideration will extend the numerical calculations considerably.

Considering equation (13) the moment yielding starts, the value of σ_{rr} (or σ_{xx}) is negligible in comparison to p. Hence for all practical purposes σ_{rr} (or σ_{xx}) can be neglected. Hence $p \cong \lambda$. Putting this value of σ_2 (-p) in equation (3) gives the value of λ associated with yielding. Hence equation (3) on simplification reduces to

$$I = \frac{r^{k} S_0}{(1 - 2h)}$$ for axisymmetric compression.

References

1. P. Ramakrishnan, Proc. Int. Seminar on Metal Working Technology Today and Tomorrow, Ranchi, India, 1980, 43-46.
2. A. K Jha and S. Kumar, Int. J. Mach. Tool Des. Res., 1983, 23, 201-210.
3. A. K Jha and S. Kumar, Adv. Tech Plast., 1984, 1, 353-357.
4. A. K Jha and S. Kumar, J. Inst. Eng. Ind., 1985, 65, 169-174.
5. T.Tabata.,S.Masaki and K. Hosokawa, Int. J. Powder Metallurgy Powder Tech., 1980, 16, 149-161.
6. T. Wonklin, Proc. First WCIT, 1972, Paper No.- F-7.
7. B. V.Deryagin, Izd. Akad. Nauk,1952, U.S.S.R.
8. B. W. Rooks, 15th Int. MTDR Conf., Birmingham, UK, Macmillan, London, 1975, 487-495.
9. T. Tabata, S. Masaki and Y. Abe, J. Jpn. Soc, Technol. Plast., 1977, 18, 373-382.
10. M. Oyane and T. Tabata, J. Jpn. Soc. Plast., 1974, 18, 373-381.

FABRICATION OF ANNULAR MOX FUEL PELLETS FOR FBTR AND PFBR

M.K.Yadav#, Neeraj Kumar, Y.G.Nehete, S.K.Shrotriya, K.Subbarayal, B.K.Shelke, P.M.Khot, B.Surendra, A.K.Mishra, Mohd Afzal and Dr J.P.Pannakkal

Advanced Fuel Fabrication Facility, Bhabha Atomic Research Centre, Tarapur, India

Absract:

Advanced Fuel Fabrication Facility (AFFF),Tarapur has gained considerable experience in fabrication of MOX fuel for various thermal and fast reactors.MOX fuels of different composition have been fabricated here for both thermal and fast reactors. MOX fuel for hybrid core of FBTR was fabricated at AFFF, BARC Tarapur. Hybrid core of FBTR sub-assemblies consist of Mark-I carbide and MOX fuel. MOX fuel for FBTR contains 44 wt% of PuO_2 along with natural UO_2.Annular MOX fuel of two compositions ie 21% and 28% PuO_2 were being fabricated for PFBR. Both these fuels are fabricated by powder metallurgical technique involving various steps like mixing &milling, precompaction, granulation, final compaction and sintering in reducing atmosphere. Final compaction of MOX annular pellets were carried out in rotary press with modified tool design so as to fabricate intricate annular pellets. An online top plunger cleaning system was introduced in Rotary Press for final compaction which has led to low man-rem and increase productivity by reducing downtime utilized in manual cleaning of plunger. The present paper compares different fabrication steps and characterization of the fuel like α-autoradiography,dissolution test of FBTR and PFBR MOX fuel.

INTRODUCTION:

Advanced Fuel Fabrication Facility, B.A.R.C., Tarapur has been fabricating Mixed Oxide [MOX] fuel for thermal reactors like Boiling Water Reactor (BWR), Pressurized Heavy Water Reactor (PHWR) and fast reactors [1,3]. MOX fuel for the hybrid core of FBTR was fabricated at AFFF which contains 44 wt% of PuO_2 and rest natural UO_2 . AFFF is presently fabricating MOX fuel pins for first core of PFBR which contains $DDUO_2$- 21% PuO_2 and $DDUO_2$-28% PuO_2. Conventional powder pelletisation route (POP) is adopted for fabrication of MOX fuel which involves mixing/milling, precompaction, granulation, final compaction, sintering and dry centreless grinding. Fabrication of annular pellets having small core diameter were a great challenge [1]. In order to fabricate annular pellets, multistation rotary press with modified tooling set were used for final compaction.

This paper describes in detail the experience gained during fabrication of annular MOX fuel for FBTR and PFBR .Various modifications are done in tool design like online top plunger cleaning system to get annular pellets [4].It also the compares effects of plutonium on dissolution test and α-autoradiography .

FABRICATION OF FUEL PELLETS:

POWDER PROCESSING AND COMPACTION

Weight of UO_2 and PuO_2 powders were taken in specified proportion to make a batch of 5 kg. Poly Ethylene Glycol (binder) and Oleic acid (lubricant) were added to the powders to facilitate compaction [2]. Mixing and milling were done in attritor for one hour. After this, homogenous milled powders were precompacted at 5-6 TSI and granulated in oscillatory granulator using #20 mesh sieve to get free flowing granules. Granules were finally compacted in multistation rotary press at 18-20TSI. Parameters for press were set to get reproducible pellets of good quality. Flow sheet for fabrication of annular pellets given in Fig-1.

SINTERING AND DRY CENTRELESS GRINDING:

Sintering of green pellets were done in batch type resistance heating furnace under reducing atmosphere (mixed N_2+7%H_2 gas) at 1600°C for 4-6Hours.Oversize pellets were ground to acceptable size by dry centreless grinding machine. Physical and chemical specification of sintered pellets for FBTR and PFBR were given in Table 1.Result of dissolution test were given in Table 2.

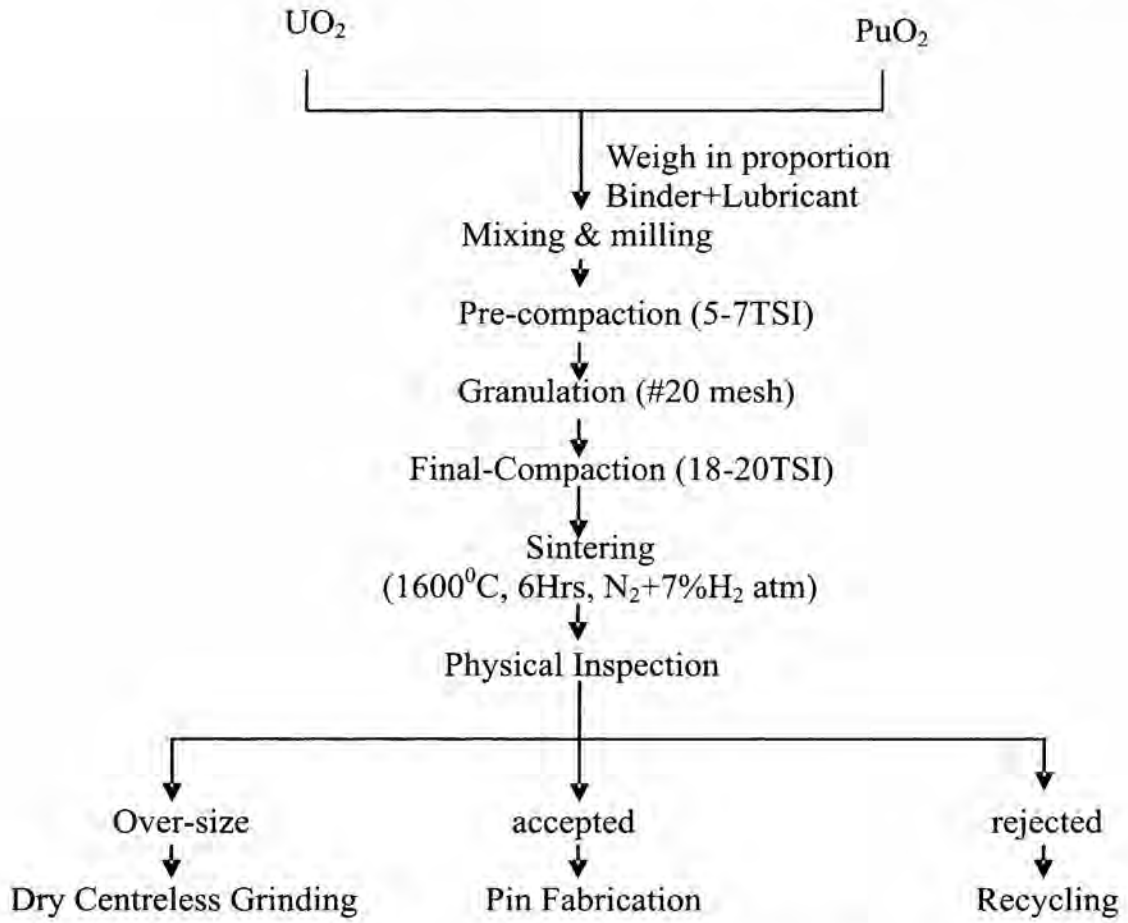

Fig-1: Flow sheet of FBTR/PFBR fuel fabrication

TABLE 1: Physical and Chemical Specification of Sinter Pellet

S.NO	CHARACTERISTICS	PFBR	FBTR/MOX
1	Outer Diameter of pellet	5.55±0.05 mm	5.52±0.08 mm
2	Inner diameter of pellet	1.8±0.2 mm	1.8±0.2 mm
3	Length of pellet	7.0 mm (nominal)	7.0 mm (nominal)
4	Linear Mass of pellet	2.25±0.15 gm/cm	2.20±0.10 gm/cm
5	PuO_2 enrichment (nominal)	21 ±1% & 28±1 %	44±1%
6	Fissile Content	(%)PuO_2xPu Equivalent 1663±110 for (21±1)% PuO_2 2218±110 for (28±1)% PuO_2	Pu(239&241) 74±3%
7	Equivalent Hydrogen Content	<3 ppm	<3 ppm
8	Total Concentration of Impurities	<5000 ppm	<5000 ppm

TABLE 2: Dissolution Test of FBTR and PFBR Fuels

Reactor	Residue Left (wt%)	Condition
FBTR	8%	10M HNO_3,10 Hr, reflux
PFBR	1%	12M HNO_3,08 Hr, reflux

DEVELOPMENT:

Annular pellets were cylindrical of diameter 5.550.05 mm having a core diameter 1.80.2 mm .Fabrication of such pellets having small core diameter is a great challenge. Choosing proper press for final compaction with annular core feature were a challenge. Multi-station rotary press had been chosen for fabrication of large quantity of annular pellets. Proper tooling sets were designed after lot of experiments with alumina and natural UO_2 powder. Tools sets used for fabrication of annular MOX pellets was shown in Fig 2. During FBTR campaign, it had been observed that frequent manual cleaning of top plunger required after 10-15 rotation due to choking of top plunger which leads to failure of core rod. Manual cleaning of top plungers leads to more man-rem to operator because of handling radiotoxic powder. Thus online top plunger cleaning system had been developed in plant to clean blocked top plunger. With continued experience, several modifications were done in tooling to get high production rate with minimum manual interference which in turn reduces personnel exposure.

RESULT AND DISCUSSION:

1- Results obtained during fabrication of FBTR & PFBR annular fuel pellets are given in Table 3.

2-Results of alpha-auto radiography shows micro-homogeneity.

3-Results of dissolution test are given in table 2. This shows macro-homogeneity.

4- It has been observed that sintering temperature for FBTR were 25°C (approx) lower than PFBR due to high PuO_2 content. This is due to more sinteractive PuO_2 powder than UO_2 powder.

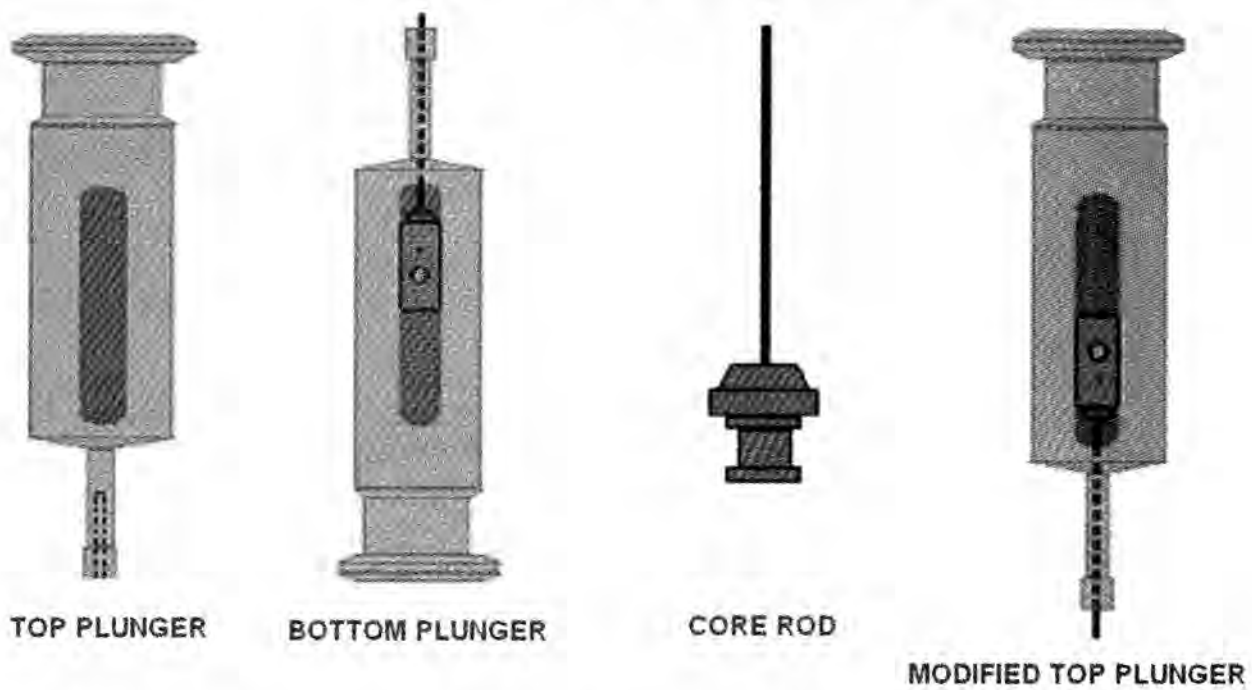

FIG 2 TOOLS USED FOR FABRICATION OF ANNULAR MOX PELLETS

TABLE -3 Details of Linear Mass of Green and Sintered Pellets

MOX Campaign	Die for final compt Φ mm	Green Pellets Φ mm	Green Linear mass gm/cm	Sintered Linear mass gm/cm
PFBR	6.7	6.75-6.79	1.95-2.05	2.15-2.38
FBTR	6.7	6.74-6.78	1.90-2.05	2.1-2.37

CONCLUSION:

Following points were concluded during fabrication of annular fuel pellets for FBTR and PFBR

1. Fuel pellets for FBTR and PFBR are fabricated successfully meeting specifications. Total 8- sub-assemblies of FBTR pins are fabricated.
2. Result of Alpha-auto radiography & Dissolution Test of both FBTR & PFBR shows complete solid solution formation.
3. Online top plunger cleaning system had been developed in plant to clean blocked top plunger. With experience, several modifications are incorporated in tooling to get high yield.

ACKNOWLEDGEMENT:

Authors are very thankful to Shri H.S.Kamath, Director, Nuclear Fuel Group, BARC for his keen interest in this work. Authors also wish to thank all the staff members of Oxide Fuel Section for their active support in carrying out this work.

REFERENCES:

1. P.S.Somayajulu,Y.G.Nehete,P.D.Sughathan, S.Mishra, A.K.Mishra, Arun Kumar& H.S.Kamath ,"New Technique in Powder Processing and Pelletisation in Nuclear Fuel Fabrication",PMAI, 2000
2. S K Shrotriya,B K Shelke,Y G Nehete,B Surendra,K Subbarayal,M K Yadav,Niraj Kumar,A K Mishra,P.S.Somayajulu,Dr J.P.Pannakkal &H.S.Kamath "Use of Na-stearate in Fabrication of Mixed Oxide Annular Pellets for FBTR" PMAI,Jan,2006 at Hyderabad.
3. P.S.Somayajulu, A K Mishra ,Y.G.Nehete,B K Shelke, S K Shrotriya, Arun Kumar,Dr J.P.Pannakkal &H.S.Kamath "PFBR Fuel Pellet Fabrication for Experimental Irradiation" CQCNF,Dec,2002 at Hyderabad
4. S K Shrotriya,B K Shelke,Y G Nehete,A K Mishra,Mohd Afzal "Development of Automated Cleaning Technique of Top Plungers Inducted in Rotary Press Used for the Fabrication of PFBR size Annular Fuel Pellets" PMAI,Feb,2009

FABRICATION OF (Th-U) MIXED OXIDE FUEL PELLETS FOR EXPERIMENTAL IRRADIATION

P.M. Khot, Y.G.Nehete, B.K.Shelke, S.K.Shotriya, K.Subbarayal, Neeraj Kumar, B.Surendra, M.K.Yadav, A.K.Mishra, Mohd Afzal and J.P.Panakkal.*

Advanced Fuel Fabrication Facility, Bhabha Atomic Research Centre, Tarapur, India

Abstract:

Thorium utilization has been an important aspect for long term sustainability of Indian three stage nuclear power program. As a step towards this, Advanced Heavy Water Reactor (AHWR) has been designed where (Th-^{233}U) O_2 mixed oxide fuel along with (Th-Pu) O_2 will be used.

In order to simulate actual condition, AHWR (Th-U) MOX fuel pins for experimental irradiation in research reactors have been fabricated at Advanced Fuel Fabrication Facility (AFFF), BARC, Tarapur. The fuel for the experimental irradiation is ThO_2-10% enriched Uo_2. ThO_2 powder derived from oxalate route is milled in attritor to break platelet morphology for making it 'sinteractive'. As received ammonium diuranate (ADU) powder is calcined to obtain enriched U_3O_8 powder. After co-milling, milled powder is precompacted, granulated and cold compacted followed by sintering in reducing atmosphere at 1650°C to get fuel pellets with density around 95 % TD. The fuel pellets which have been fabricated from co-milling with ThO_2, enriched U_3O_8 powder shows nearly same diametrical as well as axial shrinkage. On the other hand fuel pellets fabricated from co-milling of milled ThO_2 and enriched U_3O_8 powder resulted in much higher diametrical shrinkage (16%) than axial shrinkage (8.22%). Extensive trials are carried out with optimal process parameters to get pellets of desired specifications. Fabrication of ThO_2-10% enriched UO_2 fuel pellet which meets all desired specification have been carried out successfully. The present paper highlights the details of fabrication and characterization (Th-U) MOX fuel pellets.

INTRODUCTION:

AFFF has gained vast experience in the fabrication of plutonium based MOX fuel of various types for thermal and fast reactors. Experimental irradiation in research reactor is planned for studying irradiation behavior of thoria based fuel in terms of fission gas release, fuel centerline temperature, fuel pellet swelling, and fuel grain growth. The fuel simulates actual condition of AHWR MOX fuel pin. Advanced Fuel Fabrication Facility (AFFF), BARC, Tarapur has taken up responsibility of (Th-U) MOX fuel pin fabrication for experimental irradiation. Figure 1 shows the flow sheet for fabrication of Th-10% enriched UO_2 MOX pellets through conventional powder metallurgical process using ThO_2 and U_3O_8 as a starting material. All the operations are carried out in glove boxes.

The physical and chemical specifications of (Th-U) MOX fuel pellets are given in table 2 & 3.

FABRICATION OF MIXED (Th-U) OXIDE FUEL PELLETS:

ThO_2 based fuel generally fabricated by conventional powder metallurgical route which consists of milling of as received ThO_2 powder in planetary ball mill, mixing and milling of milled ThO_2 powder along with U_3O_8 powder, binder and lubricant, double precompaction of mixed milled powder, granulation, final compaction of granulated powder followed by sintering [1].

TABLE 1 Characteristics of ThO_2 and U_3O_8 powders

Sr.No	CHARACTERISTICS	ThO_2 POWDER	U_3O_8 POWDER
i)	Apparent density (gm/cm^3)	0.70	1.2
ii)	Specific Surface Area (m^2/gm)	1.53	2.15
iii)	Theoretical density (gm/cm^3)	10.00	8.34
iv)	Oxygen to Metal Ratio	2.00	2.66
v)	Total impurities (ppm)	<1200	< 800

POWDER PROCESSING:

Powder treatment:

Enriched UO_2 powder was supplied in the form of ammonium diuranate (ADU).ADU powder was calcined in air at around 700°C for 2hrs so as to convert it in U_3O_8 form.

Powder processing involves process steps such as milling, binder and lubricant addition, mixing and milling, precompaction and granulation. The ThO_2 powder derived from oxalate route has a flat, square platelet morphology, which requires milling to break platelet morphology for making it 'sinteractive'.

Batch No 1:

As received ThO_2 powder was milled in attritor at 200 rpm for 40 min using high chromium steel ball to break its platelet morphology. Milled ThO_2 powder, U_3O_8 powder, and organic binder as Polyethylene Glycol and lubricant as Oleic Acid were weighted in specified proportion and milled in attritor at 200 rpm for 40 minutes.

Batch No. 2:

As received ThO_2 powder, enriched U_3O_8 powder, Polyethylene Glycol and Oleic Acid were weighted in specified proportion and co-milled in attritor at 200 rpm for 40 minutes.

Proper choice of binder and lubricant has a considerable significance in achieving desired specification of pellets [2]. The speed and duration of milling should be chosen such that adequate homogeneity of powder should be obtained after mixing and milling process of both starting powders. Mixed powder was precompacted in double acting hydraulic press at 6-8 TSI and pre-compacts were granulated in oscillatory granulator and sieved through # 8 mesh.

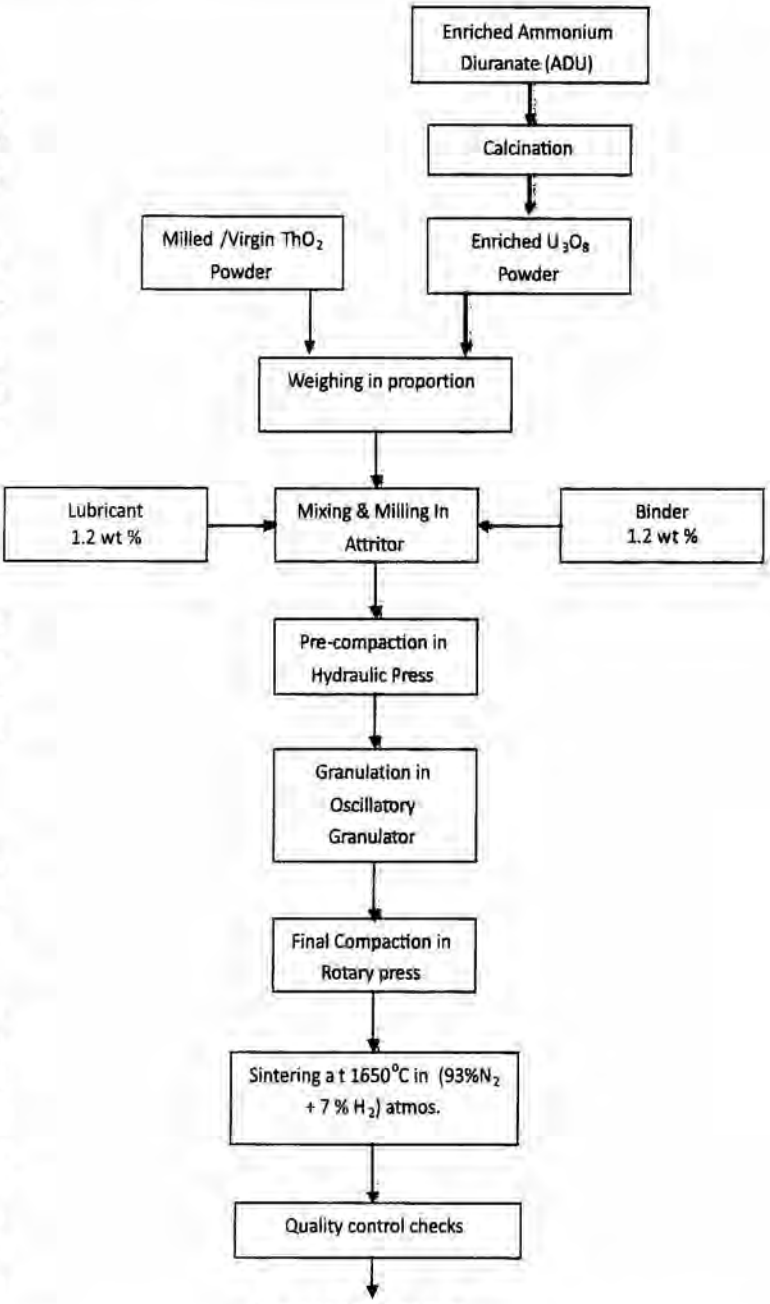

Fig 1 Fabrication flow sheet for mixed (Th-U) oxide fuel pellets

COLD COMPACTION AND SINTERING:

Final compaction of granulated powder from two batches was done using tooling size of proper diameter at 18-20 TSI in mechanical rotary press so as to attain the green density of compact in the range of 6.00 to 6.20 gm/cm^3. Green compacts were sintered in batch type molybdenum resistance furnace at 1650 ± 25 °C for 4 hours in presence of reducing atmosphere. Extensive trials were carried out using various size of tooling in final compaction and sintered at different temperature for obtaining sintered to size pellets.

TABLE 2: Physical specifications of (Th-U) MOX fuel pellets.

Sr.No	CHARACTERISTICS	SPECIFICATIONS
i)	Density of the pellet	90-95 % of T.D
ii)	Diameter of the pellet	9.7± 0.10 mm
iii)	L/D Ratio	0.5 to 1.0
iv)	Grain Size	5 to 50 μ

TABLE 3: Chemical specifications of (Th-U) MOX fuel pellets.

Sr.No	CHARACTERISTICS	SPECIFICATIONS
i)	Enrichment	1± 0.1 % $^{235}UO_2$
ii)	O/M ratio	1.98-2.00
iii)	Total impurities	< 2500 ppm
iv)	E.B.C	<2.5 ppm

Details of green and sintered pellet

Batch No.	Starting Material for Co-milling	Tool size (mm)	Green pellet data			Sintered pellet data		
			Diameter (mm) Nominal	Height (mm) Nominal	Green density (gm/cc)	Diameter (mm) Nominal	Height (mm) Nominal	Sintered density (gm/cc)
1	Milled ThO_2 + Virgin U_3O_8	11.1	11.195	10.008	5.94	9.352	9.185	9.46
2	Virgin ThO_2 + Virgin U_3O_8	11.1	11.211	10.441	6.20	9.631	8.985	9.42

RESULT AND DISCUSSION:

1) Details of Batch:

Fuel pellet from batch 1 which uses milled ThO_2 and virgin U_3O_8 as a starting material for co-milling shows lower green density with higher sintered density as compared to pellet from Batch 2. It has been observed that fuel pellets from Batch 1 showed higher diametrical shrinkage (16.462 %) as compared to axial shrinkage which was around 8.22 %. Fuel pellets of Batch no. 2 with virgin ThO_2 and U_3O_8 as starting materials for co-milling showed nearly same diametrical (14.68 %) and axial (13.94 %) shrinkage. The use of milled ThO_2 and Virgin U_3O_8 as a starting material for co-milling increased tooling size required to achieve desired pellet specification. Furthermore it increased process steps which in turn increased man-rem to operator without any significant improvement in sintered density of pellet.

2. Metallic impurities:

Trace impurities in nuclear fuel can significantly affect its performance in a reactor due to their metallurgical and neutron absorption properties.

The metallic impurities of sintered (Th-U) MOX pellet determined by Atomic Emission Spectroscopy (AES) using D.C. arc as an excitation source are shown in table 4. All the metallic elements including critical elements B, Cd were found to be within specification limits.

Table 4: Metallic impurities in ThO_2 - 10% UO_2 pellet

Elements	Concentration (ppm)	Elements	Concentration (ppm)
Al	337	Mn	35
B	0.5	Mo	47
Be	0.2	Ni	<10
Ca	239	Pb	<10
Cd	0.5	Si	165
Co	<10	Sn	32
Cr	31	V	46
Cu	37	W	110
Fe	197	Zn	126
Mg	70		

3. α- autoradiography:

Homogeneity of fuel pellet was evaluated by α- autoradiography. The presence of fissile rich zone in mixed oxide fuel pellet leads to higher fission gas release and fuel failure [3]. So it was necessary that size of agglomerate should be as low as possible and its distribution through the matrix should be uniform.

Fig 2 shows α- autoradiograph of Th-10% UO_2 pellet from batch 2 fabricated by POP route indicating uniform distribution of uranium in thorium matrix. Size of uranium agglomerate was less than the specified value.

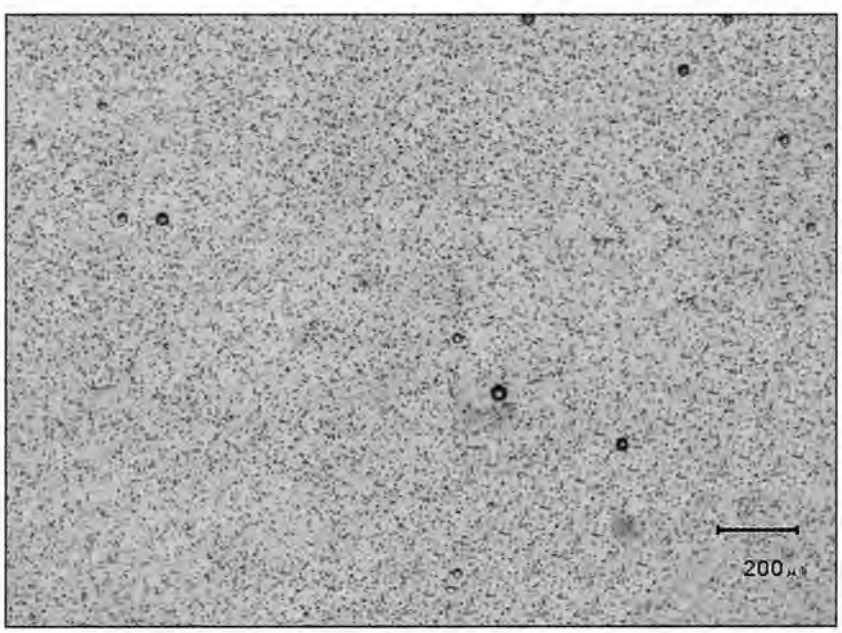

Fig.2 α-autoradiograph of ThO_2-10%UO_2 pellet fabricated by POP route sintered in N_2-7%H_2 at 1650°C for 4 Hr

CONCLUSION:

- Significant quantity of mixed (Th-10% enriched UO_2) oxide fuel pellets have been fabricated successfully using existing facility of AFFF, Tarapur for experimental irradiation in research reactor.
- Selection of starting material for co-milling play vital role in achieving sintered to size pellets.
- The selection of appropriate size of tooling used in final compaction has played vital role in elimination of grinding process during fabrication of mixed (Th-10% Enriched UO_2) oxide fuel pellets.
- From α - autoradiograph it was observed that the various milling and sintering parameters chosen for fabrication of (Th-U) MOX fuel was optimum.

ACKNOWLEDGEMENT:

Authors are very thankful to Shri H.S.Kamath, Director, Nuclear Fuels Group, BARC for his keen interest in this work. Authors also wish to thank all the staff members of Oxide fuel section and Quality control section for their active support in carrying out this work.

REFERENCES:

[1] T.R.G. Kutty a,*, P.V. Hegde a, K.B. Khan a, T. Jarvis a, A.K. Sengupta a, S. Majumdar a, H.S. Kamath, "Characterization and densification studies on ThO_2–UO_2 pellets derived from ThO_2 and U_3O_8 powders ", Journal of Nuclear Materials 335(2004), 462-470.

[2] Mishra, S.N.Rahul, I.D.Godbole, A.K.Mishra, Arun Kumar and H.S.Kamath," Use of Polyethylene Glycol and Oleic acid in Fabrication of Nuclear fuel pellets", PMAI conference 1999 S.

[3] Status and advances in MOX technology, technical report series no.415, IAEA Vienna-2003.

CNTINUOUS HYDROTHERMAL SYNTHESIS OF ZnO PARTICLE

Mustaqueem Ahmad

Department Of Chemical Engineering Aligarh Muslim University , Aligarh, India

Abstract:

This presentation provide an excellent process of producing ZnO particle continuously. this is an environmental friendly process for the production of valuable metal oxide, currently most particle synthesis are performed in batch reactor which take long time to produce particles. Nano - micro particle can be produce by several technique (precipitation, spray, pyrolysis , thermal decomposition, hydrothermal) etc. Hydrothermal process offered excellent control of morphology (spherical, cubical, fibrous and plate like) size from couple of nanometer to ten of micron .The characteristic can be controlled in wide ranges using thermodynamic variables such as, temp , type of the reaction, concentration etc. It can also be done by controlling non thermodynamic (kinetic) variables..

INTRODUCTION

Typically, hydrothermal process conducted with a batch process. An aquaes solution is heated slowly to 373-5730k and then aged for several ours and days [1] .During the heat up time, hydrothermal action taken place to produce nuclei and than crystal grow, As ZnO become more soluble in water comparing with other metal oxide such as TiO2 and ZrO2 .Hydro thermal synthesis of nano size fine particle is an especially different problem with out any surfactant. Because the conventional production of various kind of nano particles has been carried out in batch operations, There are problem such as considerable time and effort required for maintenance including charging reaction solutions and washing in each batch.

From the past decade, the research on nano scale science has been going considerably due to the potential application of nano material in electronics, material science, chemical or mechanical industries, as well as technologies with them, including super conductor, catalyst drug carriers, sensors, magnetic material pigment and in the structural and electronic material[2] It is well known that material can be modulated to exhibit improved or novel properties usingNanotechnologies because at nano scales, there property differ from both those of individual atoms and molecules and from bulk material [3]

Merit Of Hydrothermal synthesis.

Hydrothermal synthesis offers many advantage over conventional and non conventional synthesis method .All form of ceramic can be prepared with hydrothermal synthesis namely ,Powder, Fiber, single crystals, monolithic ceramics bodies and coatings on metals, polymers and ceramics. From the stand point of ceramic powder production there are for fever time and energy consuming processing steps since high temperature calcinations, mixing and milling steps are either not necessary or minimized. Moreover the ability to precipitate already crystallized powder regulate the rate and the uniformity of the nucleation, growth and aging, which result in improve control of size morphology of crystallites and significantly reduced aggregation level that is not possible with many other synthesis process.

Hydrothermal process can take place in wide variety of combination of aqueous and solvent mixture based synthesis. In general processing with liquids allows for automation of wide range of unit operations such as charging, transportation, mixing and product separation. Moreover, relative to solid state process liquid give a possibility for acceleration of diffusion, adsorption, reaction and crystallization under hydrothermal condition. However ,unlike many advanced method that can prepare large variety of form and chemical combination such as chemical vapor based method the respective cost of instrumentation energy and precursors are less for hydrothermal method ,which can be attributed in part to energy conserving low processing temperature, absence of milling, ability to recycle and safe and convenient disposal of waste that can be recycled[4].

Another important technology advantage of the hydrothermal technique is its capability for continuous

fabrication of ceramics powders[5]. Moreover hydrothermal crystallization can be monitored in-situ using a range of technique[6], which allows determination of crystal growth mechanism and better control of the hydrothermal synthesis.

There are several method of synthesis of nanoparticle. Material synthesis of nanoparticle via high-temperature processing technique is promising tool that offer a good route to production of high purity nanoparticle with specifically tailored chemical and physical properties. However, the transformation of the gaseous precursor to the final particle is a complex physical process involving nucleation of the particulate phase, condensation and coalescences between particles

Nano particle generated by ***gas phase*** process are usually atre in the form of aggregates, due to their coagulation at high temperature Electro spray- assisted chemical vapor deposition process, non – agglomerated, spherical nanoparticle of silicon, titanium and Zirconium oxide can be prepared.

Preparation of nano particulates via **liquid phase route**, such as chemical reduction, sol-gel reverse micelle, hot-soap, pyrolysis and spray hydrolysis etc. Particle synthesis through these methods have controlled characteristics, including size ,size distribution, morphology agglomeration and composition. These process are low cost and involve continuous operatiuon and high production rate. Many researcher have synthesis the nanoparticle of Sio_2, ZnO, CdSe, FePt, etc.

In the vapor phase process, condition are created where the vapor phase mixture thermodynamically unstable relative to formation of the solid material to be prepared in the nanoprticulate form. This include usual situation of a super saturated vapor. It also include chemical super saturation in which it is thermodynamically favorable for the vapor phase molecules to react chemically to form a condensed phase. If the degree of super saturation is sufficient, and the reaction/ condensation kinetics permits, particles will nucleate homogeneously. Once nucleation occurs, remaining super saturation can be relived by condensation or reaction of the vapour-phase molecules on the resulting particles, and particle growth will occur rather than further nucleation. Once particle form in the gas phase, they coagulate at a rate that is proportional only the square of their number concentration and that is weakly dependent on the particle size. At sufficiently high temperature, particle coalesces (sinter) faster than they coagulate, and spherical particle are produced.[7].

Producing the nanoparticle using *solid precursors*, in this method the material vaporize into a background gas and than gas is cooled. Inert gas condensation is the most common method. In this method the solid is evaporated in to a back ground gas and than vapor is mix the vapor with cold gas to reduce the temperature. in this way particle is produced, since many method since many metal evaporate at reasonable rate at attainable temperatures. By including a reactive gas, such as oxygen, in the cold gas stream, oxides or other compounds of the evaporated material can be prepared.[8] Ohio prepared Si / In, Ge / In, AI / In and AI /Pb composite nanoparticle by condensation reactor Si, Ge , or AI particles prepared by inert gas condensation and brought directly into a second condensation reactor.

In *pulser laser ablation*, rather than simply evaporating a material to produced super saturated vapor, one can use a pulsed laser to vaporize a plume of material that is tightly t confined both spatially and temporally this method can generally only produces small amount of nano particle. Through this method ,magnetic oxide nanoparticles by shinde et. Al.,titania nano particles by Harano et al.[9].,and hydrogenated-silicon nano-particles by makimura et al

In *spark discharge generation* , vaporizing metal is to charge electrodes made of the metal to be vaporized in the presence of an inert back ground gas until the break down voltage is reached. The arc(spark) formed across the electrodes than vaporized a small amount of metal. Through this method very small amount of nanoparticle can be produced. Weber et al,[10],produced well-characterized nickel particle

for study their catalytic studies activities in the absence of any support material.

Vaporization of solid via *Ion sputtering* with a beam of inert gas .Urban et al. [11] demonstrated formation of nanoparticles of a dozen different metals using magnetron sputtering of metal targets. They formed collimated beams of nanoparticle and deposited them as nanostructured films on silicon substrates this was the low pressure process.

Yet another means of providing the energy needed to induced reaction that leads to super saturation and particle nucleation's to inject the precursors into a *thermal plasma.* This generally decomposes them fully in to atoms, which can than react or condense to form particles when cooled by mixing with cool gas or expansion through nozzle. Heberlein et al. [12] have applied these methods for producing of nanoparticle of SiC and TiC for nano phase hard coatings.

In the flame *synthesis technologies.* which is most commercially successful approach to nanoparticle synthesis, which is producing millions of tons of carbon black and metal oxides. The synthesis of particle is carried out within the flame, so that the heat needed is produced in situ by the combustions. It is primarily useful for making metal oxides. However, the coupling of the particle production to the flame chemistry make this a complex process that is rather difficult to control. Wegner et. al [13] control the size and morphology of titanium nanoparticles by extracting them from the flame through a critical flow nozzle, quenching particle growth and agglomeration.

For particular materials, it is possible to react vapor phase precursors directly without external addition of heat, and without significant production of heat.this technology is known as low temperature reactive synthesis.

Spray *pyrolysis* (SP) method gives promising result for nanoparticle production, in which precipitation, thermolysis(SP)(ie calcinations) and sintering stages of powder synthesis can be integrated in to a single continuous process. To prepare fine particle by sp, a ..... solution is usually is prepared by dissolving the solvent.The drop let are automized from the starting solution with an automizer, and then droplets are placed in the furnace. A variety of activity may occure inside the furnace during formation of the final product including evaporation of the solvent, diffusion of the solute, drying, precipitation, reaction between the precursor and surrounding gas, pyrolysis and sintering generally, a one droplet-to-one-product particle(ODOP) con is considerd the typical particle formation mechanism in conventional spray pyrolysis(CSP). There are several spray pyrolysis method is available such as salt assisted spray pyrolysis[....]. lowpressure pyrolysis[LPSP] [14] flame assisted spray pyrolysis[FASP].Though the salt assisted pyrolysis method that introduced salt in to the precursor solution.Through this method a wide range of nanoparticle from simple oxide to multi component material can be produced

Laser energy for heating the precursors to induce reactions and homogeneous nucleation .Compared to heating the gases in a furnace, this allow high localized heating and rapid cooling, since only the gase or(or portion of the gas) is heated, and its heat capacity is small. Heating is generally done usually an infrared (CO_2) laser, whose energy is either absorbed by one of the precursors or by inert photosensitize such as sulfur hexafluoride. Nanoparticles of many material have been made using this method. A few recent example are MoS_2 nanoparticle produced by Boresella et al SiC nanoparticle prepared by Kamlag et al.[13],and si nanoparticle produced by Ledoux et al by using a pulsed CO2 laser, there by shortening the reaction time and allowing preparation of even smaller particle.

Material and Method:

This is a Edisonian approach in which extra chamber is added For the synthesis of nano particle the experimental set up is shown in ***fig. 1***. .The ZnO powder for experimentation was procured from the market(L.R) grade .The temperatures for experiment was selected as 60, 80, 90^{0C}, The ZnO is dissolved in a container having stirrer which move at a defined

constant rpm. The solution from this container is fed in to a pre filter with the help of a pump having the by pass to control the flow.. In the pre filter the un-dissolved ZnO. Is removed and the collected solution is than fed in to the tubular heater from where the heat is added with the help of electric tape heater at a constant temperature which can be regulated as per the process requirement(in our case 60,80.90$^{0C)}$ This solution is further fed in to the aging chamber which is maintained at the constant temperature. The temperature of the aging chamber kept at the defined temperature. (60,80 ,90^{0C}). The solution is fed from the bottom of the aging chamber and the aging chamber is insulated to prevent the heat loss to the environment.. During the heat-up time hydrothermal reaction take place to produce nuclei and than grow. The temperature of the aging chamber is within control with negligible temperature gradient as the leaving temperature of the solution is the temperature of the aging chamber there is continuously flow of the product from the aging chamber, the temp in aging chamber is controlled. The temperature gradient is negligible the inlet and out let temperature of the flow is constant. The solution is then fed in to the cooling system where it looses the heat .The cooling system is design in such a way that by regulating the flow rate of the cooling water, the temperature of the cooling system can be adjusted and the heat extraction can be regulated in this way. Then the solution is fed in to the continuous filtration unit from where the particle is collected and dried.

RESULT AND DISCUSSION

Primarily particle size appear to be determined by competition between the nucleation rate during crystallization. The nucleation rate is a function of temperature, degree of super saturation and interfacial tension(s), where growth rate mainly dependent on the diffusivity of the solute. In the continuous synthesis process, as a laboratory approach an aging chamber is added to get the micro to nano particle with different control this On comparing The quantities and quality of the particle keeping the temperature same in batch processing[1]. and in this experiment it is found that the quantity and quality of the particle was entirely different. the particle found in good shape. as the particle size is depend upon the residence time .It can be changed by regulating the inflow with the help of the pump provided in the system, on higer temp the particle shape found more uniform

FURTHER DESIGN CONSIDERATION:

Instead of Edisonian approach, which is used in this case, for a given precursor system the effect of concentration, temperature and pressure can be modeled to define the process variable space over which phases of interest are stable. Moreover, many different type of precursor system can be compared and the experiment modified to make material that has never been previously prepared in hydrothermal solution. In way the production of particle can be done at a industrial level with less environmental burden.

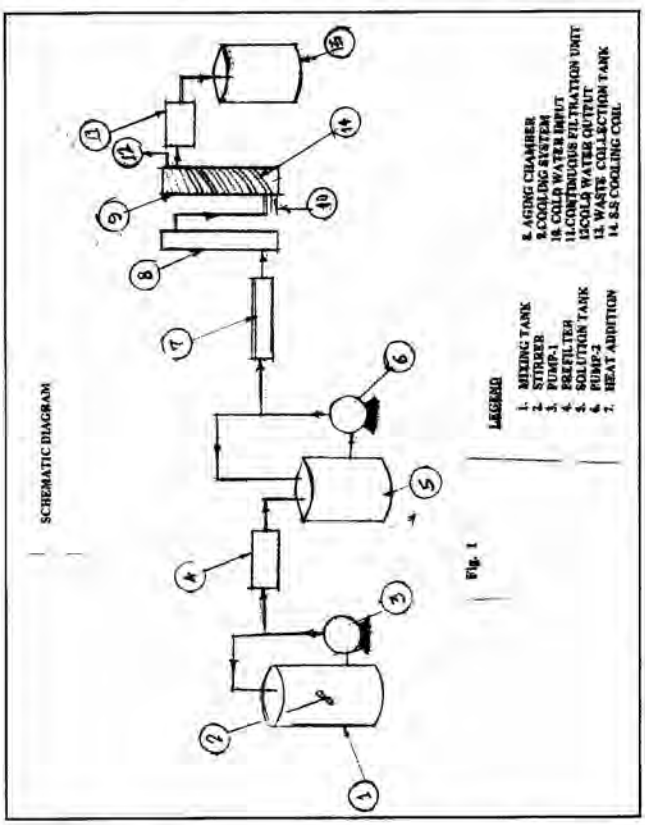

Fig.1 Experimental setup for Synthesis of Nanoparticles